EXTREME ENVIRONMENT ELECTRONICS

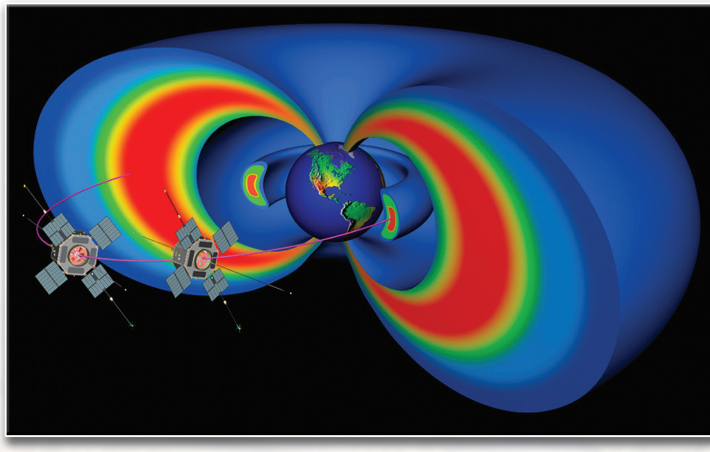

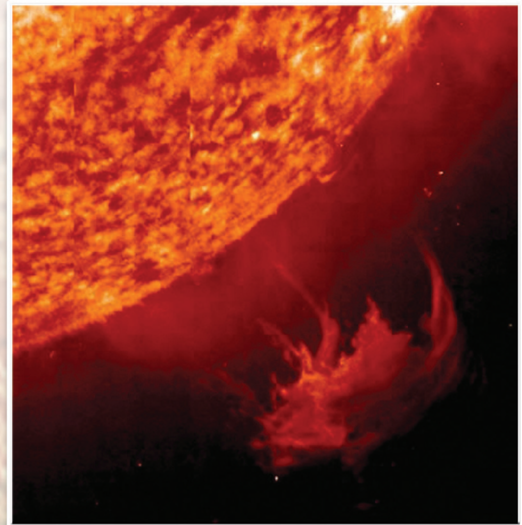

Edited by
John D. Cressler
H. Alan Mantooth

CRC Press
Taylor & Francis Group

EXTREME ENVIRONMENT ELECTRONICS

INDUSTRIAL ELECTRONICS SERIES

Series Editors:

Bogdan M. Wilamowski

J. David Irwin

PUBLISHED TITLES

Extreme Environment Electronics, *John D. Cressler and H. Alan Mantooth*

Renewable Energy Systems: Advanced Conversion Technologies and Applications, *Fang Lin Luo and Hong Ye*

Multiobjective Optimization Methodology: A Jumping Gene Approach, *K.S. Tang, T.M. Chan, R.J. Yin, and K.F. Man*

The Industrial Information Technology Handbook, *Richard Zurawski*

The Power Electronics Handbook, *Timothy L. Skvarenina*

Supervised and Unsupervised Pattern Recognition: Feature Extraction and Computational Intelligence, *Evangelia Micheli-Tzanakou*

Switched Reluctance Motor Drives: Modeling, Simulation, Analysis, Design, and Applications, *R. Krishnan*

FORTHCOMING TITLES

Power Electronics and Control Techniques for Maximum Energy Harvesting in Photovoltaic Systems, *Giovanni Spagnuolo, Nicola Femia, Giovanni Petrone, and Massimo Vitelli*

Industrial Wireless Sensor Networks: Applications, Protocols, Standards, and Products, *Vehbi Cagri Gungor and Gerhard P. Hancke*

Multilevel Converters for Industrial Applications, *Sergio Alberto Gonzalez, Santiago Andres Verne, and Maria Ines Valla*

Smart Grid Technologies: Applications, Architectures, Protocols, and Standards, *Vehbi Cagri Gungor, Carlo Cecati, Gerhard P. Hancke, Concettina Buccella, and Pierluigi Siano*

Sensorless Control Systems for AC Machines: A Multiscalar Model-Based Approach, *Zbigniew Krzeminski*

EXTREME ENVIRONMENT ELECTRONICS

Edited by
John D. Cressler
H. Alan Mantooth

CRC Press
Taylor & Francis Group
Boca Raton London New York

CRC Press is an imprint of the
Taylor & Francis Group, an **informa** business

CRC Press
Taylor & Francis Group
6000 Broken Sound Parkway NW, Suite 300
Boca Raton, FL 33487-2742

Version Date: 2012907

International Standard Book Number-13: 978-1-4398-7431-8 (eBook - PDF)

Visit the Taylor & Francis Web site at
http://www.taylorandfrancis.com

and the CRC Press Web site at
http://www.crcpress.com

From John D. Cressler:

I celebrate my many students
Who shared in my passion and love
For this fascinating field chocked full with wonder and awe.
I am indebted to each of you for your dedication,
your keen insights, and your many imaginings.

And …

For my Maria:
My beautiful wife, best friend, and soul mate for these 30 years.
For Matthew John, Christina Elizabeth, and Joanna Marie,
And now Michael and Mary Ellen:
You are God's awesome creations,
And our very precious gifts.
May your journey of discovery never end.

From H. Alan Mantooth:

In 2004, a fine team of collaborators assembled by Dr. Mohammad Mojarradi at Jet Propulsion Laboratory was fortunate to win a grant from NASA to explore silicon-germanium (SiGe) technology for the purpose of extreme environment electronics in space applications. This team was led out of Georgia Tech (Cressler) and had as its participants Arkansas (Di, Mantooth), Auburn (Dai, Johnson, Niu), BAE Systems (Berger), Boeing (Peltz), IBM (Joseph), JPL (Mojarradi), Lynguent (Holmes), Maryland (McCluskey), Tennessee (Blalock), and Vanderbilt (Alles). To this point in my career, I can honestly say that I have not worked with a finer team across the board than the "SiGe team." And, while the names listed above are the team leaders, there were scores of other engineers and students behind them performing outstanding research. Our association was, and continues to be even though the project ended in 2010, collaborative, respectful, professional, personal, productive, and most of all fun! I am proud of what our team accomplished and of having had the wonderful opportunity to play in this sandbox with these great people. They are truly national treasures because of the impact they have and continue to make in all facets of their lives.

No less than two dozen University of Arkansas (UA) graduate students, all listed among my students in the Preface, contributed to our SiGe team during the 5+ year effort in analog and digital circuit design and semiconductor device modeling. I would like to begin my dedication of this book to all of those students who made those contributions. For all the long hours, unwavering commitment, teamwork, patience, persistence, and professionalism, this book serves as a monument to your collective achievements. Within this esteemed group of students are those whose efforts truly made a big difference: Aaron Arthurs, Matt Barlow, Richard Broughton, Kim Cornett, Chris Lee, Hung Phi Hoang, Avinash Kashyap, Mihir Mudholkar, and Javier Valle. Dr. Hoang paid the ultimate sacrifice, succumbing to lung cancer in 2009 and never complaining one time. He worked in the lab until two weeks before being hospitalized while none of his team knew of his condition.

I would like to complete my dedication to my lovely wife and best friend of 25 years, Mary Lynn, and our beautiful daughters, Deanna Lynn, Laura Kathryn, and Maureen Elaine. Thank you for your patience, understanding, and love, now and forever. You ladies are the wind beneath my wings for all that I do!

(photo of Dr. Mantooth's name in Senior Walk at the UA)

Contents

PART III Environments and Prediction Tools

PART IV Semiconductor Device Technologies for Extreme Environments

PART V Modeling for Extreme Environment Electronic Design

PART VI Device and Circuit Reliability in Extreme Environments

PART VII Circuit Design for Extreme Environments

PART VIII Examples of Extreme Environment Circuit Designs

PART XII Appendices

Preface

The invariable mark of wisdom is to see the miraculous in the common.

Ralph Waldo Emerson

Motivation

Extreme Environment Electronics represents a very important niche industry within the trillion dollar global electronics infrastructure and entails the design, implementation, and deployment of electronic devices, circuits, subsystems, and systems capable of operating robustly in environmental surroundings lying outside the traditional domain of conventional commercial or military electronics specifications. Such extreme environments include a diverse collection of "nasty" situations, including, in an approximate order of importance, the following:

- Operation in radiation-rich environments
- Operation in low-temperature environments
- Operation in high-temperature environments
- Operation in cyclic, wide temperature range environments
- Operation in vibrationally intense environments
- Operation in chemically corrosive environments
- Operation in intense magnetic field environments
- Operation under conditions that bring together many extreme environments

This latter catch-all environment is actually quite common (e.g., consider putting a satellite into Earth orbit and conducting a ten-year mission there for remote sensing) and can be considered worst case. Needless to say, there are degrees of "extreme" within each subcategory, some of which are far more challenging than others, and some of which no one in their right mind would ever attempt (e.g., a mission to the moons of Jupiter comes to mind as among the more challenging in the solar system!). In general, extreme environment electronic systems are by definition low-volume, but high-value-added propositions, and hence can be extremely expensive to deploy. It is a truism that extreme environments are "unfriendly" to conventional electronic devices, circuits, and systems and thus from a broad perspective represent a very serious "reliability challenge" to designers and mission architects.

As one can easily imagine, environmental "hardening" of electronics to ensure robust operation in a given extreme environment typically comes with a high price tag and is a large part of the reason for the high cost associated with, say, operating a satellite system in space or sending a rover to Mars or the Moon. The "holy grail" in the context of extreme environments is an integrated circuit technology platform that is capable as-built for operation in any extreme environment in which the device/circuit/subsystem/system finds itself. Said another way, the desire would be that if we design electronics for standard (terrestrial) operation they should also work well in whatever extreme environment you care to use them in, with no added design or test overhead, enhanced degradation in reliability, or increase in cost. Such an extreme environment electronics technology solution does not exist, and likely never will exist. Simply put, this book you hold in your hands explores at length what is required to operate electronics in extreme environments, what the overarching reasons for those complexities entail, and how one ultimately achieves success.

It can be fairly stated that *Extreme Environment Electronics* represents the first truly comprehensive exposition of this field. We address a remarkably wide array of topical coverage, ranging from the extreme environments themselves, to basic physics of the various interactions between devices and environments, to the detailed aspects of electronic design, to modeling of devices through systems, to packaging design, to reliability and quality assurance, to ultimately a wide class of interesting end-use applications intended for real extreme environments. The "best practice" approaches required to ensure success are constantly emphasized, and many industry examples are given. Not surprisingly, the contributors to this book represent a veritable "who's who" in the extreme environment electronics field, and given its exceptionally broad coverage, its depth, and the expertise of the contributing authors, this book is expected to become "the" seminal go-to reference of the field.

Audience

So who exactly should buy this 1000+ page "beast"? *Extreme Environment Electronics* is intended for a number of different audiences and venues. It should prove to be a useful resource as (1) a hands-on reference for practicing engineers and scientists working on various aspects of extreme environment electronics; (2) a hands-on research resource for graduate students in electrical and computer engineering, physics, or materials science; (3) a textbook for use in graduate-level instruction in this field; or (4) a reference for technical managers and even technical support/technical sales personnel in the industry. It is assumed that the reader has some modest background in basic electronics (say, at the advanced undergraduate level), but each chapter is self-contained in its treatment, and there are numerous appendices with more basic background.

Contributors

In this age of ultra-busyness and information overload, in which all of us are seriously pressed for time and overworked (and likely in need of a raise!), our success in getting such a large collection of rather well-known people to commit their precious time to our vision for this project was immensely satisfying. We are happy to say that our authors made the process quite painless (well, most of you!), and we are extremely grateful for their help.

The list of contributors to this book, impressive by any standard, should be regarded as "go-to" people in their respective areas. We would like to formally thank each of our colleagues for their hard work and dedication in helping execute our vision of producing a lasting extreme environment electronics "bible." In order of appearance, the "gurus" of our field include the following:

Elizabeth Kolawa, Jet Propulsion Laboratory
Dana Brewer, NASA Headquarters
Janet Barth, NASA Goddard Space Flight Center
Andrew S. Keys, NASA Marshall Space Flight Center
Gary W. Hunter, NASA Glenn Research Center
Dennis Culley, NASA Glenn Research Center
Jonathan A. Pellish, NASA Goddard Space Flight Center
Lewis M. Cohn, Naval Research Laboratory
Kurt A. Moen, Georgia Tech
Robert Reed, Vanderbilt University
Kenneth F. Galloway, Vanderbilt University
Ronald D. Schrimpf, Vanderbilt University
Michael Xapsos, NASA Goddard Space Flight Center
James H. Adams, Jr., NASA Marshall Space Flight Center
Robert A. Weller, Vanderbilt University
Alexander B. Lostetter, Arkansas Power Electronics International
Peter Wilson, University of Southampton
Lloyd W. Massengill, Vanderbilt University
Aravind C. Appaswamy, Texas Instruments
Rajan Arora, Georgia Tech
Jiahui Yuan, Sandisk
Philip G. Neudeck, NASA Glenn Research Center
Edward P. Wilcox, NASA Goddard Space Flight Center and MEI Technologies, Inc.
Trevor J. Thornton, Arizona State University
William Lepkowski, SJT Micropower
Seth J. Wilk, SJT Micropower
Mohammad Reza Ghajar, Arizona State University
Asha Balijepalli, Arizona State University
Joseph Ervin, Arizona State University
Shyh-Chiang Shen, Georgia Tech
Cheryl J. Marshall, NASA Goddard Space Flight Center
Michael L. Alles, Institute for Space and Defense Electronics, Vanderbilt University
Richard W. Berger, BAE Systems
Paul S. Fechner, Honeywell
Jerry Yue, Honeywell
Bruce Ohme, Honeywell
Guofu Niu, Auburn University
Ashok Raman, CFD Research Corporation
Marek Turowski, CFD Research Corporation
Stanley D. Phillips, Georgia Tech
Lan Luo, Auburn University
A. Matt Francis, Ozark Integrated Circuits
Avinash S. Kashyap, General Electric Global Research Center
Ty R. McNutt, Arkansas Power Electronics International
Jeffrey S. Kauppila, Institute for Space and Defense Electronics, Vanderbilt University
Jim Holmes, Sherlock MBV Consulting, LLC
Fernando Guarín, IBM
Stewart Rauch, IBM
Yuan Chen, NASA Langley Research Center
Jeffrey D. Black, Sandia National Laboratory
Benjamin J. Blalock, University of Tennessee
Robert Rudolf, University of Southampton
Reuben Wilcock, University of Southampton
Laleh Najafizadeh, National Institutes of Health
Fa Foster Dai, Auburn University
Desheng Ma, Auburn University
Yuan Yao, Auburn University
Zhenqi Chen, Auburn University
Melanie Berg, NASA Goddard Space Flight Center and MEI Technologies, Inc.
Kenneth Li, NASA Goddard Space Flight Center
Michael Johnson, NASA Goddard Space Flight Center
Mohammad Mojarradi, Jet Propulsion Laboratory
Philippe Adell, Jet Propulsion Laboratory
Marcelo Schupbach, Arkansas Power Electronics International
Jia Di, University of Arkansas
Scott C. Smith, University of Arkansas
T. Daniel Loveless, Vanderbilt University
Stephen J. Horst, Georgia Tech
Sachin Seth, Georgia Tech
Joeseph C. Bardin, University of Massachusetts, Amherst
Michael J. Krasowski, NASA Glenn Research Center
N.F. Prokop, NASA Glenn Research Center
Michael Goryll, Arizona State University
Keith Holbert, Arizona State University
Bertan Bakkaloglu, Arizona State University
Chip Webber, Lynguent
R. Wayne Johnson, Auburn University

Linda Del Castillo, Jet Propulsion Laboratory
Jared Hornberger, Arkansas Power Electronics International
Brice McPherson, Arkansas Power Electronics International
Brandon Passmore, Arkansas Power Electronics International
Ryan M. Diestelhorst, Georgia Tech
Troy D. England, Georgia Tech
Colin McKinney, Jet Propulsion Laboratory
Shahid Aslam, NASA Goddard Space Flight Center
Akin Akturk, CoolCAD Electronics, LLC
Gerard Quilligan, NASA Goddard Space Flight Center
David A. Sunderland, Boeing
William Kuhn, Kansas State University
Yogesh Tugnawat, Kansas State University
Randy Norman, Perma Works, LLC
Alexander A. Grillo, University of California, Santa Cruz
Veljko Radeka, Brookhaven National Laboratory
Gianluigi de Geronimo, Brookhaven National Laboratory
Shaorui Li, Brookhaven National Laboratory
Tushar Thrivikraman, Jet Propulsion Laboratory
Paul W. Marshall, Consultant
Ronald Pease, Consultant
Martha O'Bryan, MEI Technologies, Inc.
Richard L. Patterson, NASA Glenn Research Center
Ahmad Hammoud, NASA Glenn Research Center

We both offer each of you a heartfelt thank you for a job well done!

Acknowledgments

We would each also like to thank our graduate students and postdocs, past and present, for their dedication and tireless work in helping evolve this fascinating field. We rest on their shoulders.

Cressler's students include the following:

Former PhD students: David Richey, Alvin Joseph, Bill Ansley, Suraj Mathew, David Sheridan, Shiming Zhang, Gang Zhang, Ying Li, Zhiyun Luo, Zhenrong Jin, Qingqing Liang, Tianbing Chen, Enhai Zhao, Amit Bavisi, Jon Comeau, Lance Kuo, Bhaskar Banerjee, Ram Krithivasan, Yuan Lu, Chendong Zhu, Xiangtao Li, Joel Andrews, Marco Bellini, Curtis Grens, Akil Sutton, Laleh Najafizadeh, Aravind Appaswamy, Jiahui Yuan, Tom Cheng, Tushar Thrivikraman, Anuj Madan, John Poh, and Steve Horst.

Current PhD students: Prabir Saha, Partha Chakraborty, Duane Howard, Kurt Moen, Ryan Diestelhorst, Jeremy Hicks, Stan Phillips, Sachin Seth, Seungwoo Jung, Michael Oakley, Subu Shankar, Troy England, Saeed Zeinolabedinzadeh, and Farzad Inanlou.

Former MS students: Lakshmi Vempati, Greg Bradford, Kartik Jayanarayanan, Juan Roldan, Stacey Salmon, Usha Gogineni, Gaurab Banerjee, Krish Shivaram, Becca Haugerud, Adnan Ahmed, Mustayeen Nayeem, Mustansir Pratapgarhwala, Steven Finn, Nand Jha, Dylan Thomas, Ted Wilcox, and Richie Mills.

Current MS students: Adilson Cardoso, Rob Schmid, Nelson Lourenco, Chris Coen, Eleazar Kenyon, Peter Song, and Uppili Raghunathan.

Former postdocs: Guofu Niu, Rao Rapeta, Emery Chen, Jongsoo Lee, Gnana Prakash, and Bongim Jun.

Mantooth's students include the following:

Former PhD students: Matt Francis, Mihir Mudholkar, Javier Valle, Erik Johnson, Avinash Kashyap, Hung Phi Hoang, Obadiah Kegege, Osama Saadeh, Tiejun Cao, Ty McNutt, Wei Zheng, Xiaoling Huang, and Beth Woods.

Current PhD students: Ashfaq Rahman, Matt Barlow, Jared Hornberger, Mike Glover, Paul Shepherd, Ranjan Lamichhane, Rui Mao, Mahmood Saadeh, and Shamim Ahmed.

Former MS students: Kacie Woodmansee, Alvin Ong, Caleb Gutshall, Chandra Givens, Chary Vadla, Chip Webber, Chris Lee, Daniel Hotz, Davin Moorman, Dimitre Dimitrov, Edgar Cilio, Greg Hupp, Hari Gunupudi, Hieu Nguyen, Ivonne Escorcia, Jianhua Mao, John Garrett, Khoa Phan, Kim Cornett, Lauren Megee, Luke Post, Mohit Sharma, Naveed Hingora, Omair Abbasi, Phaniraj Joshi, Pinki Mallick, Sabya Mallick, Rashed Hoque, Richard Broughton, Seth Henry, Seung Gwon Yang, Sharath Vallamkonda, Sharmila Mounce, Tahir Ahmad, Tea Williams, Ting Liu, Tsedeniya Abraham, Tung Le, Tushar Bajaj, Uma Annamalai, Chandu Vemulapally, Venu Allipuram, Weifeng Li, Xiaohong Zhang, Yong Gao, Yue Yu, and Vivek Chaudhary.

Current MS students: Brett Shook, Brian Stalling, Jacob Williams, Nick Chiolino, Tavis Clemmer, Thomas White, and Zihao Gong.

Former postdocs: Alexander Lostetter, Guoyuan Fu, and Yongfeng Feng

As any professor knows, financially supporting these many students requires some serious funding, and we are both grateful to a number of sponsors for their vision and support for our own work, including NASA, JPL, DTRA, DoE, ARPA-e, NSF, DARPA, and a variety of industry partners. One project, in particular, deserves special mention: NASA ETDP's "SiGe Integrated Electronics for Extreme Environments," a 5+ year, $12 million program that brought together six universities and four industry partners to do a lot of fun stuff! This project solidified many lasting collaborations and friendships, and in fact set this book in motion. Our hats are off to Andrew Keys of NASA-MSFC, in particular, for his role as project manager of the NASA ETDP SiGe effort.

Finally, we are grateful to Nora Konopka of CRC Press for helping launch this project and Jessica Vakili for supporting us along the way with day-to-day details. We would also like to thank Deepa Kalaichelvan, the project manager at SPi Global, India, and Richard Tressider, project editor at CRC Press for their able assistance (and patience!).

Extreme environment electronics is a complex and nuanced field, and in our humble opinion makes for some fascinating subject matter and darned good reading. But this is no mere academic pursuit. In the grand scheme of things, the extreme environment electronics industry is already helping reshape the way electronic devices, circuits, and systems are developed and deployed and is influencing the architecture of new exploration missions in the solar system. All of this new activity is in turn helping change the way life on planet Earth will transpire in the twenty-first century and beyond. The world would do well to pay attention to our efforts. It has been immensely satisfying to see this book come to fruition. We hope our efforts please you. Enjoy!

John D. Cressler
School of Electrical and Computer Engineering
Georgia Institute of Technology
Atlanta, Georgia

H. Alan Mantooth
Department of Electrical Engineering
University of Arkansas
Fayetteville, Arkansas

MATLAB® Disclaimer

MATLAB® is a registered trademark of The MathWorks, Inc.
For product information, please contact:

The MathWorks, Inc.
3 Apple Hill Drive
Natick, MA, 01760-2098 USA
Tel: 508-647-7000
Fax: 508-647-7001
E-mail: info@mathworks.com
Web: www.mathworks.com

Editors

John D. Cressler received his PhD from Columbia University in 1990. He was at IBM Research from 1984 to 1992 and on the faculty of Auburn University from 1992 to 2002. Since 2002, he has been on the faculty of Georgia Tech, where he is currently Ken Byers Professor of Electrical and Computer Engineering. His research interests include Si-based (SiGe/strained-Si) heterostructure devices and technology, mixed-signal circuits built from these devices, radiation effects, cryogenic electronics, device-to-circuit interactions, noise and reliability physics, device-level simulation, and compact circuit modeling. He and his team have published over 500 papers in these fields. He is the coauthor of *Silicon-Germanium Heterojunction Bipolar Transistors* (2003); the author of *Reinventing Teenagers: The Gentle Art of Instilling Character in Our Young People* (2004) and *Silicon Earth: Introduction to the Microelectronics and Nanotechnology Revolution* (2009); and the editor of *Silicon Heterostructure Handbook: Materials, Fabrication, Devices, Circuits, and Applications of SiGe and Si Strained-Layer Epitaxy* (2006). He has just finished his debut novel, *Emeralds of the Alhambra*, a love story set in fourteenth-century Muslim Spain.

During his academic career, he has graduated 38 PhD students and 37 MS students. He has served as associate editor for the *IEEE Journal of Solid-State Circuits*, the *IEEE Transactions on Nuclear Science*, and the *IEEE Transactions on Electron Devices*. He is presently editor-in-chief of the *IEEE Transactions on Electron Devices*. He has also been active on numerous IEEE conference program committees, including as the technical program chair of the *1998 IEEE International Solid-State Circuits Conference (ISSCC)*, the *2004 IEEE Topical Meeting on Silicon Monolithic Integrated Circuits in RF Systems (SiRF)*, the *2007 IEEE Nuclear and Space Radiation Effects Conference (NSREC)*, and the *2011 IEEE Bipolar/BiCMOS Circuits and Technology Meeting (BCTM)*.

Cressler has served as a distinguished lecturer of the IEEE Electron Device Society (1994–2012) and the IEEE Nuclear and Plasma Sciences Society (2006–present) and was awarded the 1994 Office of Naval Research Young Investigator Award, the 1996 C. Holmes MacDonald Outstanding Teacher Award by Eta Kappa Nu (a national award), the 1996 Auburn University Alumni Engineering Council Research Award, the 1998 Auburn University Birdsong Merit Teaching Award, the 1999 Auburn University Alumni Undergraduate Teaching Excellence Award, the 2007 Georgia Tech Outstanding Faculty Leadership in the Development of Graduate Students Award, the 2010 Class of 1940 W. Howard Ector Outstanding Teaching Award (Georgia Tech's highest award for teaching), an IEEE Third Millennium Medal in 2000, and the 2011 IEEE Leon K. Kirchmayer Graduate Teaching Award (an IEEE Field Award, the IEEE's highest award for graduate teaching). He was elected IEEE Fellow in 2001 "for contributions to the understanding and optimization of silicon and silicon-germanium bipolar transistors."

On a more personal note, John's hobbies include hiking, gardening, reading, writing, bonsai, all things Italian, collecting (and drinking!) fine wines, cooking, history, and carving walking sticks, not necessarily in that order. He considers teaching to be his primary vocation. John has been married to Maria, his best friend and soul mate, for 30 years, and they are the proud parents of three: Matthew John (28), Christina Elizabeth (26), and Joanna Marie (23).

H. Alan Mantooth received his BS (summa cum laude) and MS in electrical engineering from the University of Arkansas in 1985 and 1986, respectively, and his PhD from the Georgia Institute of Technology in 1990.

Dr. Mantooth is a distinguished professor of electrical engineering and the holder of the 21st Century Endowed Chair in Mixed-Signal IC Design and CAD at the University of Arkansas. He serves as the executive director of the National Center for Reliable Electric Power Transmission and its two constitutive centers of excellence: the NSF Industry-University Cooperative Research Center for GRid-connected Advanced Power Electronic Systems (GRAPES) and the NSF Vertically Integrated Center for Transformative Energy Research (VICTER), all of which he founded. Dr. Mantooth has been at the University of Arkansas for 13 years. Prior to his return to academia, he worked for Analogy, Inc. for eight years, eventually rising to the rank of principal engineer in charge of modeling and modeling tool research. He was named Distinguished Member of Technical Staff at Analogy in 1996. Dr. Mantooth's general research area is electronics: particularly power electronics, integrated circuit design, and modeling of devices, circuits, and systems. He and his team have authored over 200 refereed articles on circuit design and CAD. He also authored the first book on modeling with analog hardware description languages (*Modeling with an Analog Hardware Description Language,* Kluwer, Boston, MA, 1995) and holds three patents on software design. He has conducted R&D projects for many funding agencies, including the National Science Foundation, the Electric Power Research Institute (EPRI), the Department of Energy, DARPA, the Office of Naval Research, and NASA, and many industrial organizations such as Texas Instruments, American Electric Power, Honeywell, United Technologies, General Electric, Toyota, Rohm, and Consolidated Edison of New York.

Dr. Mantooth has received numerous teaching, service, and research awards since returning to the University of Arkansas: Eta Kappa Nu Electrical Engineering Faculty of the Year (1999–2000, 2003–2004); Arkansas Academy of Electrical Engineering Outstanding Faculty Award (2000, 2001, 2003, 2005); William D. and Margaret A. Brown Faculty Excellence Award (2008–2009); Outstanding Teacher Award in Electrical Engineering (2000–2001, 2006–2007); Outstanding Service to Students Award in Electrical Engineering (2004–2005); Outstanding Researcher Award in Electrical Engineering (2001–2002, 2002–2003, 2003–2004, 2009–2010); 2001 Fred M. Carter Award (highest score on the PE exam in Arkansas); UA Academic Advising Council College of Engineering Outstanding Undergraduate Advisor (2007); UA Outstanding Mentor (2006, 2007, 2008); UA Gold Medal Mentor Award (2007); UA John A. White Award for Outstanding Faculty–Student Collaborations (2008–2009); and R&D 100 Award for World's First Silicon Carbide Power Module Operational to 250°C (rating = 1200 V, 150+ A) (2009).

In 2002, Dr. Mantooth was elected to the Georgia Tech Council of Outstanding Engineering Alumni, and in 2006, to the Arkansas Academy of Electrical Engineers. In 2011, Professor Mantooth was selected to receive the John L. Imhoff Award for the Outstanding Researcher in the College of Engineering as well as the Arkansas Alumni Association Distinguished Research Award, a university-wide award. He served as a guest editor for the *IEEE Transactions on Computer-Aided Design*, the *IET Computers and Digital Techniques*, and as an IEEE Circuits and Systems Society Distinguished Lecturer (2003–2004). He currently serves the profession as a member of the Power Electronics Society Advisory Committee as director of the society's Standards Committee. He is a fellow of the IEEE, a member of Tau Beta Pi and Eta Kappa Nu, and a registered professional engineer in Arkansas.

He has been married to Mary Lynn for 25 unforgettable years and has three beautiful daughters—Deanna Lynn (18), Laura Kathryn (16), and Maureen Elaine (13)—and seven hungry Siberian Huskies. He enjoys running the dogs, woodworking, golf, and hiking in the mountains and, as a former Razorback football player, is deeply passionate about his Hogs!

Contributors

James H. Adams, Jr.
The Center for Space Plasma and Aeronomic Research
University of Alabama in Huntsville
Huntsville, Alabama

Philippe Adell
Jet Propulsion Laboratory
California Institute of Technology
Los Angeles, California

Akin Akturk
CoolCAD Electronics, LLC
College Park, Maryland

Michael L. Alles
Department of Electrical Engineering and Computer Science
and
Institute for Space and Defense Electronics
Vanderbilt University
Nashville, Tennessee

Aravind C. Appaswamy
Texas Instruments
Dallas, Texas

Rajan Arora
Georgia Institute of Technology
Atlanta, Georgia

Shahid Aslam
Goddard Space Flight Center
National Aeronautics and Space Administration
Greenbelt, Maryland

Bertan Bakkaloglu
School of Electrical, Computer and Energy Engineering
Arizona State University
Tempe, Arizona

Asha Balijepalli
School of Electrical, Computer and Energy Engineering
Arizona State University
Tempe, Arizona

Joseph C. Bardin
Department of Electrical and Computer Engineering
University of Massachusetts Amherst
Amherst, Massachusetts

Janet Barth
Goddard Space Flight Center
National Aeronautics and Space Administration
Greenbelt, Maryland

Melanie Berg
Goddard Space Flight Center
National Aeronautics and Space Administration
and
MEI Technologies, Inc.
Greenbelt, Maryland

Richard W. Berger
BAE Systems
London, United Kingdom

Jeffrey D. Black
Sandia National Laboratories
Albuquerque, New Mexico

Benjamin J. Blalock
Department of Electrical Engineering and Computer Science
The University of Tennessee, Knoxville
Knoxville, Tennessee

Dana Brewer
Headquarters
National Aeronautics and Space Administration
Washington, District of Columbia

Yuan Chen
Langley Research Center
National Aeronautics and Space Administration
Hampton, Virginia

Zhenqi Chen
Department of Electrical and Computer Engineering
Auburn University
Auburn, Alabama

Lewis M. Cohn
Naval Research Laboratory
Washington, District of Columbia

John D. Cressler
School of Electrical and Computer Engineering
Georgia Institute of Technology
Atlanta, Georgia

Dennis Culley
Glenn Research Center
National Aeronautics and Space Administration
Cleveland, Ohio

Fa Foster Dai
Department of Electrical and Computer Engineering
Auburn University
Auburn, Alabama

Linda Del Castillo
Jet Propulsion Laboratory
California Institute of Technology
Los Angeles, California

Jia Di
Department of Computer Science and Computer Engineering
University of Arkansas
Fayetteville, Arkansas

Ryan M. Diestelhorst
School of Electrical and Computer Engineering
Georgia Institute of Technology
Atlanta, Georgia

Troy D. England
School of Electrical and Computer Engineering
Georgia Institute of Technology
Atlanta, Georgia

Joseph Ervin
School of Electrical, Computer and Energy Engineering
Arizona State University
Tempe, Arizona

Paul S. Fechner
Honeywell
Plymouth, Minnesota

A. Matt Francis
Ozark Integrated Circuits, Inc.
Fayetteville, Arkansas

Kenneth F. Galloway
Department of Electrical Engineering and Computer Science
and
Institute for Space and Defense Electronics
Vanderbilt University
Nashville, Tennessee

Gianluigi de Geronimo
Brookhaven National Laboratory
Upton, New York

Mohammad Reza Ghajar
School of Electrical, Computer and Energy Engineering
Arizona State University
Tempe, Arizona

Michael Goryll
School of Electrical, Computer and Energy Engineering
Arizona State University
Tempe, Arizona

Alexander A. Grillo
Santa Cruz Institute for Particle Physics
University of California, Santa Cruz
Santa Cruz, California

Fernando Guarín
IBM
Semiconductor Research and Development Center
East Fishkill, New York

Ahmad Hammoud
ASRC Aerospace Corporation
Greenbelt, Maryland

Keith Hobert
School of Electrical, Computer and Energy Engineering
Arizona State University
Tempe, Arizona

Jim Holmes
Sherlock-MBV Consulting, LLC
Fayetteville, Arkansas

Jared Hornberger
Arkansas Power Electronics International, Inc.
Fayetteville, Arkansas

Stephen J. Horst
Georgia Institute of Technology
Atlanta, Georgia

Gary W. Hunter
Glenn Research Center
National Aeronautics and Space Administration
Cleveland, Ohio

Michael Johnson
Goddard Space Flight Center
National Aeronautics and Space Administration
Greenbelt, Maryland

R. Wayne Johnson
Department of Electrical and Computer Engineering
Auburn University
Auburn, Alabama

Avinash S. Kashyap
General Electric Global Research Center
Niskayuna, New York

Jeffrey S. Kauppila
Department of Electrical Engineering and Computer Science
and
Institute for Space and Defense Electronics
Vanderbilt University
Nashville, Tennessee

Andrew S. Keys
Marshall Space Flight Center
National Aeronautics and Space Administration
Huntsville, Alabama

Elizabeth Kolawa
Jet Propulsion Laboratory
California Institute of Technology
Los Angeles, California

Michael J. Krasowski
Glenn Research Center
National Aeronautics and Space Administration
Cleveland, Ohio

William Kuhn
Department of Electrical and Computer Engineering
Kansas State University
Manhattan, Kansas

William Lepkowski
School of Electrical, Computer and Energy Engineering
Arizona State University
Tempe, Arizona

and

SJT Micropower Inc.
Fountain Hills, Arizona

Kenneth Li
Goddard Space Flight Center
National Aeronautics and Space Administration
Greenbelt, Maryland

Shaorui Li
Brookhaven National Laboratory
Upton, New York

Alexander B. Lostetter
Arkansas Power Electronics International, Inc.
Fayetteville, Arkansas

T. Daniel Loveless
Department of Electrical Engineering and Computer Science
and
Institute for Space and Defense Electronics
Vanderbilt University
Nashville, Tennessee

Lan Luo
Department of Electrical and Computer Engineering
Alabama Microelectronics Science and Technology Center
Auburn University
Auburn, Alabama

Desheng Ma
Department of Electrical and Computer Engineering
Auburn University
Auburn, Alabama

H. Alan Mantooth
Department of Electrical Engineering
University of Arkansas
Fayetteville, Arkansas

Cheryl J. Marshall
Goddard Space Flight Center
National Aeronautics and Space Administration
Greenbelt, Maryland

Paul W. Marshall
Consultant
Brookneal, Virginia

Lloyd W. Massengill
Department of Electrical Engineering and Computer Science
and
Institute for Space and Defense Electronics
Vanderbilt University
Nashville, Tennessee

Colin McKinney
Jet Propulsion Laboratory
California Institute of Technology
Los Angeles, California

Ty R. McNutt
Arkansas Power Electronics International, Inc.
Fayetteville, Arkansas

Brice McPherson
Arkansas Power Electronics International, Inc.
Fayetteville, Arkansas

Kurt A. Moen
School of Electrical and Computer Engineering
Georgia Institute of Technology
Atlanta, Georgia

Mohammad Mojarradi
Jet Propulsion Laboratory
California Institute of Technology
Los Angeles, California

Laleh Najafizadeh
Department of Electrical and Computer Engineering
Rutgers, The State University of New Jersey
Piscataway, New Jersey

Philip G. Neudeck
Glenn Research Center
National Aeronautics and Space Administration
Cleveland, Ohio

Guofu Niu
Department of Electrical and Computer Engineering
Alabama Microelectronics Science and Technology Center
Auburn University
Auburn, Alabama

Randy Normann
Perma Works, LLC
Albuquerque, New Mexico

Martha O'Bryan
MEI Technologies, Inc.
Houston, Texas

Bruce Ohme
Honeywell
Morristown, New Jersey

Brandon Passmore
Arkansas Power Electronics International, Inc.
Fayetteville, Arkansas

Richard L. Patterson
Glenn Research Center
National Aeronautics and Space Administration
Cleveland, Ohio

Ronald Pease
RLP Research
Albuquerque, New Mexico

Jonathan A. Pellish
Goddard Space Flight Center
National Aeronautics and Space Administration
Greenbelt, Maryland

Stanley D. Phillips
Georgia Institute of Technology
Atlanta, Georgia

N.F. Prokop
Glenn Research Center
National Aeronautics and Space Administration
Cleveland, Ohio

Gerard Quilligan
Goddard Space Flight Center
National Aeronautics and Space Administration
Greenbelt, Maryland

Veljko Radeka
Brookhaven National Laboratory
Upton, New York

Ashok Raman
CFD Research Corporation
Huntsville, Alabama

Stewart Rauch
IBM
Semiconductor Research and Development Center
East Fishkill, New York

Robert Reed
Department of Electrical Engineering and Computer Science
and
Institute for Space and Defense Electronics
Vanderbilt University
Nashville, Tennessee

Robert Rudolf
Department of Electronics and Computer Science
University of Southampton
Southampton, United Kingdom

Ronald D. Schrimpf
Department of Electrical Engineering and Computer Science
and
Institute for Space and Defense Electronics
Vanderbilt University
Nashville, Tennessee

Marcelo Schupbach
Arkansas Power Electronics International, Inc.
Fayetteville, Arkansas

Sachin Seth
Texas Instruments Inc.
Dallas, Texas

Shyh-Chiang Shen
Georgia Institute of Technology
Atlanta, Georgia

Scott C. Smith
Department of Electrical Engineering
University of Arkansas
Fayetteville, Arkansas

David A. Sunderland
Boeing Space and Intelligence Systems
Los Angeles, California

Trevor J. Thornton
School of Electrical, Computer and Energy Engineering
Arizona State University
Tempe, Arizona

and

SJT Micropower Inc.
Fountain Hills, Arizona

Tushar Thrivikraman
Jet Propulsion Laboratory
California Institute of Technology
Los Angeles, California

Yogesh Tugnawat
Department of Electrical and Computer Engineering
Kansas State University
Manhattan, Kansas

Marek Turowski
CFD Research Corporation
Huntsville, Alabama

Chip Webber
Independent Consultant
Ozark Integrated Circuits, Inc.
Fayetteville, Arkansas

Robert A. Weller
Department of Electrical Engineering and Computer Science
and
Institute for Space and Defense Electronics
Vanderbilt University
Nashville, Tennessee

Reuben Wilcock
Department of Electronics and Computer Science
University of Southampton
Southampton, United Kingdom

Edward P. Wilcox
Goddard Space Flight Center
National Aeronautics and Space Administration
Greenbelt, Maryland

and

MEI Technologies, Inc.
Houston, Texas

Seth J. Wilk
School of Electrical, Computer and Energy Engineering
Arizona State University
Tempe, Arizona

and

SJT Micropower Inc.
Fountain Hills, Arizona

Peter Wilson
Department of Electronics and Computer Science
University of Southampton
Southampton, United Kingdom

Michael Xapsos
Goddard Space Flight Center
National Aeronautics and Space Administration
Greenbelt, Maryland

Yuan Yao
Auburn University
Auburn, Alabama

Jiahui Yuan
SanDisk Corporation
Milpitas, California

Jerry Yue
Honeywell
Plymouth, Minnesota

I

Introduction

Introduction

To properly set the stage for this book, we begin in Chapter 1, by John D. Cressler of Georgia Institute of Technology, with a general motivation of the field, the "big picture" if you will, and then follow that with a brief history. Chapter 1 sets the stage by motivating how NASA sees the extreme environment electronics picture. In Chapters 2 and 3, by Elizabeth Kolawa, Mohammad Mojarradi, and Linda Del Castillo of JPL and by Dana Brewer of NASA-HQ and Janet Barth of NASA-GSFC, NASA's broad-based science and exploration vision is presented, together with a discussion of the requisite role to be played by extreme environment electronics in that vision. Chapter 4, by Andrew S. Keys of NASA-MSFC, highlights a very successful extreme environment electronics effort at NASA, while Chapter 5, by Gary W. Hunter and Dennis Culley of NASA-GRC, addresses the current and future needs for extreme environment electronics in NASA's various aeronautics systems. Finally, Chapter 6, by Jonathan A. Pellish of NASA-GSFC and Lewis M. Cohn of NRL, summarizes NASA and DoD's extensive learning on what integrated circuit technologies are best-suited for operation in NASA/DoD-relevant extreme environments, and the necessary trade-offs entailed in mission design.

1

Big Picture and Some History of the Field

John D. Cressler
Georgia Institute of Technology

1.1 Extreme Environment Electronics: The Big Picture

"Extreme environment" electronics represents a very important niche industry within the trillion dollar global electronics infrastructure, and entails the design and implementation of electronic devices, circuits, subsystems, and systems capable of operating robustly in environmental surroundings lying outside the traditional domain of conventional commercial or military electronics specifications. Needless to say, there are degrees of "extreme," some of which are far more challenging than others, and some of which no one-in-their-right-mind would ever attempt! In general, extreme environment electronics' systems are by definition low-volume, but high value–add propositions, and hence can be extremely expensive to deploy. As an example, consider putting a weather satellite up into Earth orbit to monitor hurricanes; a very extreme environment, hence very costly to put in place and operate, but exceptionally important.

So what are the prevalent extreme environments folks want to do business in? Well, extreme environments are diverse, but include, in an approximate order of importance:

- *Operation in radiation-rich environments*: Radiation comes in many forms, few of which are benign, and system designers must account for three major classes of radiation effects: ionization effects (high-energy charged particles that ionize materials as they pass through), displacement effects (in which high-energy particles with mass displace lattice atoms), and/or a diverse set of single event phenomena (ranging from burnout of gate oxides, to destructive latchup, to more benign digital bit flips and error propagation). The prototypical radiation-rich environment would be space, either in Earth orbit for a remote sensing satellite or perhaps a communications satellite, or interplanetary space travel, or even exploration of the outer planets as we hunt for life beyond our borders.
- *Operation in low-temperature environments*: In general, any temperature below the standard commercial temperature range specification (0°C to +85°C) or the military specification (mil-spec) temperature range (−55°C to +125°C) would be considered a low-temperature extreme environment. Such environments are often termed "cryogenic" environments (hence, "cryoelectronics"), so-named because of the prevalent use of liquid cryogens to achieve them (e.g., liquid nitrogen = 77.3 K = −195.9°C = −320.5°F and liquid helium = 4.2 K = −270.0°C = −452.1°F—refer to Appendix B). Some highly desirable physical effects mandate operation in cryogenic environments (e.g., superconductivity). Most planetary bodies represent cryogenic environments (e.g., the poles of Mars can reach −143°C in winter). Deep space is another example (e.g., the detector electronics of the James Webb Space Telescope [which is in the dark] operates at 27 K). In addition, many electronic instrumentation packages require operation at cryogenic temperatures in order to improve system sensitivity (e.g., transistor noise scales linearly with temperature; dark current in detector diodes decreases exponentially with temperature). Such cooled detector applications are diverse, ranging from medical imaging systems, to astronomical instruments, to satellite receivers, and even high-performance computer systems.
- *Operation in high-temperature environments*: In general, any temperature above the standard commercial temperature range specification (0°C to +85°C) or the mil-spec temperature range (−55°C to +125°C) would be considered a high-temperature extreme environment. Important examples include automotive electronics,

various on-engine aerospace electronics systems, energy exploration (e.g., oil and gas well drilling), and the power industry. In such applications, robust operation to 200°C–300°C is often desired. Certain space exploration goals require exceptionally high temperatures (e.g., the surface temperature of Venus can reach 600°C).

- *Operation in cyclic, wide-temperature range environments*: Particularly in space exploration, extremes in temperature can come in the form of wide temperature ranges, which place additional constraints on system designers since then tend to be cyclic. That is, from a circuit and packaging reliability perspective, temperature swings low to high and high to low are far more challenging for ensuring long-term reliability than simply operating at a given low temperature or a given high temperature (though such needs are challenging in themselves). A classical example would be operation on the surface of the Moon, where temperature reaches +120°C in the sunlight and −180°C during the lunar night (and even down to −230°C in the shadowed polar craters). This exceptionally aggressive >300°C temperature swing is also cyclic (on a 28 day cycle) and represents one of the most challenging environments one could hope to encounter.
- *Operation in vibrationally intense environments*: While electronic devices and circuits are not especially sensitive to vibrations, the packaging of such components can be, and require, "shock-and-vibe" (shock-and-vibration) testing. A classical example would be the vibrational environment associated with rocket launch, but vibrations inside the drill head of a deep oil or gas well, or sensor suites placed on engines, also present challenges for long-term reliability.
- *Operation in chemically corrosive environments*: Classically, one packages electronic devices and circuits to protect them from chemically corrosive environments, but this can be compromised for certain applications which mandate the direct contact of parts of the device with the environment (e.g., for chemical sensors). In addition, emerging trend of placing electronics inside the human body brings this back into consideration since conventional electronics packages cannot in general be used inside the body. In this instance, the sodium contained in bodily fluids can be lethal to many types of electronic devices.
- *Operation in intense magnetic field environments*: Certain types of medical imaging devices (e.g., CT scans, PET scans) require operation in intense magnetic fields, and this can potentially place constraints on circuit implementations and electronics packaging.
- *Operation under conditions that bring together many extreme environments*: This latter catch-all environment is actually quite common and can be considered worst case. Here, one or more or even all extreme environments are brought to the table at once, thereby dramatically complicating device, circuit, and system design. The most prevalent examples exist in space exploration missions, where low-temperature, high-temperature, wide-temperature ranges, and radiation effects all necessarily must be dealt with at once.

It is a truism that extreme environments are "unfriendly" (read: toxic!) to conventional electronic devices, circuits, and systems, and thus from a broad perspective represent a very serious "reliability challenge" to designers and mission architects. As an example, a conventional silicon MOSFET naïvely launched into space within a satellite system will quickly fail due to exposure to ionizing radiation from the so-called radiation belts (think *aurora borealis*, Figure 1.1), high-energy electrons and protons generated via the solar wind and subsequently trapped in the Earth's magnetic field. Clearly such radiation-induced damage can potentially produce very expensive ramifications, ultimately resulting in the loss of the satellite. Truth be told, we are asking a lot of our electronics in such situations. For comparison, exposure to a total ionizing dose (TID) of radiation equal to about 200–300 rad will kill a human (1 rad = 0.01 J/kg of radiation absorbed by a given material). In even the most benign Earth orbit over a 10 year mission, the electronics inside the (shielded) satellite may "see" perhaps 100,000 rad of total ionizing dose, and in a not-so-benign orbit, maybe 1,000,000 rad of radiation over the mission life. Read: Earth orbit in a pretty unfriendly place to be. To get around this, electronics usually must be "hardened" for its intended environment, by utilizing changes to the underlying fabrication flow (termed "hardening-by-process" [HBP]) and/or by changes to circuit topology and/or system architecture (termed "hardening-by-design" [HBD]). As one might imagine, such environmental hardening comes with a high price tag, and is a large part of the reason for the high cost associated with, say, operating a satellite system in space or sending a rover to Mars or the Moon.

There are compelling reasons for wanting to utilize conventional, commercial-of-the-shelf (COTS) electronic components directly in a given extreme environment, but at present this

FIGURE 1.1 (See color insert.) The northern night sky, showing the *aurora borealis*.

possibility does not exist for most application needs, and a combination of HBP and HBD are necessarily employed. The desire for wanting to use COTS is not necessarily only cost-motivated. To probe this a bit further, consider the following concrete scenario. The extreme environmental conditions on the surface of our Moon are at worst case –230°C in the shadowed polar craters where we now know water exists, and range from –180°C during the lunar night to +120°C during the lunar day, over 28 day cycles, all the while bathed in intense radiation from the solar wind and galactic cosmic rays. This environmental reality effectively precludes using conventional terrestrial electronics for sensing, actuation, and control under ambient lunar conditions. So what does one do? The legacy solution is to place all of your electronic “stuff” inside a large, heavy, shielded, heated “warm box” to protect your electronics from the extreme environments. This is a crude solution at best, and one with substantial downside with respect to system size-weight-and-power (SWaP) goals, and ultimately mission cost.

This legacy path for operation in extreme environments is decidedly problematic for space mission designers. Unmanned lunar missions necessarily combine mobility on the lunar surface (i.e., on a rover) with sensing functions, electronics, and motor/actuators for control on that rover. For instance, a lunar mission might include a mobile mineralogy station for mapping in situ resources. The sensor/actuator networks on such a lunar rover provide a distributed system to monitor the health and performance of the rover in order to sense the environment for scientific exploration or to act on the environment, for example, by using a drill to obtain a soil sample for water analysis. These rover networks consist of remote “intelligent” nodes. Since these remote electronics nodes are in principle distributed over the entire vehicle, they cannot be efficiently located within protective “warm boxes” to shield them from the ambient (extreme) environment. Presently, this need for protective electronic “warm boxes” thus critically limits the mission designer’s ability to create a truly distributed, modular electronics system for such rovers, resulting in excessive point-to-point wiring, increased system weight and complexity, lack of modularity, and an overall reduction in system reliability. The scenario for manned missions, or, if you are feeling bold, lunar or Martian colonization, is even more problematic.

Clearly, then, there is great leverage to be found in changing these limitations associated with the impact of extreme environments on electronic systems. If, for instance, the electronic components were inherently “environmentally invariant” (i.e., they could operate unattended and without protection under any environment in which they found themselves), mission designers and vehicle architects would be empowered to reimagine how such systems could and should be designed and operated. This is a big deal. A similar case could be made for virtually all present applications of extreme environment electronics: terrestrial, space, or otherwise.

The “holy grail” in the context of extreme environments is an integrated circuit technology platform that is capable as-built for operation in any extreme environment in which the device/circuit/subsystem/system finds itself. Said another way, the desire would be that if we design electronics for standard (terrestrial) operation they should also work well in whatever extreme environment you care to use them in, with no added design or test overhead, degradation in reliability, or increase in cost. Such an extreme environment electronics technology solution does not exist. And likely never will exist. Simply put, this book explores at length what is required to operate electronics in extreme environments, what the overarching reasons for those complexities entail, and how one ultimately achieves success (clearly a key goal!). We build upon earlier expositions of this or that subtopic of the overall field [1–9], but it can be fairly stated that this book represents the first truly comprehensive exposition of extreme environment electronics. We address a remarkably wide array of topical coverage, ranging from the extreme environments themselves, to basic physics of various interactions between devices and environments, to various aspects of electronic design, to modeling of devices through systems, to packaging design, to reliability and quality assurance, to ultimately a wide class of interesting end-use applications intended for extreme environments. The best practice approaches required to ensure success are constantly emphasized. Not surprisingly, the contributors to this book represent a veritable “who’s who” in the extreme environment electronics field, and given its exceptionally broad coverage, its depth, and the expertise of the contributing authors, this book is expected to become the seminal go-to reference of the field.

1.2 Some History of the Cryogenic Electronics Field

Let us digress for a moment and briefly examine a bit of the history of this fascinating field. As Newton famously said, we all “stand on the shoulders of giants.” That is, we all owe a great debt to those that came before us; those that shed light on the essential problems, those that enjoyed successes, and even those that tasted the agony of defeat. After all, science and engineering is a collective learning enterprise. I would argue (strongly) that we should all study the past to learn how our predecessors did it. By doing so, we also honor their memory and hold up high their lasting contributions.

The history outlined here is not meant to be exhaustive. Rather, it is intended only to shine a dim light backward. I will focus on the two major arenas: low-temperature (cryogenic) electronics and radiation effects. These two fields represent the lions-share of the extreme environments literature, and are instructive in this context.

Temperature is one of nature’s key system variables in the behavior of matter (refer to Chapter 7), and as such it has long been used to explore the electronic, optical, magnetic, and thermal properties of various materials. Learning to liquefy gases (to form “cryogens”—hence, the term “cryogenic”) such as nitrogen and helium dramatically accelerated this field of “low-temperature physics.” Nitrogen was first liquefied on April 15,

FIGURE 1.2 **(See color insert.)** The many marvels of liquid nitrogen (do NOT try this at home!).

1883 by the Polish physicists Z. Wroblewski and K. Olszewski (Figure 1.2), and helium-4 was first liquefied on July 10, 1908 by the Dutch physicist H.K. Onnes, who used it to subsequently discover superconductivity. Due to their abundance and inert nature, nitrogen and helium remain far-and-away the most commonly employed cryogens today.

When semiconductors first came into vogue in the mid-1940s in the famous quest for the transistor, it soon became obvious that cooling them would enable an exploration of their properties [10–12]. Once transistors were around and in wide use (early 1950s), doing all of this neat low-temperature physics begged for some electronics (e.g., amplifiers) to study property *X* or *Y*, and due to the experimental constraints associated with thermal isolation, signal integrity, cabling, etc., inevitably a preference for locating the electronics in the cryogenic environment itself emerged. This prompted folks to begin cooling electronic "stuff" to see how it would function in such extreme environments, leading to the first publication on cryogenic electronics in 1951 [13]. The rest is history, so they say.

As cryogenic experiments began to proliferate in the 1950s, with an increasing eye toward potential commercial applications, regenerative, closed-cycle (helium-based) refrigerators provided an valuable alternative to using liquid cryogens, and small and efficient Sterling cycle "cryocoolers" reached the market by 1954 [14]. Gifford-McMahon cryocoolers soon followed. The field of cryogenics blossomed in the 1960s as attention shifted to the understanding and utilization of superconductivity [15], and in the 1970s and 1980s the potential of Josephson junction (JJ) technology to potentially revolutionize computer system design drove the field forward [16]. While the JJ effort was eventually abandoned as impractical, the development of high-T_C superconductors [17,18] sparked a new interest in the application of superconductivity which continues to this day.

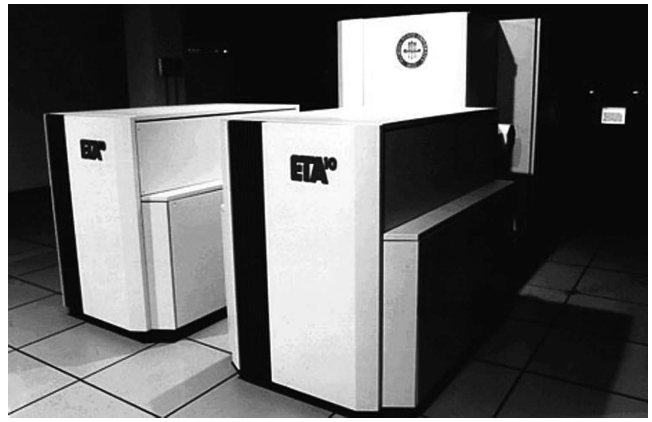

FIGURE 1.3 The ETA^{10} liquid nitrogen–cooled supercomputer.

Meanwhile, the field of cryogenic electronics (cryoelectronics) thrived (for a comprehensive list of early papers, refer to [1], and also see [19] for an early assessment of the suitability of various semiconductors and devices for the cryogenic environment). The 1970s brought the first serious investigations of using MOSFETs at cryogenic temperatures in computing systems [20,21], research that continues to this day. Silicon bipolar transistors were discounted early on (1981) as contenders for cryogenic operation [22], but this picture has changed dramatically with the advent of bandgap engineered silicon–germanium (SiGe) heterojunction bipolar transistors (HBTs) [23,24].

Serious consideration of (CMOS-based) cryogenic computers began to emerge in the mid-1980s, bringing new excitement to the field, and culminating in the announcement in 1986 of the (sadly, now-defunct) Control Data Systems ETA^{10}, a liquid nitrogen–cooled supercomputer (Figure 1.3). It should be noted that while cryogenically cooled supercomputers are not commercially available today, many high-end supercomputers do employ active liquid cooling and are plumbed for cryogens should they be needed. If and when the constraints which will necessarily be faced in classical Moore's law scaling reach a breaking point, there may well be a resurgence of interest in cryogenic computers as a more cost-effective alternative to (eventually) crippling bottlenecks associated with scaling. Time will tell.

In the mean time, the design and use of cryogenic electronics continue to blossom in interesting and healthy ways, with applications ranging from basic science experiments, to medical imaging systems, to remote sensing, to superconductivity, to a diverse set of astronomical instruments, to a wide class of high-sensitivity instrumentation systems.

1.3 Some History of the Radiation Effects Field

Let us turn now to the history of radiation effects in electronics. Radioactivity was discovered accidentally in 1896 by Henri Becquerel, who was investigating phosphorescence in uranium salts. These penetrating radioactive emissions were subsequently studied by Rutherford, Villard, Pierre, and Marie Curie, and shown to be fundamentally different from the recently discovered x-rays (high-energy photons). In 1903, Becquerel shared the Nobel Prize in Physics with Pierre and Marie Curie "in recognition of the extraordinary services he has rendered by his discovery of spontaneous radioactivity." The danger posed by radiation to genetic material (our DNA), including a consequent increase in cancer risk, was recognized as early as 1927 by Hermann Muller, who was awarded the Nobel prize for his pioneering work in 1946 (the date is no coincidence). The science and engineering leading up to the construction (and sadly, detonation) of a nuclear device at the end of World War II clearly brought into sharp focus all things radiation, but it was not until the launch of the U.S. space program that the impact of radiation on electronic "stuff" came center stage. Conceived during the Eisenhower presidency, NASA's Apollo program exerted significant technology "pull" on began in earnest after President John F. Kennedy proposed in a speech to Congress on May 25, 1961 a national goal (with funding to match) of "landing a man on the Moon and returning him safely to the Earth" by the end of the 1960s (Figures 1.4 and 1.5). It is an under-appreciated fact that NASA's Apollo program exerted significant technology "pull" on the development of the fledgling electronics industry, and given that electronics would necessarily accompany the astronauts into space, it was just a matter of time before an electronics-meets-radiation scenario emerged. The rest is history.

The impact of the various types of radiation on electronic devices, circuits, and systems is many and varied (refer to Chapters 8 and 9 for the basics of radiation) and consists of ionization effects (TID), atomic displacement effects (displacement damage [DD]), and a wide variety of single event effects (SEE), where we will begin.

FIGURE 1.4 **(See color insert.)** The launch of Apollo 11 on July 20, 1969. (Courtesy of NASA, Washington, DC.)

FIGURE 1.5 **(See color insert.)** The famous view of the Earth from the Moon. (Courtesy of NASA, Washington, DC.)

The history of SEE* began in 1962 [26]† with the prescient inference that the ever-increasing packing density of transistors in the rapidly evolving integrated circuit would eventually make them susceptible to high-energy cosmic rays. This prediction was confirmed experimentally in 1975 by Binder et al. [27], who reported upsets in digital flip-flop circuits in orbital satellites due to cosmic rays, claimed (correctly) that they were due to "iron group" cosmic rays, and even showed how to calculate upset rates. In 1978, the world was introduced to soft errors due to alpha particles in semiconductor memories (even in terrestrial environments) with experimental results reported by May and Woods [28] and a model for the observations developed by Pickel and Blandford [29]. The year 1979 proved to be a banner year for soft error activity. After alphas came neutron- and proton-induced memory upset observations by Wyatt et al. [30] and Guenzer et al. [31] in 1979, the latter correctly identifying proton-induced nuclear reactions as the cause of the soft errors. Following this was the first observation of heavy ion–induced latchup, reported by Kolasinski et al. [32], an investigation of sea-level cosmic rays and the errors they produce in computer memories by Ziegler and Landford [33], and two additional papers by Bradford [34,35] defining some of the fundamentals of this new emerging field. These papers set the stage for what has followed since in the SEE world.

The 2003 Commemorative Special Issue of the *IEEE Transactions on Nuclear Science* (TNS) [25], and the papers contained within it, chronicle the history of radiation effects in electronics in substantial detail and will not be repeated here. The interested reader is directed there for further information.

* The history of SEE in electronics presented here follows that given by E. Wolicki and which is contained in Ref. [25].

† Again, the timing is no coincidence. A reminder that transistor and integrated circuit evolution was famously predicted by Gordon Moore of Intel in 1965 based upon only four data points (starting in 1961) from the developments of the brand-new electronics industry.

It should be noted that the *IEEE Transactions on Nuclear Science*, together with its companion conference, the *IEEE Nuclear and Space Radiation Effects Conference* (NSREC), and more recently the *IEEE Radiation Effects on Components and Systems* (RADECS), its European cousin, have become the premier venues for the publication of research in radiation effects in electronic materials, devices, circuits, and systems, and the NSREC, in particular, from its inception in 1964, has averaged about 80 papers a year over the past 35 years (the best of which end up in *IEEE TNS*), by any measure a substantive body of literature.*

One particularly interesting editorial paper in the 2003 *IEEE TNS* Special Issue, by Galloway [36], examines the "high-impact" papers of the radiation effects field, and includes the most highly cited papers in the field (to 2003), the NSREC Outstanding Papers, and an interesting section on "first reports, overlooked papers, and others." We note here only several seminal papers dealing with TID effects in devices. The earliest reports of total ionizing dose effects in MOS devices actually appeared in 1964 by Hughes and Giroux [37] and in 1965 by Raymond et al. [38]. Enhanced low dose rate sensitivity (ELDRS), a major concern in the hardness assurance community for the last 20 years, was first reported in silicon bipolar devices in 1991 by Enlow et al. [39], and the first report of the inherent total dose tolerance of SiGe HBTs first appeared in 1995 [40,41] by Babcock et al.

The interested reader is directed to [36] and the other excellent articles within the 2003 *IEEE TNS* Special Issue as a good starting point for a detailed history of the radiation effects field. The coming 2013 Special Issue will bring this history up to date.

References

1. R.K. Kirschman (Ed.), *Low-Temperature Electronics*. New York: IEEE Press, 1986.
2. P. Lall, M.G. Pecht, and E.B. Hakim, *Influence of Temperature on Microelectronics and System Reliability*. Boca Raton, FL: CRC Press, 1997.
3. E.A. Gutierrez, M.J. Deen, and C. Claeys, *Low-Temperature Electronics: Physics, Devices, Circuits, and Applications*. San Diego, CA: Academic Press, 2001.
4. F. Balestra and G. Ghibaudo (Eds.), *Device and Circuit Cryogenic Operation for Low Temperature Electronics*. Dordrecht, the Netherlands: Kluwer, 2001.
5. F.P. McCluskey, R. Grzybowski, and T. Podlesak (Eds.), *High Temperature Electronics*. Boca Raton, FL: CRC Press, 1997.
6. R.K. Kirschman (Ed.), *High-Temperature Electronics*. New York: IEEE Press, 1998.
7. G.C. Messenger and M.S. Ash, *Single Event Phenomena*. New York: Chapman & Hall, 1997.
8. C. Claeys and E. Simoen, *Radiation Effects in Advanced Semiconductor Materials and Devices*. Berlin, Germany: Springer, 2002.
9. R.D. Schrimpf and D.M. Fleetwood (Eds.), *Radiation Effects and Soft Errors in Integrated Circuits and Electronic Devices*. Riveredge, NJ: World Scientific, 2004.
10. G.L. Pearson and J. Bardeen, Electrical properties of pure silicon and silicon alloys containing boron and phosphorus, *Physical Review*, 75, 865–883, 1949.
11. A.K. Jonscher, Semiconductors at cryogenic temperatures, *Proceedings of the IEEE*, 52, 1092–1104, 1964.
12. B.V. Rollis and E.L. Simmons, Long wavelength infrared photoconductivity in silicon at low temperatures, *Proceedings of the Physical Society (London)*, B65, 162–168, 1953.
13. A.N. Gerritsen and F. van den Burg, The possibility for using an amplifier at low temperatures, *Physica*, 17, 930–932, 1951.
14. G. Walker and E.R. Bingham, *Low-Capacity Cryogenic Refrigeration*. Oxford, U.K.: Clarendon Press, 1994.
15. T. van Duzer and C.W. Turner, *Principles of Superconductive Devices and Circuits*. New York: Elsevier, 1981.
16. M.B. Ketchen, D.J. Herrell, and C.J. Anderson, Josephson cross-section model experiment, *Journal of Applied Physics*, 57, 2550–2574, 1985, and references within.
17. J.G. Bednorz and K.A. Mueller, Possible high-T_C superconductivity in the Ba-La-Cu-O system, *Zeitschrift fur Physik*, 64, 189–193, 1986.
18. M.K. Wu, J.R. Ashburn, C.J. Torng, P.H. Hor, R.L. Meng, L. Gao, Z.J. Huang, Y.Q. Wang, and C.W. Chu, Superconductivity at 93 K in a new mixed-phase Y-Ba-Cu-O system at ambient pressure, *Physical Review Letters*, 58, 908–910, 1987.
19. R.K. Kirschman, Cold electronics: An overview, *Cryogenics*, 25, 115–122, 1985, and references within.
20. R.W. Keyes, E.P. Harris, and K.L. Konnerth, The role of low temperatures in the operation of logic circuitry, 58, 1914–1932, 1970.
21. F.H. Gaensslen, V.L. Rideout, E.J. Walker, and J.J. Walker, Very small MOSFETs for low-temperature operation, *IEEE Transactions on Electron Devices*, 24, 218–229, 1977.
22. W.P. Dumpke, The effect of base doping of the performance of Si bipolar transistors at low temperatures, *IEEE Transactions on Electron Devices*, 28, 494, 1981.
23. J.D. Cressler and G. Niu, *Silicon–Germanium Heterojunction Bipolar Transistors*. Boston, MA: Artech House, 2003.
24. J.D. Cressler (Ed.), *Silicon Heterostructure Handbook: Materials, Fabrication, Devices, Circuits, and Applications of SiGe and Si Strained Layer Epitaxy*. Boca Raton, FL: CRC Press, 2006.
25. T.R. Oldham, F.W. Sexton, and J.R. Srour, Guest editorial introduction to the commemorative special issue, *IEEE Transactions on Nuclear Science*, 50, 454–456, June 2003.
26. J.T. Wallmark and S.M. Marcus, Minimum size and maximum packing density of non-redundant semiconductor devices, *IRE Proceedings*, 50, 286, 1962.
27. D. Binder, E.C. Smith, and A.B. Holman, Satellite anomalies from galactic cosmic rays, *IEEE Transactions on Nuclear Science*, 30, 2675, 1975.

* These important IEEE TNS Special Issues have a decade cycle time, with another TNS Commemorative Special Issue planned for 2013. Stay tuned.

28. T.C. May and M.H Woods, Alpha particle induced soft errors in dynamic memories, *IEEE Transactions on Electron Devices*, 26, 2, 1979.
29. J.C. Pickel and J.T. Blandford, Cosmic ray induced errors in MOS memory cells, *IEEE Transactions on Nuclear Science*, 30, 1166, 1978.
30. R.C. Wyatt, P.J. McNulty, P. Toumbas, P.L. Rothwell, and R.C. Filz, Soft errors induced by energetic protons, *IEEE Transactions on Nuclear Science*, 26, 4905, 1979.
31. C.S. Guenzer, E.A. Wolicki, and R.F. Allas, Single event upset of dynamic RAMs by neutrons and protons, *IEEE Transactions on Nuclear Science*, 26, 5048, 1979.
32. W.A. Kolasinski, J.B. Blake, J.K. Anthony, W.E. Price, and E.C. Smith, Simulation of cosmic ray induced soft errors and latchup in integrated circuit computer memories, *IEEE Transactions on Nuclear Science*, 26, 5087, 1979.
33. J.F. Ziegler and W.A. Landford, Effect of cosmic ray on computer memories, *Science*, 206, 776, 1979.
34. J.N. Bradford, A distribution function for ion track lengths in rectangular volumes, *Journal of Applied Physics*, 50, 3799, 1979.
35. J.N. Bradford, Cosmic ray effects in VLSI in space systems and their interaction with Earth's space environment, *Progress in Astrophysics and Aerophysics*, 71, 549, 1980.
36. K.F. Galloway, High-impact papers presented at the *IEEE Nuclear and Space Radiation Effects Conference: The View in 2003*, *IEEE Transactions on Nuclear Science*, 50, 457–465, 2003.
37. H.L. Hughes and R.A. Giroux, Space radiation affects MOSFETs, *Electronics*, 37, 58–60, 1964.
38. J. Raymond, R. Steele, and W. Chang, Radiation effects in metal-oxide-semiconductor memories, *IEEE Transactions on Nuclear Science*, 12, 457–463, 1965.
39. E.W. Enlow, R.L. Pease, W. Combs, R.D. Schrimpf, and R.N. Nowlin, Response of advanced bipolar processes to ionizing radiation, *IEEE Transactions on Nuclear Science*, 38, 1342–1351, 1991.
40. J.A. Babcock, J.D. Cressler, L.S. Vempati, S.D. Clark, R.C. Jaeger, and D.L. Harame, Ionizing radiation tolerance and low-frequency noise degradation in UHV/CVD SiGe HBTs, *IEEE Electron Device Letters*, 16, 351–353, 1995.
41. J.A. Babcock, J.D. Cressler, L.S. Vempati, S.D. Clark, R.C. Jaeger, and D.L. Harame, Ionizing radiation tolerance of high-performance SiGe HBTs grown by UHV/CVD, *IEEE Transactions on Nuclear Science*, 42, 1558–1566, 1995.

2

Extreme Environments in NASA Planetary Exploration

Elizabeth Kolawa
Jet Propulsion Laboratory
California Institute of Technology

Mohammad Mojarradi
Jet Propulsion Laboratory
California Institute of Technology

Linda Del Castillo
Jet Propulsion Laboratory
California Institute of Technology

2.1 Introduction to Planetary Extreme Environments

One of the biggest challenges of solar system exploration is the variety of extreme environments that orbiters, landers, and probes must encounter and survive. For example, exploration of the Venus surface requires engineering systems and science instruments that can withstand intense heat (480°C) and pressure (92 bar). A spacecraft that dwells in the equatorial plane of Jupiter, or that orbits any of the inner Galilean satellites, must be designed to handle an extremely harsh radiation environment. Table 2.1 [1] summarizes planetary extreme environments. The planetary environments are organized by extremes in temperature; however, it is evident that missions will often encounter multiple extremes simultaneously. An adequate technical solution for coping with only one or the other of these environments may not work when they are presented simultaneously. For example, at Venus and Jupiter, high temperatures are typically coupled with high pressures, requiring technical developments that integrate solutions for both extreme conditions. Europa's surface couples low temperatures and high radiation levels, requiring radiation-hard electronics that also function at low temperatures. In general, an important consideration is also the timing of the encounter with the extreme environment. This varies with the target. Examples include the following:

- *Venus*: The temperature and pressure increase steadily during descent until extremes are reached at the surface. The surface exploration platform (lander, probe, etc.) may have to pass through sulfuric acid clouds (Figure 2.1).
- *Jupiter*: Extreme temperatures and pressures increase during the descent phase into the atmosphere.
- *Europa*: High radiation is experienced as the spacecraft enters the Jovian radiation environment, with a substantial fraction received prior to entering orbit. A combination of high radiation and low temperature characterize Europa's surface.

Therefore, determining the technology needs requires a good understanding of the planned mission architecture. For example, the radiation tolerance required of the electronics to be used in Europa missions depends strongly on the mission target (orbit, surface, or subsurface) and mission duration. On the other hand, while both Venus and Jupiter present similar environmental conditions, the challenges for mission designers differ substantially. Highest temperatures and pressures on Venus are experienced at the surface, while at Jupiter they vary with the depth of the descending probe. Therefore, although Venus surface mission success depends on the capability of the spacecraft to survive the ambient environment, the major challenge for a probe missions to Jupiter is the thermal protection during descent and the probe's ability to communicate with the orbiter.

2.2 Future Planetary Exploration

The National Research Council (NRC) of the National Academies summarized our current knowledge of the universe, outlined science objectives, and provided prioritized future exploration plans in the Solar System Exploration Decadal Survey in [2]. Table 2.2 summarizes future missions recommended by this Decadal Survey.

TABLE 2.1 Extreme Environments in the Solar System

Mission Stage	Space	Entry		In Situ					
Target	Radiation (krad/Day)	Heat Flux at Atmospheric Entry (kW/cm²)	Deceleration (g)	High Pressure (bar)	Low Temperatures (°C)	High Temperatures (°C)	Day Length (Earth Days)	Chemical Corrosion	Physical Corrosion
High temperatures and high pressures									
Venus surface		30	400	92		500	400	H_2SO_4	
Jupiter (gas giants)		42		100		450			
Low temperatures									
Lunar permanently shadowed regions					−230				
Comet nucleus		0.5[a]			−270				
Titan surface					−185			CH_4	
Low temperatures and high radiation									
Europa orbit	40								
Europa surface	20				−180				
Europa subsurface	0.3 at 10 cm								
Thermal cycling									
Moon					−180	120	27		Dust
Mars					−120	+20			Dust

[a] This heat flux describes the heat flux at Earth for returned missions. A returned sample mission from a cometary surface is discussed further in Chapter 3. However, this heat flux will apply to any returned sample mission.

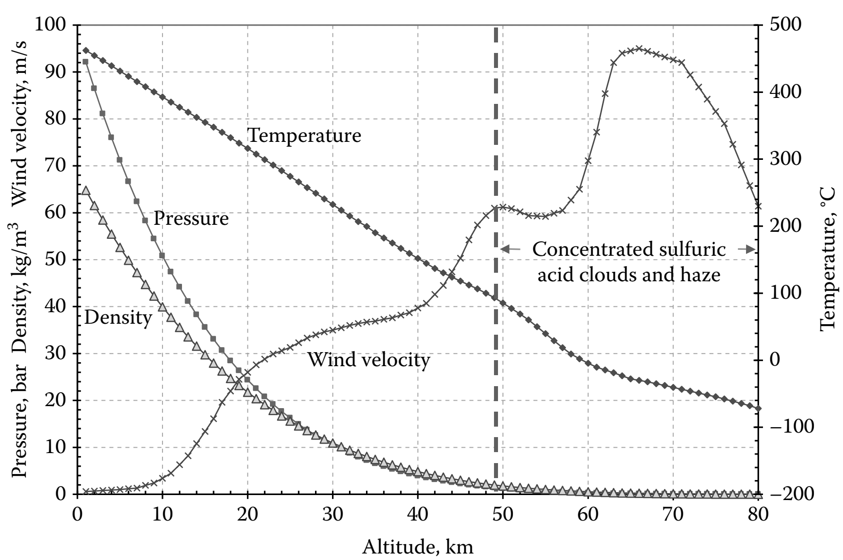

FIGURE 2.1 Profile for Venus atmospheric temperature and pressure. (From Hall, J.L. et al., *Venus Flagship Mission Study: Report of the Venus Science and Technology Definition Team*, NASA, Washington, DC, 2009.)

TABLE 2.2 Extreme Environments Planetary Missions Recommended by the Decadal Survey

	Mission Science Objectives	Extreme Environments
	New Frontiers Missions	
Lunar South Pole-Aitken Basin Sample Return (NF4)	Return samples from this ancient and deeply excavated impact basin to Earth for characterization and study.	40 K
Venus In-situ Explorer (NF4)	Examine physics and chemistry of Venus' atmosphere and crust. This mission aims to characterize variables that cannot be measured from orbit, including detailed composition of the lower atmosphere, and elemental and mineralogical composition of surface materials. The mission architecture consists of a lander that acquires atmospheric measurements during descent, and briefly carries out remote sensing and in situ measurements on the planet's surface.	780 K, 92 bar
Comet Surface Sample Return (NF4)	Acquire and return to Earth a macroscopic sample from the surface of a comet nucleus using a sampling technique that preserves organic material in the sample. The mission would also use additional instrumentation to determine geologic and geomorphologic context of the sampled region.	90 K
Trojan Tour and Rendezvous (NF4)	Examine two or more small bodies sharing the orbit of Jupiter, including one or more flybys followed by an extended rendezvous with a Trojan object.	
Saturn Probe (NF4)	Determine the structure of Saturn's atmosphere, noble gas abundances and isotopic ratios of oxygen, hydrogen, carbon, and nitrogen. The flight system consists of a carrier-relay spacecraft and a probe to be deployed into Saturn's atmosphere. The probe makes continuous in situ measurements of Saturn's atmosphere as it descends ~250 km from its entry point and relays measurement data to the carrier spacecraft.	10 krad
Io Observer (NF5)	Determine the internal structure of Io and to investigate the mechanisms that contribute to the satellite's intense volcanic activity.	
Lunar Geophysical Network (NF5)	Characterize the Moon's internal structure, seismic activity, global heat flow budget, bulk composition, and magnetic field. Mission duration would be several years, allowing detailed study of lunar seismic activity and internal structure. This mission consists of several identical landers distributed across the lunar surface, each carrying geophysical instrumentation.	90–300 K thermal cycling
	Flagship Missions recommended for 2013–2022 (priority order)	
Mars Astrobiology Explorer Cacher MAX-C	The first of three components of a joint NASA-ESA Mars Sample-Return campaign. The MAX-C rover is responsible for characterizing a landing site that has been selected for high science potential, and for collecting, documenting, and packaging samples for return to Earth. The rover is also capable of conducting high priority in situ science on the martian surface.	150–290 K thermal cycling
Jupiter Europa Orbiter	Characterize Europa's ocean and interior, ice shell, chemistry and composition, and the geology of prospective landing sites. The preliminary mission timeline includes a 30-month jovian system tour phase, followed by a 9-month Europa orbital phase. The mission also makes observations of Jupiter.	~3000 krad
Uranus Orbiter and Probe	Make in situ measurements of noble gas abundances and isotopic ratios for an ice giant atmosphere, using a small atmospheric probe deployed from the spacecraft.	
Enceladus Orbiter	Investigate the saturnian satellite's cryovolcanic activity, habitability, internal structure, chemistry, geology, and interaction with other bodies of the Saturn system.	
Venus Climate Mission	Address science objectives concerning the Venus atmosphere, including CO_2 greenhouse effects, dynamics and variability, surface/atmosphere exchange, and origin. The mission architecture includes a carrier spacecraft, a gondola/balloon, a mini-probe, and 2 drop sondes. The mini-probe and drop sondes each have 45-min. science missions as they descend to the surface, and the gondola/balloon system carries out a 21-day science campaign as it travels at a ~55 km float altitude.	780 K, 92 bar
	Flagship Missions deferred to the next decade for consideration (alphabetical order)	
Mars Sample Return Lander and Orbiter	The second component of the Mars Sample Return campaign. It consists of a fetch rover to retrieve cached samples on the martian surface and an ascent vehicle to launch the samples into Mars orbit.	150–290 K thermal cycling
Mars Geophysical Network	Characterize the internal structure, thermal state, and meteorology of Mars. The mission includes two or more identical, independent flight systems, each consisting of a cruise stage, an entry system, and a lander carrying geophysical instrumentation.	150–290 K thermal cycling
Titan Saturn System Mission	Address key science questions regarding Saturn's satellite Titan as well as other bodies in the Saturn system. The baseline mission architecture consists of an orbiter supplied by NASA, and a lander and Montgolfière balloon supplied by ESA. These components will examine Titan, concentrating on the prebiotic chemical evolution of the satellite.	90 K

2.3 Electronics for Extreme Environments: State of Practice

During the past 40 years, NASA, the Soviet Union Space Agency, and the European Space Agency (ESA) have sent landers to the Moon, Mars, and Venus, as well as atmospheric probes to Jupiter, Venus, and Titan. Generally, all of these missions were designed to minimize the exposure of subsystems to the ambient environment by protecting the payload, avionics, navigation, power, and telecom subsystems from the environment, using elaborate thermal, radiation, and pressure control.

2.3.1 High-Pressure and High-Temperature Environments

High-pressure and high-temperature environments have been experienced by the Soviet and U.S. missions to the deep atmosphere and surface of Venus. The Soviets sent their first probe to Venus before the severity of the surface conditions was known. By the time of the last mission, however, they had developed the technology for surviving, making measurements in the surface environment, and acquiring samples within the constraints of a mission limited to 2 h of surface time. They also appear to have developed methods for coping with the corrosive aspects of the environment—not only for sulfuric acid in the upper atmosphere (using Teflon-coated Vega balloons), but also carbon dioxide in a supercritical state in the lower atmosphere.

Pioneer Venus, NASA's only mission to the deep atmosphere of Venus, was purely intended as an atmospheric probe and neither designed nor equipped for surface observations. Unlike the Soviet probes, Pioneer Venus probes were only tested in a nitrogen environment at the temperature and pressure conditions of the Venus surface.

2.3.2 Cold-Temperature Environments

Severe cold-temperature environments are inherent to exploration of the outer solar system and are experienced in the inner solar system during the exploration of airless bodies (Moon, Mercury, asteroids) as well as Mars, a body with a thin atmosphere and extreme diurnal temperature changes. Short-duration missions, such as the Huygens probe to Titan [3], have coped with environments as cold as −180°C (Figure 2.2). The Mars Exploration Rover (MER) mission, a multiyear mission, experiences deep diurnal temperature cycles between −120°C and +20°C. Figure 2.3 summarizes surface pressures and temperatures for Mars. Electronic components that will not function over this range are protected in a warm electronics box. The warm electronic box used for MER is shown in Figure 2.4 [1].

2.3.3 Severe Radiation Environments

While ionizing radiation environments are ubiquitous in space, the most severe environments are encountered in the Jupiter radiation belts. In its multiyear mission, the Galileo orbiter not only provided the most complete characterization of this environment, but also was exposed to a cumulative dose of 600 krad, which is much higher than any other planetary spacecraft [4,5]. To cope with the Jovian environment, Galileo employed extensive use of shielding, radiation-tolerant electronic parts, and operational methods for recovering from radiation damage. The extensive base of experience from Galileo on the nature of the Jovian environment, its effects on spacecraft components, and methods of mitigating these effects were all applied to the design of Juno (Jupiter Orbiter), which is currently on its way to Jupiter.

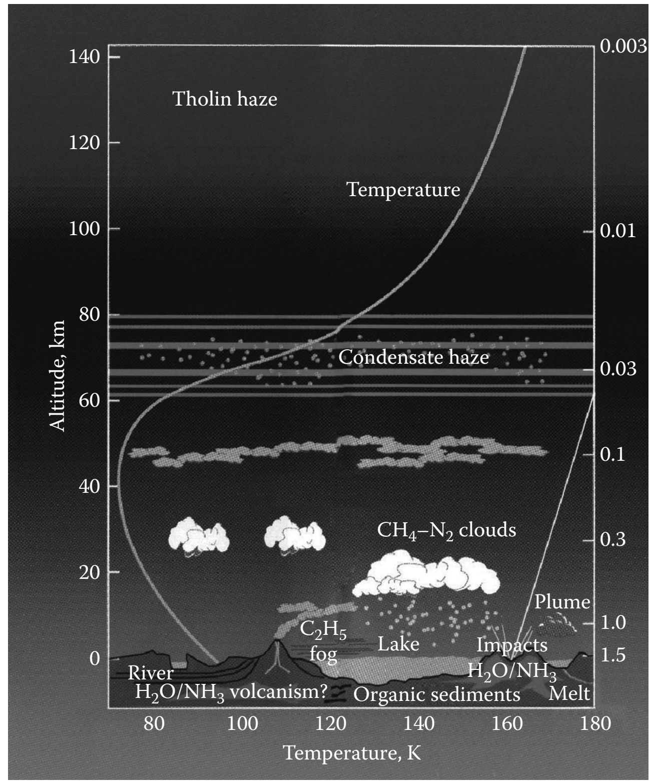

FIGURE 2.2 **(See color insert.)** Diagram of the subsurface, surface, and atmosphere of Titan, demonstrating the relevant chemistry in each region and how all three are interconnected. (From Reh, K. et al., *Titan Saturn System Mission (TSSM) Flagship Mission Study Report*, NASA, Washington, DC, 2009.)

2.4 Impact of Extreme Environment Technologies on Future NASA Missions

2.4.1 High Temperatures and High Pressures

Prior landed missions to Venus have been limited to surface lifetimes of 2 h. Missions to Venus recommended by Decadal Survey are listed in Table 2.2.

The recently completed Venus Flagship Mission (Figure 2.6) study [6] identified key technologies required to implement its Design Reference Mission and other important mission

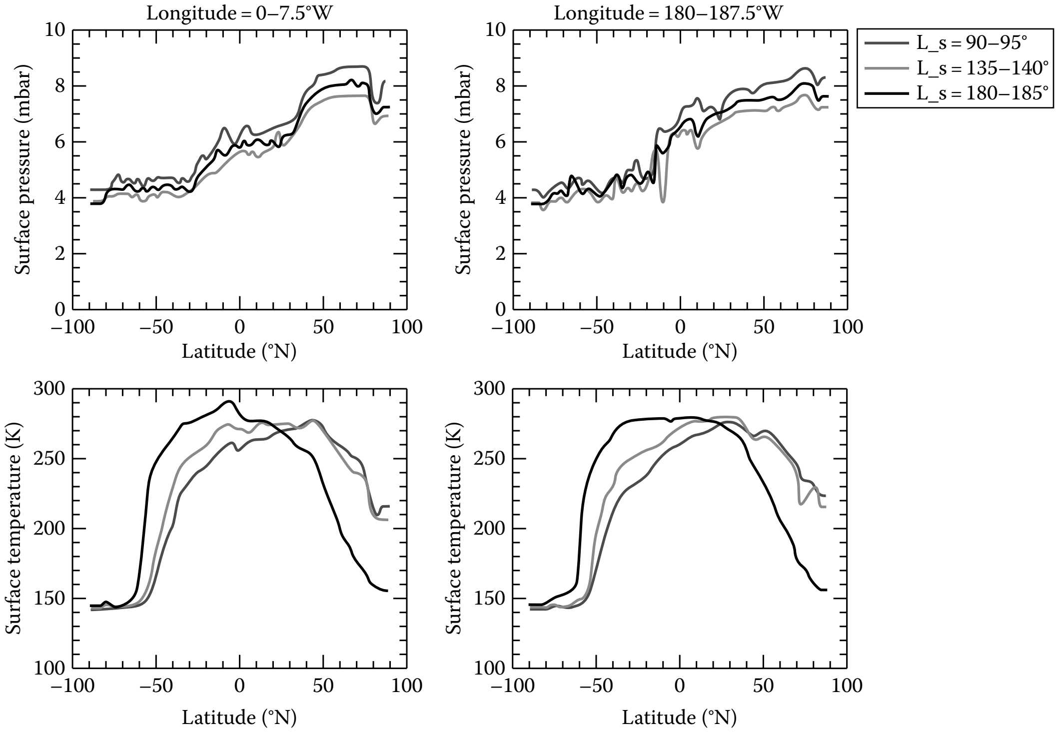

FIGURE 2.3 Surface pressure and temperatures of Mars. (From McGuire, P.C. et al., *IEEE Trans. Geosci Remote Sens.*, 46(12), 4020–4040, December 2008.)

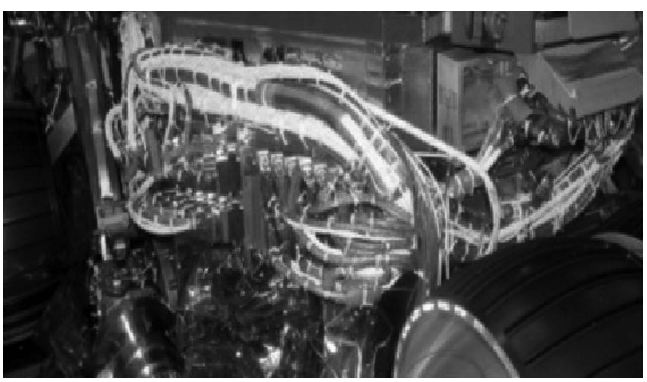

FIGURE 2.4 MER warm electronics box. (From Kolawa, E. et al., Extreme environment technologies for future space science missions, Technical Report JPL D-32832, 2007, NASA, Washington, DC, September 19, 2009, http://vfm.jpl.nasa.gov/files/EE-Report_FINAL.pdf)

options. Some of these technologies would also be applicable to deep probe missions to Jupiter, Saturn, and other outer planets. Missions such as the Venus Mobile Explorer (VME), which would be planned to operate at the surface of Venus for several months, would also require surface power generation, active cooling technologies, and high-temperature electronics to achieve the long-lifetime objectives. Sample acquisition mechanisms would necessarily be exposed to the environment and advances in components would have major advantages.

Through the implementation of advanced technologies, there are numerous scientific investigations that can yield extraordinary science return for understanding the Venus environmental and planetary system [6,7]. One of the highest priority science objectives of the Venus community is to develop an understanding of the structure and dynamics of the interior of the planet. Fundamental questions such as the thickness of the thermal lithosphere, the behavior of the mantle, the current rate of internal activity, and the nature of Venus nonmagnetic core must be addressed in order to understand the unique geologic history of Venus. Some volcanic and tectonic features are familiar, and some are not. Comparisons with partially understood geology on Earth will increase our understanding of these processes in ways that could not be done by studying the Earth's geologic record alone. Direct seismic measurements will be very useful in addressing these questions, making seismometry one of the highest priority alternative investigations. The successes of the Mars Exploration Program have shown the crucial importance of exploring geologically diverse terrains in situ. At Venus, this motivates the use of long duration and/or mobile exploration platforms that can access those diverse terrains and survive long enough for extensive scientific investigations. A far better understanding of Venus atmospheric chemistry and dynamics could be obtained by multiple dropsondes.

The ability to select target rocks and soils for excavation and analysis, and to base measurement decisions on new data, requires moderately extended lander lifetimes on the order of 24 h or more. Selection of targets for geochemical, mineralogical, and elemental analyses would provide a much greater chance for obtaining a good understanding of how the atmosphere and surface interact, and the nature of geologic processes that shaped the surface of Venus. Discoveries can lead to new targeted investigations that would not be possible with autonomous or preprogrammed spacecraft. Mission risk can also be reduced if the mission team can interact with the lander and help troubleshoot any problems that arise.

A passive thermal architecture to achieve extended surface lifetime performance appears to be within the realm of possibility, but it will require technology development. There are a number of ideas in the literature that describe a "long-life" architecture [6]. These generally involve the use of a phase change material such as lithium nitrate trihydrate ($LiNO_3 \cdot 3H_2O$) to absorb thermal energy generated by electronics inside the pressure vessel and a water evaporative cooling system to absorb the energy coming from the Venus environment. A water-based heat absorption system can take advantage of the solid to liquid phase change and the liquid to vapor phase change. Any improvements in the elevated temperature capabilities of the electronics would reduce the cooling requirements and improve the lifetime of the passive thermal system.

Balloons are probably the most scientifically capable platforms for deep and extended in situ investigations of atmospheric circulation and chemistry, for exploring the Venus greenhouse effect, and for understanding how the clouds form. Very-long-duration balloons could circumnavigate the planet multiple times, probing the winds and sampling the gases and clouds to build up a picture of the atmosphere of Venus unobtainable in any other way. Long-duration balloons might eventually reach the polar vortices and be swept downward toward the poles, obtaining dynamical and chemical measurements until they were destroyed. Balloons operating at 55 km, like Vega balloons [8], do not require extreme environments electronics.

2.4.1.1 Extended Surface Life Landers

A highly capable long-lived lander (months or longer) on Venus surface would be mankind's first extended outpost on a planet with an extreme greenhouse effect. A lander that could survive for long enough to track the weather and obtain a range of seismic events would also be able to more thoroughly explore its nearby environment. The lander could also serve as a relay station for science data being gathered by in situ instruments such as the seismic/meteorological planetary network. Being able to drill to depths of up to a meter and to acquire soil and rock samples at a variety of locations would greatly enhance the ability to provide the crucial information of how pristine Venus rocks reacted with the atmosphere. The illusion of static volcanic plains from the Venera lander images obscures the fact that visually, the surface of Venus undergoes vast changes. Night and day with intense scattering by the thick atmosphere will change the scene dramatically, perhaps even altering the illumination of the landscape and lander workspace. Other changes, such as particles lofted by the winds, and even the changing appearance of the lander and sampled sites, would provide significant insights into the dynamic nature of Venus' surface.

Seismology and meteorology are two investigations that require long-lifetime measurements on the surface, and hence cannot be fully accomplished in a short-duration surface mission. How active is Venus? Are there Venus quakes? How deep are the basaltic plains? and What is beneath them? It is important to recognize that significant science can be accomplished with just one seismometer on the surface of Venus, while the broader goal of understanding the interior structure will require several seismic stations around the planet. A broader and more complete picture of Venus' interior, the dynamics of the mantle, and the nature of the lithosphere will require a network of at least four seismometers spaced around the planet. Based on terrestrial seismicity, such a network operating for 1 Earth year would probably be sufficient to meet these science goals. The operational requirements for Venus ground ambient environments include ~480°C operation and ~92 bar for durations from 117 Earth days to 1 Earth year. Given the current state of technology development and depending on the mission architecture, such measurements may not be feasible. Rather, measuring at least a subset of the seismic frequency range would be desirable, with significant science benefits. If the seismology experiment is a part of a refrigerated spacecraft with a radioisotope power source coupled with cooling, then it may be possible to achieve the full range of target measurement requirements. However, if the experiment is performed at ambient surface temperatures using high-temperature electronics and high-temperature power sources or/and high-temperature batteries, then some performance trade-offs may be necessary. Atmospheric super-rotation may be forced by angular momentum exchanges with the surface, although the mechanisms of upward transfer of angular momentum within the atmosphere are not understood. Meteorological stations that can weather data at two locations simultaneously over one Venus solar day would provide extremely important information on the dynamics of the near-surface atmosphere. The specific goals of the meteorology experiment, in addition to providing wind speed and direction as well as atmospheric temperature and pressure, are to determine the vertical and horizontal structure at the base of the local atmospheric boundary layer, and to observe changes at the locations with time.

The options to technologically realize a seismometer and meteorological network on the surface of Venus and secure its long-term operation from 117 days to 1 year include the following:

- Use a refrigerated pressure vessel to be able to operate a network in mild thermal environment enabling the use of conventional, space-rated components. Issues associated with measurement interfaces to the ambient surface and environment would have to be addressed.

- Use components that can fully and reliably operate in the Venus surface environment without thermal control including high-temperature sensors, high-temperature electronics and telecom system, and high-temperature power sources and batteries.
- The development of a hybrid system using both refrigeration and environmentally hardened components. The use of high-temperature components would enable the optimization of the refrigeration system to minimize its power and mass, and refrigeration can protect components that are unable to operate at Venus surface temperature and pressure.

The development of a seismic instrument, which measures across the complete frequency range, is a significant technical challenge. Given ongoing advancements in high-temperature microelectromechanical systems (MEMS) technology, such a broad range measurement device is achievable; the corresponding electronics and communication technologies for a more complex system would be very challenging. This would involve not only the development of high-temperature MEMS-based accelerometers but also more complex circuitry including memory and the data handling to support the instrument. While such an approach would provide a complete spectrum of seismic information, the remaining technical challenges are very significant and equal to developing high-temperature semiconductors to the capability of silicon-based technology.

2.4.1.2 Low-Altitude Balloons

The introduction of low-altitude mobile systems, such as low-altitude balloons, can add great scientific capability, and potentially public excitement to Venus exploration. The only locations where we can actually see what the surface of Venus looks like at visible wavelengths are the spectacular images from the Venera Landers. The only geologic context we have for Venus is provided by the global Magellan radar image dataset. In order to establish a chronology of events and to interpret the geologic history of Venus, geologists must be able to see contacts between geologic units, stratigraphic relationships, and structure. A low-level balloon which traverses at an altitude low enough to view the surface provides an effective way of surveying the regional geology of Venus. Using prevailing winds, horizontal traverses of thousands of kilometers are possible. Balloon altitude control techniques can also be used to perform vertical traverses through the atmosphere and thereby acquire atmospheric vertical profile information at multiple locations. An extremely capable balloon that could touch down, retrieve a sample, and then retreat to cooler levels could analyze sample chemistry, mineralogy, and elemental abundance at diverse locations. An important key to understanding atmospheric processes and perhaps the evolution of Venus resides in the lower 20 km of the atmospheric column, where nearly 80% of the atmospheric mass exists. Measurements of variabilities in trace atmospheric species during a low-level traverse would be very important for gaining a deeper understanding of surface atmosphere chemical interactions. Finally, low-altitude balloon traverses are an ideal way to do geological photo-reconnaissance of the Venus surface. By obtaining visible images of the surface across thousands of kilometers, it would be possible to observe diverse lithologies and their relative positions in the geologic sequence.

The technology required to implement lower altitude (<50 km) Venus balloons is not mature and faces four main challenges: (1) available polymer balloon materials and adhesives do not work at the 460°C surface temperatures; (2) most scientific instruments cannot tolerate high temperatures; (3) electrical power is difficult to obtain below the Venus clouds since the solar flux is much reduced and the operating temperature of solar panels is very high compared to terrestrial or standard spacecraft environments; and (4) the balloon's suspended payload is significantly mass limited. Therefore, the payload and internal power source needs to be both capable and light.

The ability to actively refrigerate instruments and electronics fundamentally changes the nature of any long-lived mission, including landers, low-altitude platforms, or independent in situ instruments. Such a refrigeration system has two main components: a power source and a refrigeration machine that uses the power source to pump heat from the payload back out into the environment. Radioisotope power is the only realistic long-lived power source for the surface of Venus. Typically a radioisotope power system (RPS) would be used to jointly power the electronic components of the payload as well as the refrigeration system.

Venus exploration missions also pose significant challenges for energy storage systems. Many concepts for Venus surface missions (landers and seismic/meteorological stations) require mass- and volume-efficient energy storage systems that can operate at temperatures as high as 480°C. Venus atmospheric exploration missions (aerial platforms, atmospheric probes) likewise require energy storage systems that can operate at 50°C to 480°C, depending on the altitudes.

In the United States, over the past five decades, several high-temperature energy storage technologies have been developed by and for NASA, the Department of Energy (DoE), and the Department of Defense (DoD) and as a result several battery chemistries operating above 400°C were created and qualified. High-temperature batteries that are under development and offer a promise for Venus missions can be classified into two groups: (1) thermal batteries and (2) high-temperature rechargeable batteries. Thermal batteries were developed by DoD and DoE for use in weapons and missiles. These are primary batteries and are activated thermally before use. A signal from an external source initiates the ignition of pyrotechnic materials (heat pellets) within the battery. This ignition in turn results in a melting of the electrolyte, and the battery produces electrical power for a relatively short period of time. Significant work was carried out in the 1970s and 1980s on the development of high-temperature (300°C to 600°C) rechargeable batteries. These systems include (a) LiAl–FeS_2, (b) Na–S, and (c) Na–metal chloride. Although these batteries were designed as rechargeable versions, they can also function in primary battery mode.

A range of sensors applicable to Venus missions have been and continue to be developed for a variety of target applications, including high-temperature aerospace and industrial applications. Sensor development includes high-temperature positioners, accelerometers, pressure sensors, temperature sensors, and chemical sensors. Conventional Si-based pressure sensors are temperature limited while devices such as SiC-based pressure sensors have a much wider operating temperature range. Progress has been made in both SiC pressure sensor micromachining and packaging. The resulting sensors have demonstrated the capability to withstand high temperatures with improved reliability and operation up to 600°C [6]. This mature technology has been transferred to industry and is presently being commercialized. Research efforts are geared toward integrating three functionalities in a MEMS structure: a pressure sensor, an anemometer, and a temperature differential sensor. GaN-based pressure and temperature sensors have been recently explored for extreme environments, and prototype GaN sensors operating at 480°C [6].

High-temperature physical sensors, including those for strain, temperature, heat flux, and surface flow, are required for surface measurements in propulsion system research at temperatures up to 1100°C. This technology has a long history of test stand implementation in a variety of environments, typically at temperatures well beyond those necessary for Venus.

The development of MEMS-based chemical microsensors to measure emissions in high-temperature, harsh environments has been ongoing for engine emission monitoring applications. The fundamental approach used by this technology is that each sensor is designed to be selective to the chemical species of interest intending to provide direct measurement of the chemical species predominately without the need for pattern recognition hardware or extensive processing in order to interpret the results. Sensors composed of Schottky diodes, electrochemical cells, and resistors composed of a variety of harsh environment materials are used to detect a range of species with sensor operating temperatures ranging from 500°C to 700°C.

Only limited work has been done in developing long-range, high-power, and high-temperature transmitters for Venus applications. Absence of high-frequency passive and active RF components seems to be a major issue limiting the progress in this area. Based on the current state of the art and the general Venus missions' requirements, further development of high-temperature transmitters and corresponding RF components for this purpose are needed. In addition, the passive components required to construct oscillators and amplifiers must be developed to the same level of reliability. Lastly, electronic packaging of the circuits is required. In parallel, the same type of development is necessary for other promising types of transmitter technologies. Vacuum tubes or GaN semiconductor technologies can either provide an alternative to or complement existing SiC technologies.

2.4.1.3 Dropsondes and Probes

Although dropsondes [6] provide only a snapshot of the atmosphere at a time, the simultaneity of multiple of them at globally distributed locations will provide very valuable information about the spatial variations in state of the Venus atmosphere which has not been possible to date on a global scale. These dropsondes would measure not only wind speed and direction, but also temperature and atmospheric gas abundances. This full array of data would be provided at multiple entry locations, altitudes, all at the same time. This approach depends on capable instrument suite, power, and communication systems. Such a suite of dropsondes equipped with net-flux radiometers would provide crucial information on variations of down-welling and up-welling radiation as a function of altitude, latitude, and solar zenith angle. Another advantage to this platform would be simultaneous measurements of chemical abundance profiles at several dispersed locations. Finally, if they were equipped with cameras, dropsondes could perform descent imaging at a wide variety of diverse locations.

Dropsondes or probes would have to survive for a short period of time in a wide variety of environments (increasing temperature and pressure, corrosive sulfuric acid clouds, supercritical carbon dioxide) as they descend to the surface. Depending on the sondes or probes payload and duration of operation, the combination of different design architectures and technologies will be needed to achieve the desired life and performance. If the science investigation includes descent imaging, a combination of passive thermal control and conventional space electronics and telecom can be used. The penalty would be a relatively high probe mass. In order to reduce the probe mass by minimizing thermal control requirements, the moderate temperature (~300°C) electronics could be used for data processing and communication. For probes with simple payloads (temperature, pressure, and other basic sensors), high-temperature sensors, electronics, and batteries can be used providing system survivability as the dropsondes or probes approach the surface and higher temperatures and pressures. The benefit of this approach would be a significant mass reduction and longer life (limited by battery life). The communication infrastructure for such a multicomponent probe system would have to take into account the labeling and identification of the signals and data from each sonde or probe. The orbiter would then have to adequately transmit that information with timestamp back to Earth.

2.4.2 Low Temperatures

While all missions to the outer solar system are exposed to cold temperatures, in situ missions present the greatest challenges because of their power constraints and thermal control complexities. Low-temperature electronics can enable extended operations on cold targets. For mobile vehicles with motors and actuators exposed to the surface environment, cold electronics can greatly simplify cabling. Repetitive changes in environmental conditions can cause even more stress on engineering systems than stable extreme conditions. Slowly rotating bodies such as the Moon and Mercury experienced extreme temperature excursions between night and day and electronics and components must be designed to tolerate the resulting cyclical stresses.

Cassini-Huygens has provided interesting data and has enabled us to glimpse the surface of Titan. However, it left us with many questions that require future missions to answer [9]. These include determining the composition of the surface and the geographic distribution of various organic constituents. Key questions remain about the ages of surface features, specifically whether cryovolcanism and tectonism are actively ongoing or are relics of a more active past. Ammonia, circumstantially suggested to be present by a variety of different kinds of Cassini-Huygens data, has yet to be seen. Is methane outgassing from the interior or ice crust today? Are the lakes fed primarily by rain or underground methane–ethane aquifers (more properly, "alkanofers") and how often have heavy methane rains come to the equatorial region? We should investigate whether Titan's surface supported vaster seas of methane in the past, and whether complex self-organizing chemical systems have come and gone in the water volcanism, or even exist in exotic form today in the high-latitude lakes. The presence of a magnetic field has yet to be established. A large altitude range in the atmosphere, from 400 to 900 km in altitude, will remain poorly explored after Cassini. Much remains to be understood about seasonal changes of the atmosphere at all levels, and the long-term escape of constituents to space [9].

Other than Earth, Titan is the only world in our solar system known to have standing liquids and an active "hydrologic cycle" with clouds, rains, lakes, and streams. The dense atmosphere and liquid lakes on Titan's surface can be explored with airborne platforms and landed probes (Figures 2.5 and 2.6), but the key aspect ensuring the success of future investigations is the conceptualization and design of instruments that are small enough to fit on the landed probes and airborne platforms, yet sophisticated enough to conduct the kinds of detailed chemical (including isotopic), physical, and structural analyses needed to investigate the history and cycling of the organic materials. In addition, they must be capable of operating at cryogenic temperatures while maintaining the integrity of the sample throughout the analytic process. Illuminating accurate chemistries also requires that the instruments and tools are not simultaneously biasing the measurements due to localized temperature increases. While the requirements for these techniques are well understood, their implementation in an extremely low-temperature environment with limited mass, power, and volume is acutely challenging. No such instrument systems exist today.

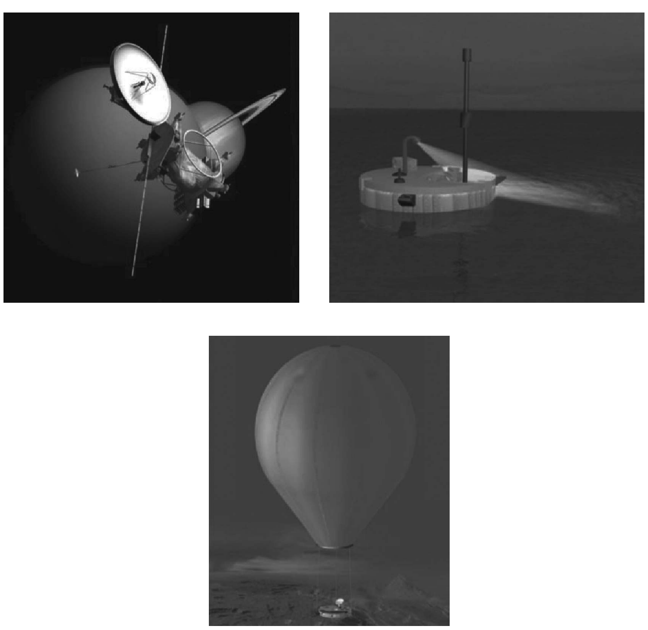

FIGURE 2.5 **(See color insert.)** The three elements of the 2009 TSSM mission architecture: a Titan orbiter, a lake lander, and a hot-air balloon. (From Reh, K. et al., *Titan Saturn System Mission (TSSM) Flagship Mission Study Report*, NASA, Washington, DC, 2009.)

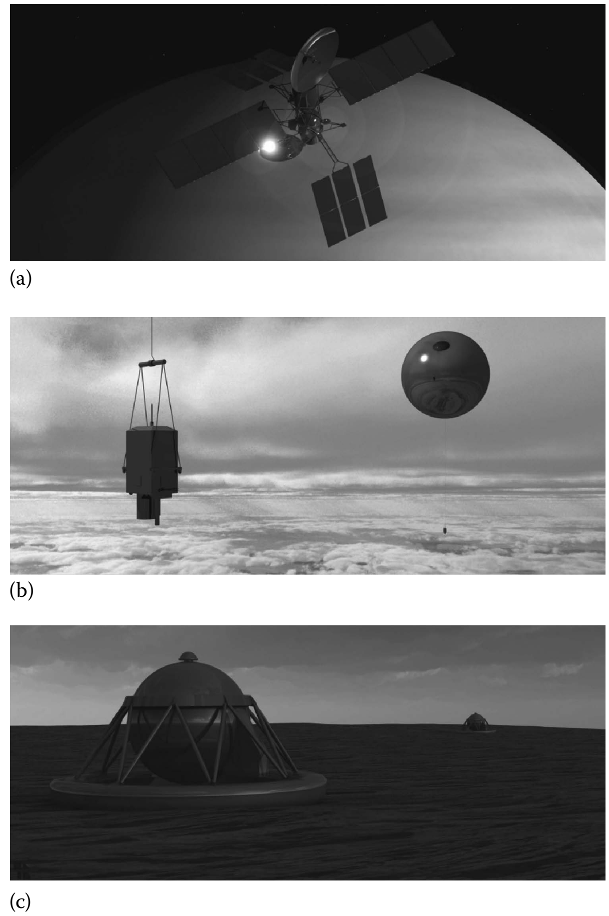

FIGURE 2.6 Three elements of the recommended Venus Flagship Mission include (a) a capable, long-lived orbiter (years) with high-resolution radar imaging and topography, (b) two instrumented balloons between 52 and 70 km (1 month), and (c) two landers with extended surface life (5 h) that also acquire detailed atmospheric data on descent. (From Hall, J.L. et al., *Venus Flagship Mission Study: Report of the Venus Science and Technology Definition Team*, NASA, Washington, DC, 2009.)

Missions to Titan are severely limited in both mass and power because spacecraft have to travel over a billion miles to get there and require a large amount of fuel, not only to reach Titan, but also to maintain the ability to maneuver when they arrive. Landed missions have additional limitations, in that they must be packaged in a sealed aeroshell for entry into Titan's atmosphere. Increases in landed mass and volume translate to increased aeroshell mass and size, requiring even more fuel for delivery to Titan. Nevertheless, missions during which such systems and instruments could be employed range from Discovery and New Frontiers class in situ probes that might be launched in the next decade, to a full-up Flagship class mission as shown in Figure 2.5. Capitalizing on recent breakthroughs in cryotechnologies, smart materials fabrication, and low-temperature electronics, advanced designs of low-temperature systems can be implemented for Titan future missions.

Designing electronics that perform well at −180°C is possible and progress has been made in recent years, but developing low-power circuits that meet the demands of many of the in situ instruments at these low temperatures is still a work in progress. To reduce mass and power, all the instruments described earlier could benefit from electronics that can function at ambient Titan temperatures. Also, relevant electronic packaging materials for long-life, low-temperature in situ Titan missions are available, but design of substrates and the characterization and testing of novel materials are critical. Ceramics, polymers, and metals all have lifetime difficulties at Titan surface temperatures. Novel power and electronics will relieve the need for Earth-like conditions within the spacecraft power and electronics housings. Bold use of materials such as carbon nanotubes and other nanostructured materials will enable new capabilities. Continued examination of geophysical techniques to explore Titan's interior without multiple networked stations is crucial given the distance to Titan and the resulting expense per kilogram of launch weight. However, although the novel geophysical techniques are important to explore (and the research should continue), it has become apparent that developing low mass and power chemical analysis system for novel Titan missions is more valuable. It is through characterization of the chemistry of Titan that an understanding of this mysterious moon will ultimately be obtained.

The dense atmosphere and diverse organic deposits on Titan's surface can be explored with airborne platforms and landed probes, but the key aspect ensuring the success of future investigations is the conceptualization and design of instruments that are small enough to fit on the landed probes and airborne platforms, yet sophisticated enough to conduct the kinds of detailed chemical (including isotopic), physical, and structural analyses needed to investigate the history and cycling of the organic materials. In addition, they must be capable of operating at cryogenic temperatures while maintaining the integrity of the instrument and sample throughout the analytic process. Illuminating accurate chemistries also requires that the instruments and tools are not simultaneously biasing the measurements due to localized temperature increases.

While the requirements for these techniques are well understood, their implementation in an extremely low-temperature environment with limited mass, power, and volume is challenging. Titan missions during which such systems and instruments could be employed range from Discovery and New Frontiers class in situ probes that might be launched in the next decade, to a Flagship class mission.

2.4.3 Ionizing Radiation

Very high ionizing radiation will be seen by Jupiter Europa Orbiter [10], a mission to orbit the Jovian satellite Europa. A typical mission profile of 2 years in Jupiter orbit followed by a 90 day mission in Europa orbit would involve radiation doses to the spacecraft five times that experienced by the Galileo mission. On the other hand, future missions that include Europa lander may experience lower dose rates than the orbiter due to Europa's self-shielding. However, lander missions are much more mass constrained than orbiters, so it is possible that the requirements on the components might be even more demanding.

2.5 Summary

NASA has not implemented a mission to a high-temperature planetary environment since the Pioneer Venus and Galileo probes, and neither was equipped with electronic components to tolerate elevated temperatures. However, developments within NASA and the commercial drivers have resulted in significant progress on components tolerant of high-temperature environments. Large bandgap semiconductors, such as silicon carbide (SiC) and gallium nitride (GaN), as well as vacuum tube–active components, can operate at 500°C for extended periods of time. In Venus surface missions, high-power electronic and telecommunications systems act as internal heat sources within the pressure vessel. Placing these systems outside the thermally protected vessel may reduce internal heating and extend the life of the mission. Small-scale integrated SiC, and GaN high-temperature technologies and heterogeneous high-temperature packaging can support this need and provide components for power conversion, electronic drives for actuators, and sensor amplifiers. Another architectural approach is the use of devices that operate at an intermediate temperature of 300°C, such as commercially available silicon-on-insulator (SOI) devices. Electronics operating at medium temperatures can reduce the difference between the outside environment and inside the thermally protected system, significantly reducing the associated power requirements for cooling.

Developments in cold-temperature electronics are important to support the needs of the next-generation Mars Rovers and the future lunar robotic missions. Commercial development of silicon germanium (SiGe) components is showing a great deal of promise. Avionics systems, transmitters, and in situ systems (using wheels, drills, and other actuators) that can directly work at cold temperatures (down to −230°C) will allow for the elimination of the warm electronics box and the implementation of distributed architectures, which will in turn enable the development of ultralow-power, efficient, and reliable systems.

At present, the space industry relies on three distinct sources for radiation-tolerant components:

1. *Commercial components*: These are components that are determined to be—perhaps serendipitously—radiation tolerant.
2. *Radiation hard by process* (RHBP): These are components manufactured with radiation-hardened material processes at specialized foundries.
3. *Radiation hard by design* (RDBD): These are components built on commercial lines with commercial materials and processes but designed to tolerate high radiation doses.

In addition to the DoD developments, NASA has carried out focused investments in rad-hard technology aimed specifically at missions to the Jupiter system under the X-2000 program in the late 1990s, and few other technology development projects. As a result, many components are now available, including those rated at a 1 Mrad total integrated dose and a broader range of components to 300 krad.

One major gap in the technology has been dense non-volatile memory (NVM). High-density solid-state recorders (SSRs) employed in Earth orbital missions use commercial flash memory devices, which are inherently rad soft. Even massive vaults may not provide the level of shielding needed for operation in the Jupiter system. However, recent progress on rad-hard memory elements in chalcogenide random access memory (CRAM) and magnetoresistive memory (MRAM) may provide a solution.

The traditional approach to the design of in situ instruments is to protect their electronic systems from diverse planetary environments. The techniques used for protection depend on the mission destination and include warm electronic boxes for low/wide temperature destinations like Mars or Moon, thermally insulated pressure vessels for high-temperature missions to Venus, and radiation shielding for high radiation environments. These techniques require high mass and power and limit the lifetime of the instruments. In the case of instruments placed on the extremities of robotic systems (arms, masts, etc.), the traditional use of these protection techniques creates a large physical distance between electronics (placed in a central thermal enclosure) and the instrument sensor/detector. Signal attenuation across this distance leads to a poorer instrument performance or must be compensated for through more complex electronics.

High-performance, low-power, low/wide operation temperature (−230°C to +125°C) electronics will benefit a large number of planetary instruments destined to operate on Mars, Titan, Moon, comets, and asteroids. In some cases, like Titan missions, developing instruments and sample acquisition system that do not dissipate heat (as a possible source that could alter the environment/samples) may be critical to achieve mission science goals. At the same time, low/wide temperature electronics will be required for next-generation, low-power, and large format imaging instruments. The bandwidth of the raw data from these imagers by far exceeds the performance of most advanced flight-like serial buses. Real-time processing of the sensor data through colocating high-performance wide temperature computational circuitry is perceived to be essential to transfer of the data from these instruments.

References

1. Kolawa, E., T.S. Balint, G. Birur, E. Brandon, L. Del Castillo, J. Hall, M. Johnson, R. Kirschman, R. Manvi, M. Mojarradi, A. Moussessian, J. Patel, M. Pauken, C. Peterson, J. Whitacre, E. Martinez, E. Venkapathy, P. Newdeck, and R. Okojie, Extreme environment technologies for future space science missions, Technical Report JPL D-32832, 2007, National Aeronautics and Space Administration, Washington, DC, September 19, 2009, http://vfm.jpl.nasa.gov/files/EE-Report_FINAL.pdf
2. National Research Council. *Vision and Voyages for Planetary Science 2013–2022*. The National Academies Press, Washington, DC, http://solarsystem.nasa.gov/multimedia/downloads/Vision_and_Voyages-FINAL1.pdf (accessed on December 15, 2011).
3. Lebreton, J.-P., O. Witasse, C. Sollazzo, T. Blancquaert, P. Couzin, A. Schipper, J. Jones, D.L. Matson, L. Gurvits, D. Atkinson, B. Kazeminejad, and M. Perez-Ayucar, An overview of the descent and landing of the Huygens probe on Titan, *Nature* 438, 758–764, December 8, 2005.
4. Fieseler, P.D., S.M. Ardalan, and A.R. Frederickson, The radiation effects on Galileo Spacecraft Systems at Jupiter, *IEEE Transactions on Nuclear Science* 49(6), 2739–2758, 2002.
5. Burdick, G., E.H. Kopf, and D.D. Meyer, The Galileo single-event upset solution and risk assessment, in *Proceedings of Annual Rocky Mountain Guidance and Control Conference*, Keystone, CO, February 1–5, 1986, pp. 199–220.
6. J.L. Hall, M. Bullock, D.A. Senske, J.A. Cutts, and R. Grammier, *Venus Flagship Mission Study: Report of the Venus Science and Technology Definition Team*, NASA, Washington, DC, 2009. http://vfm.jpl.nasa.gov/files/Venus+Flagship+Mission+Study+090501-compressed.pdf (accessed on December 18, 2011).
7. Balint, T., J. Cutts, M. Bullock, J. Garvin, S. Gorevan, J. Hall, P. Hughes, G. Hunter, S. Khanna, E. Kolawa,

V. Kerzhanovich, and E. Venkatapathy, Technologies for future Venus exploration, White Paper to the NRC Decadal Survey, http://ia600604.us.archive.org/1/items/TechnologiesforFutureVenusExploration/TiborSBalint.pdf (accessed on December 15, 2011).
8. Bertaux, J.L., T. Wideman, A. Hauchecorne, V.I. Moroz, and A.P. Ekomonov, Vega 1 and Vega 2 entry probes, *Journal of Geophysical Research* 101, 709–746, 1996.
9. Reh, K., T. Magner, D. Matson, A. Coustenis, J. Lunine, J.-P. Lebreton, C. Jones, and J. Sommerer, *Titan Saturn System Mission (TSSM) Flagship Mission Study Report*, NASA, Washington, DC, 2009. http://opfm.jpl.nasa.gov/files/08_TSSM+Final+Report_Public+Version.pdf (accessed on December 15, 2011).
10. Clark, K., T. Magner, R. Pappalardo, M. Blanc, R. Greeley, J.-P. Lebreton, C. Jones, and J. Sommerer, *Jupiter Europa Orbiter (JEO) Flagship Mission Study Report*, NASA, Washington, DC, 2009, http://opfm.jpl.nasa.gov/files/JEO-Rpt_Public-Release_090203.pdf (accessed on December 15, 2011).
11. McGuire, P.C., M.J. Wolff, M.D. Smith, R.E. Arvidson, S.L. Murchie, R.T. Clancy, T.L. Roush, S.C. et al., MRO/CRISM retrieval of surface Lambert albedos for multispectral mapping of Mars with DISORT-based radiative transfer modeling: Phase 1—Using historical climatology for temperatures, aerosol optical depths, and atmospheric pressures, *IEEE Transactions on Geoscience and Remote Sensing*, 46(12), 4020–4040, December 2008.

3

Extreme Environment Electronics in NASA's Heliophysics Vision

Dana Brewer
National Aeronautics and Space Administration

Janet Barth
National Aeronautics and Space Administration

3.1 Introduction

Heliophysics seeks to understand the variability of the sun, the response of the planets in our solar system, and the impacts of the variability and response on human society. "Helio" is taken from the personification of the sun in Greek mythology. Thus, heliosphere is the area of space including the planets that are influenced by the sun—and that area is our solar system.

3.1.1 The Sun

At the center of our solar system is the sun, our star. This star is the dominant, time-varying source of energy, plasma, and energetic particles in our solar system. Energetic particles are protons with very high energies. The plasma is comprised of high-energy electrons and protons. The energy from the sun (which is typically studied in the extreme ultraviolet wavelength range), or solar wind, can be compared to the heat radiated at the edge of a bonfire. The closer a body is to the energy source, the greater the energy incident upon the body. The edge of our solar system is coincident with the end of the effects from the solar wind.

The sun behaves as a magnetic dipole with strong magnetic field lines. During a minimum in solar activity, the magnetic field lines are aligned. High solar activity occurs when the sun's dipole is in the process of changing polarity, and the associated field lines invert relative to their starting points (see Figure 3.1). Since similar field lines repel each other, tangled magnetic field lines result is high solar activity. During times of high solar activity, there are releases of energy and/or mass, called solar flares and corona mass ejections (CMEs), respectively (see Figures 3.2 and 3.3). The flares and CMEs spurt energy and matter into the heliosphere, and these eruptions have directionality. Streamers from the flares and CMEs may loop back into the sun, and when the loops return to the sun's surface, it is called magnetic reconnection.

Solar physicists study the sun in three areas: (1) the interior of the sun called helioseismology, (2) the surface of the sun where activity is manifested as sunspots, and (3) the outer halo of the sun called the corona. Sunspots are small areas that are cooler than the remainder of the sun's surface.

3.1.2 The Earth and Other Planets with Magnetic Cores

If the flares and CMEs are directed toward the Earth, the electric and magnetic fields in the ionosphere and thermosphere of the Earth can be increased or "charged up," because the Earth's magnetic core and associated magnetic field lines attract the sun's electric and magnetic fields. When electrons and particles (i.e., high-energy protons) enter at the Earth's poles, they become trapped and build up in medium Earth orbit, bouncing from the top of a donut in high northern latitudes to top of the same donut in high southern latitudes. The populations and distribution of these trapped electrons and ions become important when designing and operating Earth-orbiting spacecraft. Figure 3.4 depicts the areas around the Earth where particles and electrons can get trapped during high solar activity. There are two areas surrounded by light shading that are the Van Allen radiation belts. The inner belt is at one to two Earth radii, and the outer belt is at two to six Earth radii. Figure 3.5 depicts the radiation processes that can be observed in and near the radiation belts with in situ observations. Creation and variation of radiation populations result from a complicated interplay of these processes.

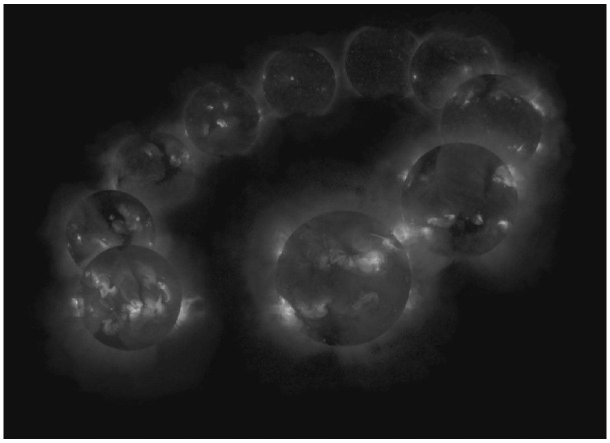

(a)

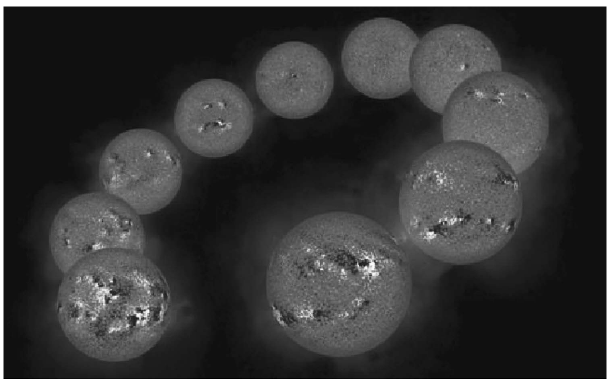

(b)

FIGURE 3.1 **(See color insert.)** Magnetic variations in solar activity during a solar cycle in two wavelengths: (a) first wavelength and (b) second wavelength. The bright pictures in the foreground were taken at solar maximum, and the dimmer pictures in the background were taken at solar minimum. The time period to transition from solar maximum, through solar minimum, and reach solar maximum again is 11 ± 2 years.

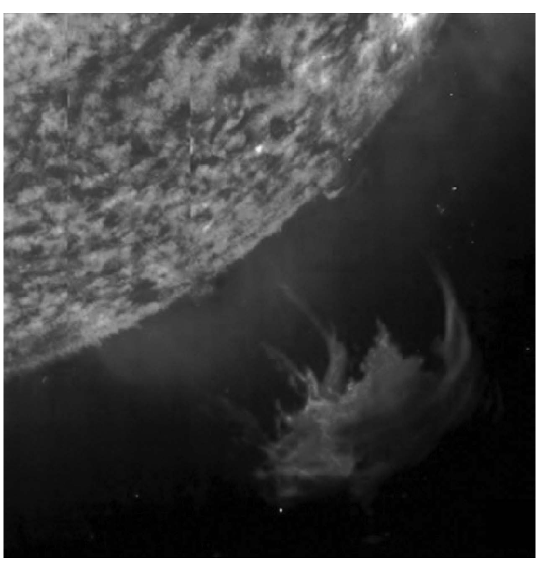

FIGURE 3.2 **(See color insert.)** Picture of a coronal mass ejection/solar flare.

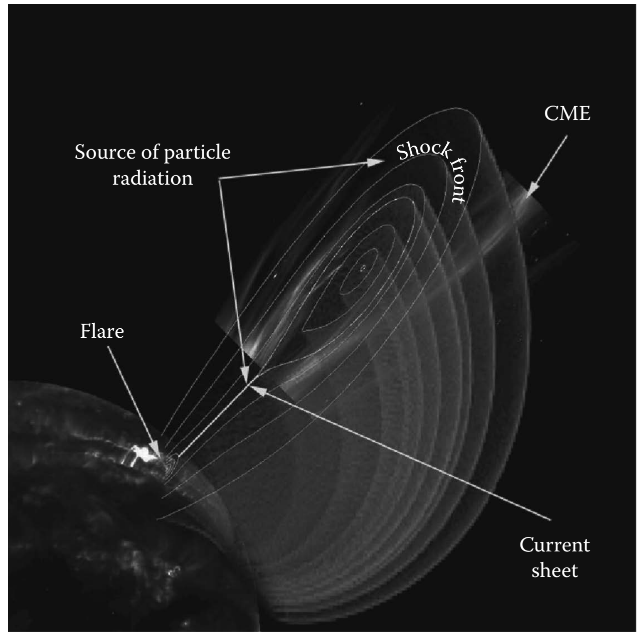

FIGURE 3.3 **(See color insert.)** Components of a solar flare.

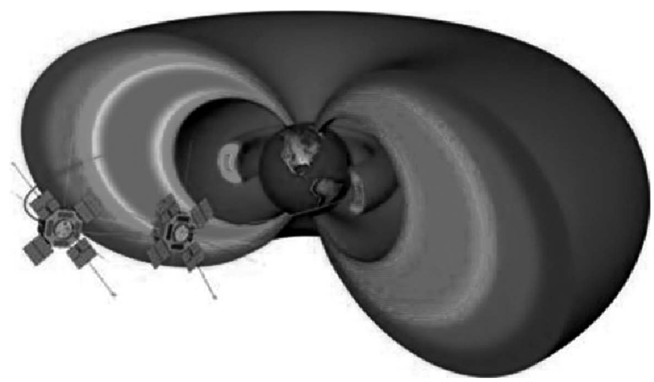

FIGURE 3.4 **(See color insert.)** Areas around the Earth, the Van Allen radiation belts, where particles and electrons can get trapped during high solar activity.

Heliophysics seeks to understand the coupling not only between the sun and the Earth but also between the sun and other planets such as Mars. It is fortunate that both Earth and Mars have magnetic cores, so heliophysics can understand the coupling of the sun with any magnetic planet in our solar system by focusing on the relatively close-in processes between the sun and Earth. Heliophysics science in its entirety investigates processes taking place throughout the solar interior and atmosphere: the evolution and cyclic activity of the sun; the origin and propagation of the solar wind and magnetic field from the sun to the heliopause (the boundary between the solar wind and the interstellar medium); the acceleration and transport of energetic particles in the heliosphere; and the interface of solar influence with the interstellar medium.

Scientists who study the physics of the interaction of the Earth and the sun are called geospace scientists. The geospace

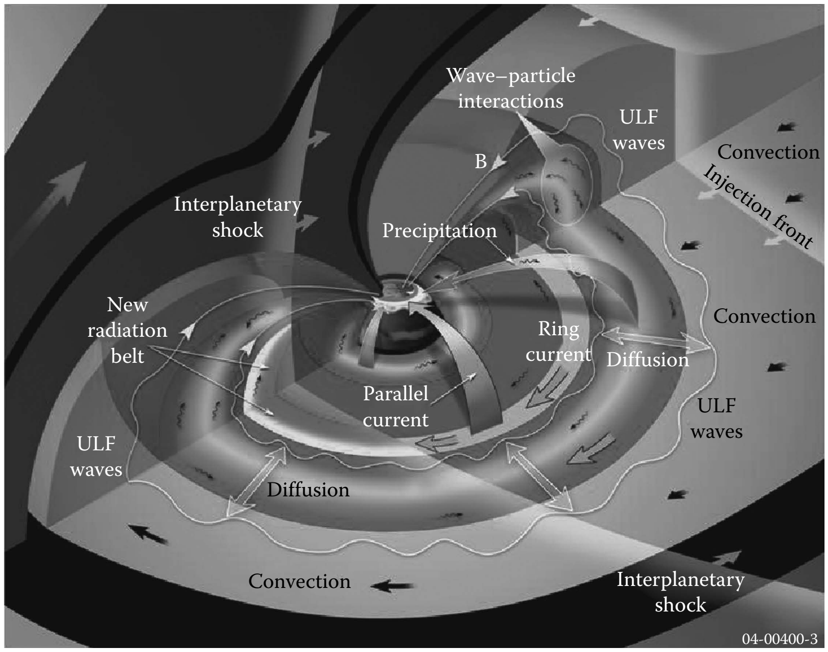

FIGURE 3.5 **(See color insert.)** The radiation belts are regions where radiation processes can be observed with in situ observations.

discipline is often further divided into the study of the interaction of the Earth's radiation belts with the remainder of the atmosphere including magnetic reconnection, and the study of the ionosphere–thermosphere.

3.1.3 Space Weather

The changes in solar activity are called space weather. The consequences of space weather are called space weather effects. These effects include

- Enhanced electromagnetic activity that can affect radio transmissions
- Aurora
- Enhanced levels of charged particles in the Van Allen–trapped radiation belts
- Enhanced radiation dose to spacecraft and aircraft crew members that fly over the poles
- Disruption in power transmission in the higher latitudes
- Single event effects in electronics, particularly in spacecraft and aircraft flying over the poles

3.2 Electronics Technology in Heliophysics Missions

Heliophysics missions are prioritized and selected for development based upon the overall heliophysics science priorities. Science investigations, which include instruments, are selected through a competitive process. The final mission destination and prime operating lifetime are driven by the science that is selected for the mission. The spacecraft attributes and orbital mechanics needed to get to the destination are defined by the selected science. Science missions typically have destinations near the sun, at Lagrange points between the sun and Earth, or near the Earth. Figure 3.6 depicts operating heliophysics missions. Understanding the magnetic and electric fields around the sun and Earth is an important area of research, so typically heliophysics spacecraft is magnetically and electrically clean in the vicinity of the science instruments. In some cases, accommodation of this cleanliness necessitates placing instruments

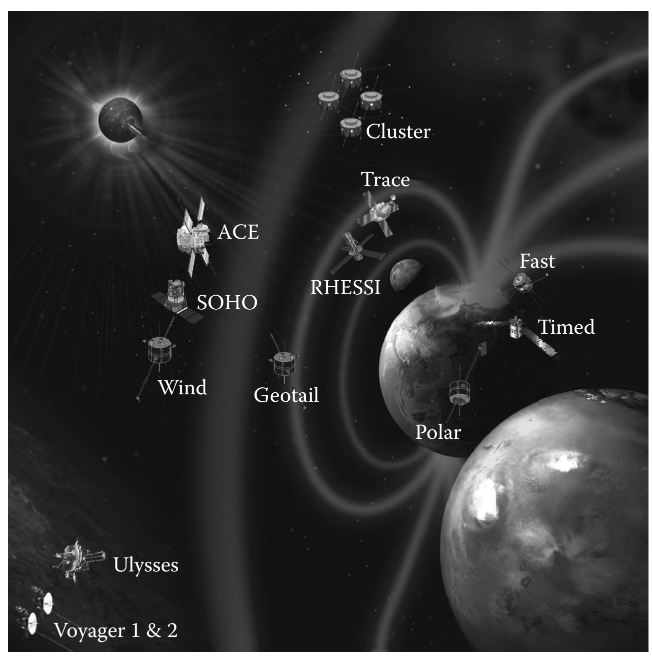

FIGURE 3.6 **(See color insert.)** Depiction of some operating heliophysics science missions.

on deployable booms. The radiation exposure or shielding on a boom may be significantly different than if the instrument was mounted inside the spacecraft, and this must be considered when electronic devices are being selected for missions with booms. In addition, the scientists require “better” data than was available from previous missions, so each mission (and hence the electronics) typically is more complex than previous missions (Figure 3.6).

3.2.1 Electronics Technology for Solar Missions

Instruments on missions that study solar science typically want to image the full disk of the sun and/or measure the particles as well as the electric and magnetic fields of the sun at a cadence coincident or better than the time period for events on the sun. Two missions can serve as examples of the electronics considerations needed in heliophysics solar missions. They are Solar Dynamics Observatory (SDO), which launched in 2010, and ESA’s Solar Orbiter mission.

The SDO mission is in Geosynchronous Earth orbit (GEO). Its instruments collect science data at 120 MB/s and downlink it through 2 Ka band antennas. Full science mission success required that twenty-four 72 day time periods of data are collected during its 5 year prime mission lifetime. In order to collect data for these extended time periods with low error rates, it was very important that the instruments operate during high solar activity. The electronics challenges for this mission were

- Being able to manufacture 2 K × 2 K charge-coupled detectors (CCD) and stitch them together into 4 K × 4 K detectors
- Ensuring that the electronic devices responsible for clearing the detectors and transferring the data for downlink had their timing synchronized (since this was the first time that these much data were being collected and downlinked using Ka band communications)
- Maintaining the data integrity and very low error rate through transmission from the spacecraft to the ground antennas and then to the scientists at locations away from the antennas
- Operating in the high-radiation GEO location which introduced possibilities for frictional electrostatic discharge and deep dielectric discharge
- Ensuring operation during periods of high solar activity

Some mitigation of the discharging was introduced by using conductive external spacecraft surfaces to bleed off excess charge and checking/rechecking that the surfaces and structure were adequately bonded together. For the spacecraft power system, parts have very little protection in the vicinity of the solar arrays, so care was needed in parts selection for the power system applications. Often Heliophysics missions use electronics in ways that are not the ways they are routinely used on Earth; that is, registers that are not routinely addressed in ground applications may be used in space applications, and the space applications may then introduce problems with parts and devices that had not been identified in the past. The market for radiation-hardened parts is limited, so it was necessary not only to procure the parts but also to verify that they operated as expected. In more than one case, the advertised and actual operating voltages did not coincide. Finally, workmanship of both parts and boards became a significant issue and required diligent inspections to meet the specifications.

The Solar Orbiter mission has a different scenario than SDO. It will be launched out of the Earth’s atmosphere, have a cruise phase that includes Earth and Venus gravity assists to increase the speed of the spacecraft, and then have an operational phase orbiting the sun. Initially it will orbit equatorially and after several orbits, it will use a series of Venus gravity assists to change the orbit from equatorial to increasingly higher heliolatitudes. The distance of closest approach to the sun will be about 62 solar radii. The Observatory’s remote sensing instruments may be taking data during the cruise phase, and both the in situ and remote sensing instruments will collect data during its orbits around the sun. The electronics for this mission will need to be selected so that they are capable of operating both during the cruise phase and during the high temperatures present close to the sun. The NASA imager has a 4 K × 4 K active pixel sensor (APS) detector. This mission will be the first time that an APS detector of this size will be stitched together and flown. The solar cells and associated power electronics will also require attention due to the operational environment and the relative inability to protect them from the heat from the sun and space weather; whether the heat will affect the materials and electronics selections has not been determined but will be addressed prior to exiting from critical design review, where 90% of the drawings are expected to be completed. The imager detector will also need to be mindful of the effect of its field of view due to light reflection by the solar arrays; devices or other means to correct for the absence of a clear field of view may be needed.

The Solar Probe Plus mission will explore the last region of the solar system to be visited by a spacecraft, the sun’s outer atmosphere, or corona as it extends out into space. Solar Probe Plus will repeatedly sample the near-sun environment, revolutionizing our knowledge and understanding of coronal heating and of the origin and evolution of the solar wind and answering critical questions in heliophysics that have been ranked as top priorities for decades. Moreover, by making direct, in situ measurements of the region where some of the most hazardous solar energetic particles are energized, Solar Probe Plus will make a fundamental contribution to our ability to characterize and forecast the radiation environment in which future space explorers will work and live. The Solar Probe Plus spacecraft will fly within 9.5 solar radii of the sun, posing challenges for the design of the electronics. As the spacecraft approaches the sun, its heat shield must withstand temperatures exceeding 2500 F and blasts of intense particle radiation. Estimating the levels of high-energy, penetrating radiation levels to which the spacecraft will be exposed is particularly challenging due to the lack of high-energy particle measurements at less than 1 astronomical units (AUs) from the Earth. This may require the use of large margins in the predicted levels of total ionizing dose and single event effects rates.

3.2.2 Electronics Technology for Geospace Missions

Geospace missions typically address one of two categories: either they are ionosphere/thermosphere (I/T) missions or they are radiation belt missions. The I/T missions address the interactions, drivers, and energy exchange between the layers of the atmosphere and how the sun influences the changes. The radiation belt missions address how and why the belts change as a function of time and solar activity.

The science for these missions requires multipoint measurements, so often missions contain multiple spacecraft that are launched from a single launch vehicle and operated independently. There are several instances where the only difference between the multiple spacecraft is the frequency with which each spacecraft is commanded from the mission operations center. Examples of multi-spacecraft missions are Magnetospheric Multiscale and Radiation Belt Storm Probes.

The geospace mission science measures the magnetic and electric fields, so the spacecraft and instrument electronics need to be magnetically and electrically clean. This is sometimes accomplished by placing instruments at the tips of long booms. The area of space where the geospace missions operate is also a very harsh environment, so even if the spacecraft is single string, selective redundancy is employed to achieve the full science success and operational lifetime. The advice for selecting electronic devices for the solar missions also applies to the geospace missions. That is, electronics may use registers that are not routinely used in applications on the ground, so verification of correct performance is essential. Workmanship problems must also be anticipated, because all the heliospheric missions are one-of-a-kind mission, and the goal of each mission's science is to advance (or be better than) the last mission.

4

Overview of the NASA ETDP RHESE Program

Andrew S. Keys
National Aeronautics and Space Administration

4.1 Introduction and Context

On January 14, 2004, President George W. Bush held a press conference at the headquarters building of the National Aeronautics and Space Administration (NASA) in Washington, DC, to announce a new direction for the nation's space agency. Almost one year prior to the announcement, on February 1, 2003, NASA and the rest of the world witnessed the tragic loss of the Space Shuttle Columbia, causing much uncertainty about the future of the space shuttle program and the still incomplete International Space Station. With this second loss of a space shuttle vehicle (the first being the 1986 loss of the Space Shuttle Challenger), there was a growing concern that the shuttle program may be suddenly, and irreversibly, ended much sooner than previously anticipated. The agency needed a new direction that would guide space exploration through the shuttle's planned Return to Flight and into a new era of space vehicle development and operation.

The announcement made by President Bush at that 2004 press conference articulated a new direction for manned and robotic exploration of the solar system. Referred to as the "Vision for Space Exploration" [1], or VSE, this inspirational plan described a framework for exploration that was scoped to be sustainable, flexible, and affordable under the predicted flat budget anticipated by the agency for years to come. The primary goal of the VSE was to advance U.S. scientific, security, and economic interests through a robust space exploration program that would, among other goals, return humans to the lunar surface by 2020.

After some initial formulation efforts, NASA conducted the *Exploration Systems Architecture Study* [2], which, in turn, was the basis for the development of the Constellation program, a set of space exploration vehicles that were specifically formulated to achieve the goals as defined within the VSE. The Constellation program was designed to have the flexibility not only to accommodate missions to the lunar surface, but also to provide the infrastructure for future missions to near earth asteroids, the small moons of Mars, and eventually the Martian surface. The Constellation program included the following elements:

- A crew exploration vehicle named "Orion"
- A new man-rated launch vehicle called the "Ares I" capable of launching the Orion capsule into low Earth orbit
- An eventual heavy-lift launch vehicle called the "Ares V" capable of propelling up to 180 metric tons of payload into Earth orbit
- A lunar lander named "Altair" that could provide cargo and human access to the lunar surface
- An Earth Departure Stage designed to be launched as an upper stage for Ares V and intended to boost the Altair and Orion spacecraft out of Earth orbit and across cislunar space
- The surface system infrastructure needed to support an outpost on the lunar surface for permanent habitability
- The Extra Vehicular Activity suits required to explore the surface of the moon
- The ground system launch and operations support for all Constellation missions

The architects of the Constellation program understood that the goals of the VSE and the elements of the Constellation program would require the development of new technologies not currently available. To provide these new technologies, NASA established a "sister program" to Constellation, the Exploration Technology Development Program (ETDP). Established in 2005, the ETDP was managed by NASA's Langley Research Center (LaRC) and consisted of 22 individual technology development projects [3]. Collectively, the projects covered the broad range of technology anticipated to be required to support and enable the success of the Constellation program. Specific to this text, one of the ETDP projects was the Radiation Hardened Electronics for Space Exploration (RHESE) project. This chapter serves to provide a justification for the RHESE project, a description of the project's multiple development tasks, and a review of project accomplishments achieved between 2005 and 2010 [4–7].

4.2 Radiation Hardening for the Space Environment

Not since 1972, with the successful launch and return of the Apollo 17 mission, have humans ventured beyond low Earth orbit. Just as with the Apollo missions, the Constellation program endeavored to launch crew and cargo into the deep space environment and on to the lunar surface. It has long been known that the deep space environment poses a particular radiation hazard to both organic and inorganic materials. In general, the high-energy particles that constitute the radiation hazard within the space environment originate from three sources [8]:

1. Proton and electron radiation trapped within the Earth's magnetic field
2. Solar coronal mass ejections
3. Galactic cosmic rays

The high-energy particles encountered in the deep space environment typically possess energies that range from the lower level of less than 1 MeV as possessed by particles in the Earth's radiation belts to beyond the predicted upper limit of ~5×10^{19} MeV (known as the Greisen–Zatsepin–Kuzmin [GZK] limit [9,10]) as inexplicably exhibited by extremely energetic galactic cosmic rays. At these energies, the particles are capable of passing deep into, and in some cases completely through, the encountered material, causing localized ionization and occasional atomic displacement. Because electronics operate based on the principle of controlled carrier diffusion within the semiconductor material, the flood of ions produced by a localized passing of a single high-energy particle easily causes the electronic device to perform unpredictably. This occurrence is generally known as a single event effect (SEE).

Though sources of space radiation are well understood and characterized, the problem still remains of how to protect the spacecraft, its occupants, and its electronics from the deleterious effects experienced when encountering space radiation. Multiple solutions exist that provide some level of protection. The most basic solution is to provide material shielding for the radiation-sensitive components of the spacecraft. By including additional material around the component to be protected, there is a much greater chance that a high-energy particle will be stopped via its interaction with the shielding material prior to reaching the component. The obvious problem with using shielding on a spacecraft is the mass penalty paid when attempting to place the entire system in orbit. One interesting approach to shielding includes the strategy for a manned mission to carry the potable and wastewater in locations that provide maximal radiation shielding [11] thus allowing the water to serve two purposes. It should also be realized that shielding will protect from lower-energy particles, but higher-energy particles may penetrate the shielding regardless of its practical thickness. Shielding also introduces the risk of induced Bremsstrahlung, or secondary, radiation caused by the interaction of high-energy particles with the constituent particles of the shielding material.

Another consideration in developing protection for a spacecraft and its contents from radiation damage includes the aspect of mission design. If it is possible to select a mission profile that minimizes the exposure of a spacecraft to environmental radiation and thermal extremes, then this should be included in the mission design trade space. As an example, if a spacecraft's orbit can be specified such that it minimizes its encounters with the trapped radiation of Earth's radiation belts, then this should be considered as a factor in the design trade space. By a similar argument, if a lunar landing location may be selected such that it minimizes direct exposure to the sun by allowing the landing site to spend half a lunar orbit with the lunar body acting as a shield from potential solar particles, then this too should be considered. However, this trade must be made against the benefits of solar exposure to lunar surface power generation systems and thermal regulation considerations.

Another approach to providing operational assurance is the process of designing critical systems to include redundant electronic strings of components, thereby reducing the chance that space radiation will cause adverse effects to the system's performance. The spacecraft designer may choose to implement triple module redundancy (TMR) within the logic circuits of the flight electronic component [12]. This approach involves using three strings of logic circuitry that all feed into a set of voting logic circuitry. Between the three circuit inputs, the majority digital state is forwarded as the solution while the minority digital state is discarded. The practice of TMR may be extended beyond the digital circuitry level to include multiple components, processors [13], and even subsystems [14] that feed an overlying layer of voting logic to determine the majority answer. This approach to radiation hardening can be loosely identified as radiation hardening by architecture (RHBA). One could argue in an extreme case of redundant system engineering that multiple and totally redundant spacecraft would statistically improve the chances of mission success [15]. However, in the case of manned missions, there are no redundant crews. Even in the case of an unmanned mission, redundant spacecraft are expensive. The process of assembly, verification, and validation of flight hardware, launch services, and operations of multiple flight systems could increase a mission's total cost considerably.

Beyond RHBA, the next level of hardening electronic components is referred to as radiation hardening by design (RHBD). RHBD implies that an electronic part or board has been radiation-hardened by virtue of the component layout and circuit architecture of on-chip gates, devices, and interconnects independent of any special fabrication process or technique. Examples of RHBD techniques include using TMR strategies within the chip layout, designing dopant wells and isolation trenches into the circuit layouts, implementing error detecting and correction circuits [16], and using device spacing and decoupling design rules. Disadvantages to these techniques include the extra devices required to implement TMR, the extra power load these devices consume, and the extra chip area required to isolate devices, gates, and latches.

Radiation hardening by process (RHBP) is the lowest level of hardening where the actual electronic transistor components of the electronic device have been fabricated with materials and process techniques that temper the component against a SEE radiation event. Material selection, insulation layers, doping levels, and proprietary processing steps are a part of RHBP. Unfortunately, this is an expensive method for radiation hardening as the process that hardens the part is dependent on dedicated foundry lines and part runs. The market for radiation-hardened devices is very limited and the expense of developing a new component using a RHBP usually does not justify the effort—particularly when the part is customized for a spacecraft application where a run of approximately 10–20 parts would completely satisfy the spacecraft's test and assembly needs. Because of the expense and special foundry requirements to produce electronics that utilize RHBP techniques, the capabilities of these RHBP radiation-hardened electronics (power consumption, processor speed, feature size, etc.) tend to lag the capabilities of commercial electronics by a decade or more.

Of course, the spacecraft designer has the option of implementing any or all of these radiation damage mitigation techniques in any combination. Depending on the criticality, value, and acceptable risk associated with the mission being developed, the specified hardness of the onboard electronics may range from commercial-grade parts assembled with no redundancy under minimal material shielding to parts that are radiation-hardened via RHBP techniques running in a TMR voting configuration under heavy localized material shielding. It is therefore obvious that the process of developing a flight system, complete with modern electronics and avionics, capable of continual operation within the extreme environments of space, is not a trivial task.

4.3 RHESE Project Description and Tasks

The process of identifying and specifying avionic systems that will properly and reliably perform within the deep space environment is a critical step in the development of modern space platforms. In fact, so critical is this process to NASA's success in spaceflight that spacecraft developers have defined a radiation hardness assurance (RHA) methodology process [17]. In general, the process may be described by the following steps:

1. Define the radiation hazard
2. Evaluate the hazard
3. Define the requirements to be met by the spacecraft's electronics
4. Evaluate the electronics to be used
5. Engineer processes to mitigate hazard damage
6. Iterate on the methodology, if and when necessary

The RHESE project was formulated to assist in providing avionic technologies to the Constellation program that are successful in mitigating the hazard damage as identified in step 5 of the RHA methodology. However, at the time of the RHESE project's establishment in 2005, the Constellation program had not yet proceeded to accomplish step 3 of the RHA methodology—to define the spacecraft's environmental requirements for avionics. The long lead time required for technology development within the RHESE project could not tolerate a developmental delay until all Constellation program environmental requirements had been established. Therefore, the project proceeded to supplement the higher-level requirements of the Constellation program with derived environmental performance requirements for electronic components based on multiple inputs including architecture studies, working group discussions, technical interchange discussions, and RHESE team-resident knowledge of system and architecture objectives.

Collectively, the defined environmental performance requirements within the RHESE project were used to specify the following project objectives:

- Improve total ionization dose (TID) tolerance
- Reduce single event upset (SEU) rates
- Increase threshold for single event latch-up
- Increase sustained processor performance
- Increase processor efficiency
- Increase speed of dynamic reconfigurability
- Reduce operating temperature range's lower bound
- Increase the available levels of redundancy and reconfigurability
- Increase the reliability and accuracy of radiation effects modeling

To quantify these objectives, the project defined key performance parameters and task capabilities. These are listed in Table 4.1 along with the threshold and goal performance levels for each parameter. Note that because RHESE technology products are very diverse in nature and span between software and hardware developments, not all of the listed capabilities and performance parameters in this table were applicable to all RHESE technology products. But the parameters do provide a standard metric for measuring and quantitatively testing the maturity of a particular technology. Measurements of the performance value through testing provided a method for determining the technology readiness level (TRL) [18] of each RHESE technology product. The Constellation program generally expected any new technology to be matured to a TRL 6 prior to the preliminary design review (PDR) of the Constellation program element that intended to use the technology. Therefore, RHESE's parent program, the ETDP, likewise required technologies to be tested

TABLE 4.1 Key Performance Parameters for RHESE Technology Development Tasks

Key Performance Parameters	Units	Threshold Value	Goal Value	TRL
Total ionizing dose (TID)	Mrad	0.1 (Si)	0.3 (Si)	6
Single event upset rate	errors/bit-day	1.00E−12	1.00E−13	6
Single event latch-up threshold	$MeV \cdot cm^2/mg$	100	Immune	6
Sustained processor performance	MIPS	500	3000	6
Sustained processor efficiency	MIPS/W	500	2000	6
Speed of dynamic reconfiguration	s	1	1.00E−03	6
Temperature range	°C	−180	−230	6
Redundancy and reconfigurability	Levels of reconfigurability	3	4	6
Radiation model accuracy	Number of technologies included	2	4	6
Storage density	GB/cm^2	1	100	6
Storage efficiency	%	95	100	6

at TRL 6 prior to their use by the Constellation program. TRL definition levels are briefly described in Figure 4.1.

The RHESE project was formulated to provide advancements in environmentally hardened flight electronics and avionic systems. Investment areas included new materials, design processes, reconfigurable hardware techniques, and software techniques. Near-term emphasis within the RHESE project began with tasks that could use existing hardware components and design technologies to prove out radiation-hardening techniques, such as the radiation hardening of commercial field programmable gate arrays (FPGA) architectures, the use of FPGA devices to study reconfigurable computing architectures, and the use of semiconductor materials (such as silicon–germanium) to develop basic circuit designs that provided tolerance to radiation events and low-temperature environments. As these technologies matured, the project planned to shift its focus to efforts requiring more advanced design work and fabrication efforts such as total processor hardening techniques and complex SiGe-based devices. Had the Constellation program continued, this phased approach to technology product development used by the RHESE project would provide hardened FPGA devices and environmentally hardened electronic units for mission infusion into early Constellation projects, such as the Orion crew exploration vehicle and, later, the Ares V launch vehicle. Once these technologies began the infusion process, the next phase of RHESE technology product development would provide hardened high-speed processors, associated hardened bulk memory, and high-density data storage for the longer duration missions such as the Altair lunar lander, the planned lunar outpost, and eventual Mars exploration missions.

The specific technology product tasks within RHESE were broad-based and diverse. They collectively included the development of total dose radiation-tolerant electronics, SEU-tolerant electronics, latch-up tolerant electronics, high-performance processors, low-temperature electronics, reconfigurable robust

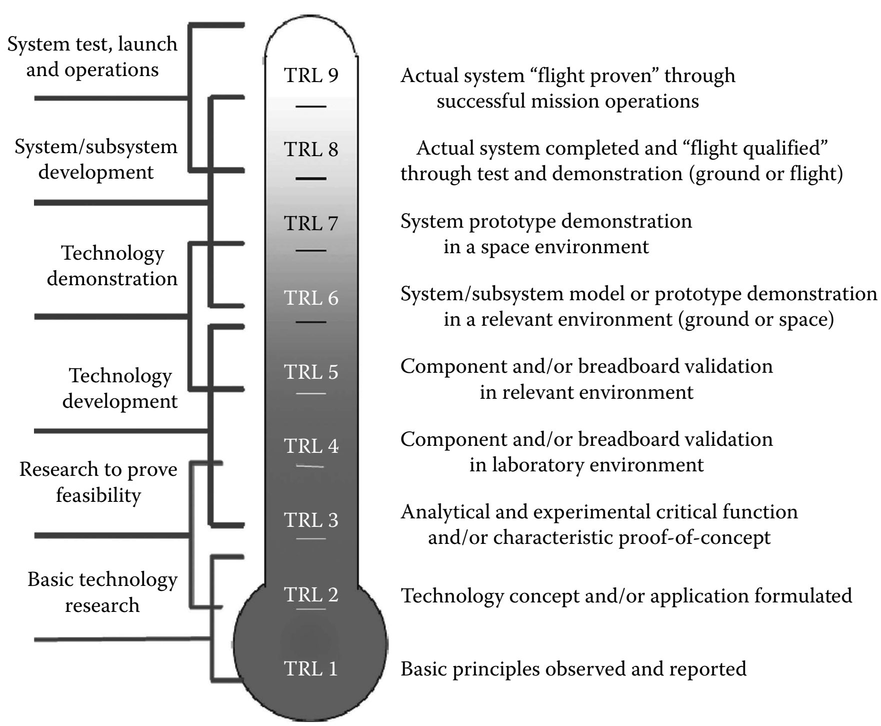

FIGURE 4.1 NASA technology readiness level definitions.

electronics, and updated models capable of predicting the effects of radiation on electronics. Specifically, the RHESE tasks were

- Modeling of radiation effects on electronics (MREE)
- SEE-immune reconfigurable FPGA (SIRF)
- Radiation-hardened high-performance processors (HPP)
- Reconfigurable computing (RC)
- Silicon–germanium (SiGe) integrated electronics for extreme environments

Following an initial description of the RHESE project management function, each of these technology product tasks is described.

4.3.1 RHESE Project Management

The RHESE project management function handled the day-to-day administrative and programmatic concerns of the project including budget planning, schedule development, accomplishment monitoring, risk assessment, and project execution. NASA's Marshall Space Flight Center (MSFC) managed the RHESE project. The RHESE project management function served to enable the technology product tasks and to represent featured accomplishments to the ETDP program office. As technologies grew to a maturity of TRL 6, it was the job of the RHESE project management function to ensure a proper infusion plan was developed and implemented. The baselined RHESE Project Management Plan captured the details concerning the programmatic management of the RHESE project and the specifics of each technology product task.

As a strategy to reduce duplicative efforts between NASA and other government-sponsored developers that may also be investing in environmentally hardened electronic and avionic technology, it was the responsibility of the RHESE project management function to be cognizant of external activities and investments made by these other U.S. government agencies, federal laboratories, academic institutes, and commercial developers. The RHESE project management function also worked in partnership and collaboration with these other organizations where appropriate. Collaborative efforts provide benefit in that they can leverage technology investments from multiple sources to deliver products that may otherwise not be realized through independent and competing efforts.

To maintain cognizance of current development activities, the RHESE project manager and task leads regularly attended reviews, presentations, and conferences where multiple other non-NASA technologists were working to improve the state of the art in radiation-hardened electronics. The RHESE project was represented at many of these gatherings to discuss and coordinate technology development activities, including the American Institute of Aeronautics and Astronautics's (AIAA's) annual SPACE conferences, the Air Force Research Laboratory (AFRL)–sponsored Radiation Hardened Electronics Technology workshops, the Institute of Electrical and Electronics Engineers (IEEE) annual Aerospace conferences, the Government Microcircuit Applications and Critical Technology (GoMACTech) annual conferences, and the IEEE Nuclear Science and Radiation Effects Conference (NSREC) annual conferences.

4.3.2 Model of Radiation Effects on Electronics Technology Task

The RHESE project's MREE task focused on developing an updated model of the detrimental effects that radiation may have on modern electronic devices. The previously used model, Cosmic Ray Effects on Micro Electronics 96 (CREME96) [19], had for years been the industry standard modeling tool for estimating the occurrence probability of SEEs in electronics. However, since its release in 1994, the state of the art in microelectronics continued to advance toward architectures and device designs that incorporate smaller feature sizes, more complex and multilayered structures, and the use of heavy metals—all of which make today's modern electronic architectures more susceptible to SEEs and radiation-induced failures. The paradigm for SEE prediction in the CREME96 model was deficient in accounting for these advanced electronic device technologies. The CREME96 model had further deficiencies in that it assumed the ionization trail left by a high-energy particle is much smaller than the minimum feature size of the affected electronic structure, an assumption that is no longer true when considering the ever-decreasing feature sizes used to create modern electronic devices. Since CREME96 was developed, the minimum feature size has shrunk by more than a factor of 100. As a result, the interaction between track microstructure and device characteristics can no longer be ignored. This assumption in CREME96 has been shown to have significant shortcomings when applied to new and emerging technologies like advanced complementary metal-oxide-semiconductor (CMOS) electronics, SiGe heterojunction bipolar transistors (HBTs), photodiodes, and infra-red focal plane arrays (IR FPAs). Also, CREME96 assumed that the SEE sensitivity of individual microcircuits could be idealized as a single sensitive junction, allowing an estimated SEE occurrence rate to be assessed through the calculation of the linear energy transfer (LET) rate of the ionizing particle versus the cross section of this single sensitive junction.

It was therefore the primary goal of the MREE task to develop a more physics-based approach to SEE prediction that provides accurate results for modern electronics parts. The resulting model code, referred to herein as CREME-MC, consists of two parts: one part for simulating the propagation of the radiation environment through the hosting spacecraft structure and into the sensitive electronic component and a second part for calculating the effects of the radiation on this electronic component. The "MC" portion of the model refers to the use of Monte Carlo modeling techniques used to provide a probability distribution for radiation particle impingement on the electronic device being assessed.

MSFC and Vanderbilt University jointly developed the CREME-MC tool with each participant being responsible for different portions of the effort. MSFC was responsible for providing the radiation environment models to be used for the estimation of SEE and total ionized dose under various space weather conditions. Models that define the space environment, including the lunar neutron environment, the galactic cosmic ray environment, and the solar particle environment, have all been updated over the past few years. MSFC also provided computer codes to propagate the external radiation environment through the actual design of the spacecraft structure to the component being investigated. During propagation, the effects of nuclear interactions and energy loss by ionization are taken into account. This allows accurate estimates to be made of total dose and single event rates for the device under investigation as positioned in its designed location within the space vehicle under any chosen external environment model and in any chosen orbit. Because the models will employ an accurate definition of the surrounding spacecraft structure to determine radiation shielding effects, this tool may provide additional benefit to NASA's efforts in assessing the protection provided by structures to biological and human crew within radiation environments. To allow the user to maintain control of the detailed computer-aided design (CAD) of his spacecraft, this part of the model is downloaded and executed on the user's local computer equipment. The result is a description of the local radiation dose and environment, internal to the spacecraft, surrounding the part of interest. Users of this code can upload this internal radiation environment to the CREME-MC code as hosted on a Vanderbilt website. Alternately, the CREME-MC website tool can be used to compute a radiation environment internal to the spacecraft as experienced by the component being assessed through the assumption of a single layer of shielding of uniform thickness that surrounds the part.

Vanderbilt University is responsible for providing users with the ability to construct a representative model of the physical structure of the microelectronic circuit within the semiconductor material and then to propagate the individual radiation particles from the calculated internal radiation environment into and through the device structure. Just as with actual transistors and junction devices, the representative model can be constructed to contain multiple sensitive volumes that are used to estimate charge collection within the modeled device. The Vanderbilt-developed code used to assess the charge collection in the modeled device is called the Monte Carlo Energy Deposition (MRED) code [20]. This code employs a Monte Carlo, repetitive sampling engine to determine a probability distribution of charge collection as based on the propagated internal radiation environment. The MRED code was built around GEomertry ANd Tracking 4 (GEANT4) software libraries [21,22]. Simulation improvements using these codes can account for nuclear-to-nuclear reactions, energy loss, and hole–electron pair creation by the ionizing particle within and nearby the microelectronic circuit components.

At the time of this writing, the CREME-MC website tool [23] is accessible online for general use, but does require the user to request a user account from the system administrator. The CREME-MC website tool is hosted on servers maintained and operated by Vanderbilt University. MSFC was responsible for the programmatic management of the MREE task.

4.3.3 SEE-Immune Reconfigurable FPGA Technology Task

The FPGA is an electronic component that has experienced widespread usage in multiple applications due to its ease of programmability. Because the FPGA can be programmably customized, it is also an inexpensive and attractive alternative to the design and development of a non-programmable, hardwired application-specific integrated circuit (ASIC). FPGAs are available in multiple architectures. The most common is the static random-access memory (SRAM)–based FPGA, which can be reprogrammable within an active system to perform a large variety of functions. But they are much like volatile memory in that most of these FPGAs require reconfiguration after each power cycle. Also, due to their CMOS-based architecture, they are susceptible to radiation events. Antifuse FPGAs solve the volatility and radiation susceptibility problem by allowing a single configuration to be permanently programmed onto the device. The nature of the antifuse architecture makes it intrinsically radiation-hardened, but the obvious disadvantage of this architecture is that it can only be programmed once prior to use.

In an effort to address the radiation hardness of a SRAM-based FPGA, the RHESE project teamed with multiple government and industry partners to support the development of a radiation-tolerant version of the Xilinx Vertex-5 FPGA. The resulting device would yield the benefits of reconfigurable hardware without the usual loss in capability typically required to harden reconfigurable devices to radiation effects, such as increased chip area, reduced speed, increased power, and increased complexity. SIRF FPGAs could be used to implement systems that incorporate radiation-tolerant reconfigurable interfaces and digital interconnects. This capability was planned to facilitate the design of common "plug-and-play" modular, adaptive, and reconfigurable subsystems. Such subsystems could be field-programmed and reprogrammed to implement multiple functions in diverse systems.

A SIRF-based processor board could, for example, be removed from a lunar storage depot and inserted into a rover navigation system. Upon insertion, the board, if developed with RC techniques, could autonomously download configuration data, configure its electrical interfaces and internal interconnects, and execute the desired functionality. It could also continuously monitor its performance and self-reconfigure to mitigate faults, should they occur. This same board could then be removed from the rover and, if needed, be moved yet again to a different platform to replace a malfunctioning board in an oxygen-generating system. Once inserted, it would autonomously configure for this application. Significant systems efficiencies including development, fault tolerance, maintenance, repair, and inventory control would result from this capability.

Since gate array–based processors demonstrate significant performance advantages over serial processors when implementing tasks that can be parallelized, a SIRF-based avionic board could be used to process high-bandwidth, back-end applications such as vision processing, radar, and LIDAR imaging.

SIRF could have the additional advantage of being able to realize this performance advantage without the inefficiencies associated with SEE mitigation techniques. Investments in the SIRF project formed the basis of the Xilinx Virtex-5QV FPGA, released in July 2010.

Though the effort was primarily supported by the SIRF task partners, NASA provided funding for the SIRF development and also provided complimentary analysis of the SIRF technology to determine applicability to future space systems. NASA's Goddard Space Flight Center (GSFC) was responsible for the programmatic management of NASA's involvement in the SIRF task.

4.3.4 High-Performance Processors Technology Task

Certain capabilities within the Constellation architecture, such as autonomous spacecraft operations, surface mobility, and hazard avoidance and landing, would require reliable computational processing power. The issue with this need is not that there are no commercial processors capable of providing the necessary computations required to handle these capabilities. This issue is that there are limited or no commercial processors that are low-power, radiation-hardened, high-throughput, and flight-validated and that are also capable of providing the necessary computations required to handle these capabilities. The RHESE HPP task sought to expand the capabilities of flight computer systems by advancing the sustained throughput and processing efficiency of high-performance, radiation-hardened processors while seeking processor architectures that minimized power consumption. The performance and power efficiency of processors developed specifically for the space environment historically lags that of commercial processors by multiple performance generations. The highest performing radiation-tolerant, commercially produced electronics offer increased performance at the expense of reduced power efficiency. The HPP task endeavored to concurrently advance the state of the art of these two metrics: sustained throughput and processing efficiency.

The need for power-efficient, high-performance, radiation-tolerant processors and related peripheral electronics required to implement modern flight systems is not unique to NASA; this capability could also benefit commercial aerospace entities and other governmental agencies that require highly capable flight processors. This task therefore sought to leverage, to the extent practical, relevant external technology and processor development projects sponsored by other government agencies. Accordingly, important factors in defining and implementing the HPP strategy and implementation were the investment plans of these organizations and cognizance of relevant prior and ongoing NASA investments.

By the time the HPP task completed in 2010, two promising processor development activities were evaluated for their suitability for use in NASA's manned spaceflight program: the HyperX and the Maestro processor architectures.

4.3.4.1 HyperX Architecture

The Coherent Logix (CLX) HyperX architecture was developed in a collaborative Department of Defense (DoD) program; partners included the AFRL, the Office of Naval Research (ONR), Defense Advanced Research Projects Agency (DARPA), Army Research Laboratory (ARL), Missile Defense Agency (MDA), the Space and Naval Warfare Systems Command (SPAWAR), and others. A follow-on collaborative effort between CLX, the RHESE project, and NASA's Innovative Partnership Program (IPP) entitled "Extremely High-Performance, Ultra-Low Power, Radiation-Tolerant Processor: An Enabling Technology for Autonomous and Computationally Intensive Capabilities" was selected for funding by the IPP. The goal of this effort was to assess the performance and radiation susceptibility of the base HyperX processor, and then formulate and implement radiation-hardening strategies. The effort was awarded in 2008 and established a baseline radiation test of the HyperX processor within ground facilities. Test results formed the basis for SEE radiation mitigation strategies that were developed in 2009 and validated in a follow-on radiation tests within ground facilities.

To further validate the radiation mitigation techniques, four HyperX processor boards were flown as a part of the Materials International Space Station Experiment-7 (MISSE-7). The MISSE series of flight experiments provided an opportunity to assess the performance and functionality of various hardware components and materials during long-duration exposure to the space environment. In 2009, the HPP task supported MISSE-7 integration efforts to deliver the flight version of the HyperX processor for integration into the MISSE-7 experiment. Launch of MISSE-7 occurred in November 2009. Onboard the experiment, two of the four Hx boards were powered and programmed to repeatedly execute Fast Fourier Transform (FFT) algorithms in an infinite loop. They were monitored for radiation-induced SEEs during the lifetime of the project. Figure 4.2 shows two photos of the HyperX hardware as flown aboard the MISSE-7 experiment.

4.3.4.2 Maestro Architecture

The second processor development activity worked within the HPP task was the assessment of the Maestro Processor chip. This effort began as a DARPA initiative to develop a flexible, multicore processor that performs with a high level of efficiency across all categories of application processing, ranging from bit-level stream processing to symbolic processing, and encompassing processor capabilities ranging from special purpose digital signal processors to general purpose processors. Known as the Onboard Processing Expandable Reconfigurable Architecture (OPERA) effort, this system combined a RHBD multicore processor chip called "Maestro" as developed by Boeing's Solid State Electronics Department and multicore compiler tools and parallel processing libraries as developed by Information Sciences Institute (ISI) East, a unit of the University of Southern California's Viterbi School of Engineering.

The Maestro processor has heritage in intellectual property from Tilera's Tile-64 chip, a non-hardened 64 processor multicore commercial chip. With this IP, the Maestro was developed to be a

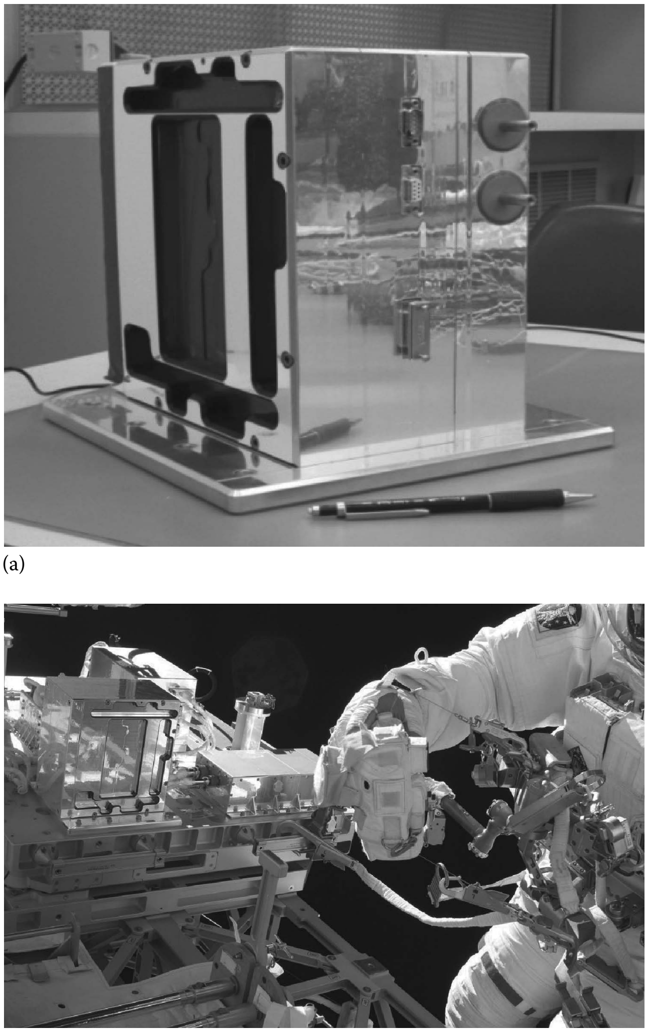

(a)

(b)

FIGURE 4.2 HyperX flight hardware (a) and HyperX experiment on-orbit during MISSE-7 installation on ISS (b).

RHBD version of the Tile-64 chip (part number TLR26480). The Maestro has 49 cores arranged in a 7 × 7 tile array. The chip was developed and fabricated using the IBM 9SF, 90 nm CMOS fabrication process. Target performance criteria included an operating clock speed of 480 MHz enabling the full complement of processors to perform up to 70 giga operations per second (70 GOPs). Power dissipation was planned to be less than 28 W with that power level being downwardly adjustable through processor programming. The radiation hardness was targeting a total ionized dose of 500 krad and a single event latch-up tolerance of greater than 100 (LET in MeV · cm^2/mg). Using these specifications to drive development, the fabricated Maestro processor wafers were delivered for testing on March 9, 2010. Radiation tests of packaged devices were performed over the summer of 2010.

Test results for the Maestro processor required a necessarily reduced clock speed from 480 to 260 MHz. This provided a resulting processing performance of 38 GOPs. Power dissipation was measured to be 14.4 W peak. The resulting throughput for the Maestro RHBD chip was consistent with HPP task objectives and metrics. However, its relatively high-power dissipation level reduces its desirability for use in numerous spaceflight systems. Future plans within NASA's current avionics development activities include the proposal of developing a multicore processor that would leverage investments made in the Maestro architecture to deliver a RHBD system with throughput comparable to Maestro, but at a significantly reduced power dissipation level.

The HPP task was programmatically managed by GSFC, with support from MSFC, LaRC, and the Jet Propulsion Laboratory (JPL).

4.3.5 Reconfigurable Computing Technology Task

The concept of RC [24] focuses on using single computational hardware assets to accomplish multiple data-intensive objectives previously handled by multiple dedicated systems. This new approach to flight computing resource utilization would result in a reduction of subsystem-level flight spare inventories, adaptability to system failures, and flexibility in connecting components through a variety of data interfaces. The RC task as managed within the RHESE project aimed to provide improved fault and error detection and correction, enablement of autonomous repair and/or replacement of defects, and the concept of requiring a single configurable processor to autonomously conform to multiple configurations performing multiple computational tasks. Accomplishment of this goal yields a reduction in flight spares required to be carried on long-duration missions, since a single computational asset would then be able to perform many diverse processing functions. Such architecture adaptability will provide mission volume and mass savings as required by extended duration missions.

Three areas of focus were identified for the RC task: internal reconfigurability, external reconfigurability, and autonomous fault detection and mitigation. Internal reconfigurability provides the ability of the core processor to emulate any form of computing resource as needed by the flight system. External reconfigurability provides a capability to interface resources to any target system by adapting communication standards, physical and electrical interconnections, and other parameters of the host system to connect multiple computing assets using a variety of standards. Autonomous fault detection and mitigation allows the computational resource to detect an internal fault and perform autonomous isolation and recovery from the fault without external involvement.

Flexibility is also bolstered by the RC task. Interface reconfiguration can allow a single processor to make connections through different external interfaces as needed. By providing external modularity, vehicle system integrity is enhanced by allowing processors to be transferred among busses and networks to replace lost functionality. This flexibility directly supports the concept of reduced flight spaces required by long-duration missions.

During fiscal year 2009, the RC task demonstrated internal modularity. A Xilinx FPGA was shown to be programmable and reconfigurable to perform three diverse activities: act as a digital motor control, perform digital signal processing (DSP) computations (via an FFT), and emulate a finite state machine (via a "turing machine" simulator). In fiscal year 2010, the RC task demonstrated one solution to external modularity and several solutions to fault detection and mitigation. These demonstrations were performed in partnership between MSFC and Montana State University (MSU). For the external modularity demonstration, MSU used two Xilinx boards as connected via a multiline bus. The boards use a soft-core picoblaze processor to monitor the lines of the bus and the data being transmitted. Should any one (or more) of the bus lines become inactive through a faulty connection or environmentally related radiation event on the other board, the controlling board implements a dynamic input/output recovery routine, routing the faulty line data to an unused bus line for continued, resilient operations [25]. For the fault detection and mitigation demonstration, MSU developed and tested a tile-based, soft processor computing system using a Xilinx FPGA. The researchers divided the FPGA into equally sized tiles which represent a quantum of resources that can implement a soft processor and can also be individually reprogrammed using partial reconfiguration (PR) of the FPGA. At any given time, three of the processors are configured in TMR with the rest reserved as spare processor tiles. In the event that the TMR voter detects a fault, a recovery process is initiated that attempts to reset, reinitialize, and resynchronize the faulted tile, allowing a mitigation technique for handling SEUs that may have occurred in the FPGA circuit fabric. If the tile reset is not successful, a spare processor is brought online from one of the unused tiles to replace the faulted circuit. Once the new TMR triplet is operational, an attempt is made to recover the previously faulted tile using PR. After PR, the recovered tile is reintroduced into the system as an available spare. This recovery process mitigates SEUs that may have occurred in the configuration SRAM of the FPGA (i.e., single event functional interrupts [SEFIs]). If the system tries to use the recovered tile for a second time and immediately experiences a fault, the tile is marked as permanently damaged, possibly from an excess of TID, and is no longer available for use. This allows the system to continue operation in the presence of TID failures in localized regions of the FPGA. The mitigation strategy and computer architecture in this project has the advantage of addressing the two main logical fault types experienced in SRAM-based FPGAs (fabric SEUs and SEFIs). Furthermore, the ability to continue operation despite localized TID damage can extend the useful life of flight hardware [26,27]. Future improvements to this effort are proposed to include the addition of a two-dimensional matrix of radiation detectors as applied to the surface of the FPGA chip, providing additional information to the FPGA controller concerning the physical location of a high-energy radiation strike and implying where within the FPGA fabric an error may be expected to occur [28].

The RC task was programmatically managed by MSFC with support from LaRC.

4.3.6 Silicon–Germanium Integrated Electronics Technology Task

The RHESE SiGe task has as its goal the development and demonstration of basic electronic components applicable to flight systems that utilize distributed avionics architectures and require exposure to extreme environments. The SiGe task was initially developed to support the Constellation program and its flight platforms that require environmental operations in the deep space and lunar surface environment. The extreme temperature conditions on the lunar surface (at worst case, −230°C in shadowed polar craters, and ranging from −180°C to +120°C lunar night to day) combined with the pervasive radiation environment of deep space preclude the use of conventional electronics. The SiGe task was formulated to address these environmental issues. Now, with the cancellation of the Constellation program, the products resulting from the SiGe development effort are being solicited for infusion on a wide variety of planned flight demonstrations, flagship-class missions, robotic precursor missions, and deep space science missions.

Fiscal year 2010 was the last year of development for the SiGe task. On August 10, 2010, the SiGe task held a final review at the Georgia Institute of Technology where the full team, including participants from Boeing, BAE Systems, IBM, JPL, Auburn University, Vanderbilt University, the University of Tennessee, the University of Maryland, Lynguent, and the University of Arkansas, jointly presented a summary of the SiGe development activity. Core to the SiGe effort was the use of low-cost, commercial SiGe technology including SiGe HBTs and CMOS devices [29–33]. Unlike other commercial off-the-shelf integrated circuit technologies, SiGe offers unparalleled cryogenic temperature performance, built-in radiation tolerance, wide temperature range capability, and optimal mixed-signal circuit design flexibility at the monolithic level. Other benefits include the ability to fabricate power-efficient, multiple breakdown voltage, high-speed SiGe HBTs on the same piece of silicon wafer as high-density Si CMOS circuits and passive components.

At the final review, the SiGe team successfully delivered the following products:

- Low-power, radiation-tolerant (to 100 krad), integrated SiGe BiCMOS mixed-signal (digital + analog + power) electronics for sensor/imager and actuator systems that can operate reliably across −180°C to +120°C, and under relevant radiation conditions
- High-density packaging of these SiGe BiCMOS electronics components (with integrated passive components) which can operate reliably across −180°C to +120°C
- Modeling and CAD tools for SiGe BiCMOS devices and packaging to accurately predict and simulate the electrical performance, reliability, and radiation tolerance of these SiGe BiCMOS mixed-signal circuits and packages across −180°C to +120°C, a range that is beyond the limits of all other existing electronics device models
- Definition and implementation of a general purpose SiGe Remote Electronics Unit (REU) prototype capable of operation across −180°C to +120°C and simultaneous relevant radiation conditions
- A final report that documents the entire SiGe development effort

Prior to the final review, the SiGe task had produced increasingly complex designs that successively built toward the fabrication of the final REU prototype system. The "CRYO" moniker was used to identify the progressive stages of the development effort. Completed in 2005, the first iteration of the CRYO series, CRYO-1, was a proof-of-concept fabrication run containing SiGe-based basic circuit building blocks such as operational amplifiers, digital-to-analog converters, and standard characterization and test structures. The final REU prototype system, or CRYO-5, included a SiGe-based REU Sensor Interface (RSI) ASIC and a Digital Control (RDC) ASIC chip. Initially scheduled to be delivered in 2009, the final REU prototype delivery was slipped until August 2010 to accommodate a re-fabrication and test of the RDC ASIC chip. The RDC ASIC experienced some design problems during the final fabrication and therefore resulted in the inability to deliver the final packaged, environmentally hardened device. Instead, the functionality of the RDC was programmed into a Xilinx FPGA that was used to perform and validate final radiation and cryogenic testing at Texas A&M University. Photographs of the individual RSI and RDC dies are shown in Figure 4.3 and a packaged version of the REU is shown in Figure 4.4.

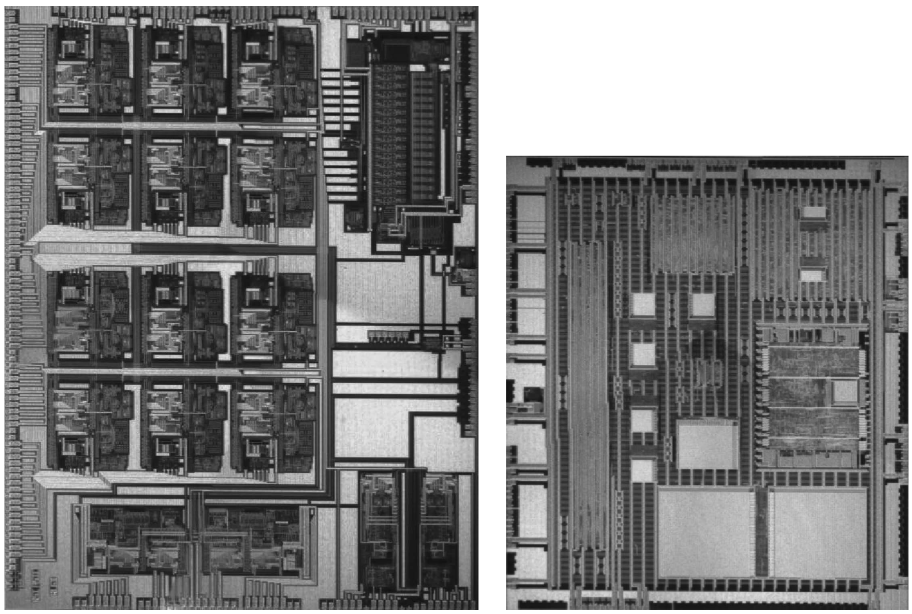

(a) (b)

FIGURE 4.3 CRYO-5 SiGe RSI ASIC (a) and CRYO-5 SiGe RDC ASIC (b).

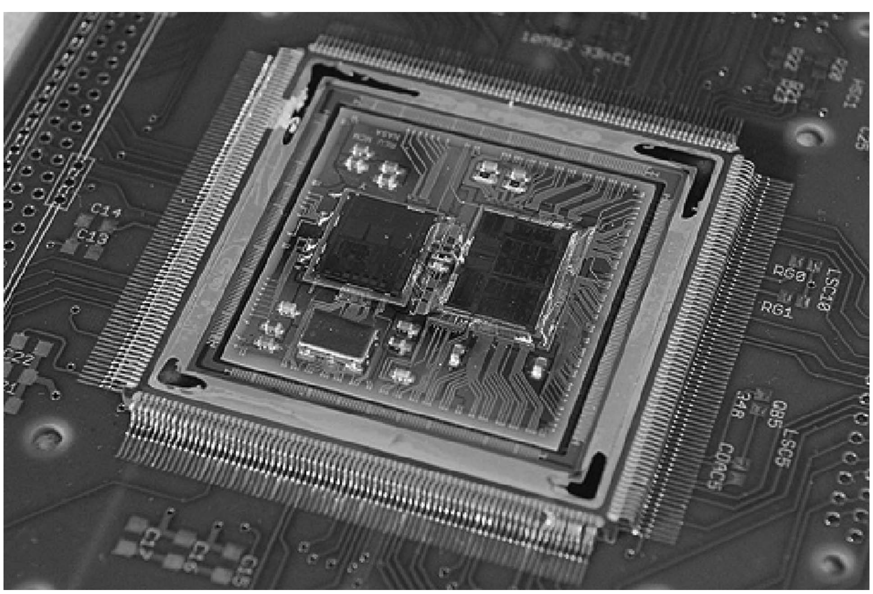

FIGURE 4.4 REU multi-chip module.

The development, test, and delivery of the SiGe-based REU successfully raised the TRL of SiGe BiCMOS extreme environment electronics technology, including packaging, from TRL 2 (feasibility of low-temperature operation of SiGe BiCMOS transistors) to TRL 6 (demonstrated integrated circuits, packaging, models, design libraries, and functional prototypes), permitting seamless technology infusion into future spacecraft architectures.

For purposes of testing the SiGe technology in the space environment, multiple flight experiments were developed to include SiGe-based electronic chips. Mounted on the MISSE-6 experiment were passive, unpackaged SiGe chips that function as a voltage reference. To protect the SiGe dies from atomic oxygen within the low Earth orbit environment while allowing exposure to other environmental conditions such as radiation and temperature, the team developed a protective coating process. MISSE-6 was retrieved from the ISS during STS-128 in August 2009. Performance tests on the SiGe die that flew on the MISSE-6 experiment were conducted by NASA's Ames Research Center (ARC).

Also in cooperation with the Boeing Company, an active, packaged SiGe-based control circuit, the CRYO-3a voltage reference design, was incorporated as an integrated portion of a Boeing experiment to monitor a thermal protection system material on the MISSE-7 experiment platform. MISSE-7 was launched aboard STS-129 in November 2009 and was mounted on the exterior of the ISS.

Though the Georgia Institute of Technology was prime contractor for the SiGe task, the contract for the SiGe task was programmatically managed by NASA's LaRC with support from the JPL.

4.4 Transition of RHESE Technology Tasks

In 2009, President Barack Obama initiated a review of NASA's plans for human spaceflight and exploration. The resulting study [34] concluded that the Constellation program, though reasonable and acceptable in its architecture, was aiming to achieve mission goals that were not commensurate with the appropriated funding or published schedule. President Obama subsequently moved to cancel the program and instead encouraged commercial programs to develop new launch vehicles able to access low Earth orbit and service the International Space Station. Congress responded with additional direction as provided in the "NASA Authorization Act of 2010" [35] to develop a new heavy-lift vehicle capable of serving as the workhorse for manned exploration beyond low Earth orbit. With the Constellation program in the process of being cancelled, the ETDP program was reformulated to accommodate not only technology development, but also several technology flight demonstrations. Renamed the Exploration Technology Development and Demonstration (ETDD) program, the constituent projects within were likewise also reformulated.

By this time, the RHESE project had been renamed to be called the Advanced Avionics and Processor Systems (AAPS) project. Since the project was a part of the closing ETDP program, the RHESE/AAPS project was officially terminated. A final RHESE/AAPS project review was conducted at MSFC on August 25, 2010. The three technology tasks that were still in development within the project, HPP, RC, and MREE, were transitioned from the closed RHESE/AAPS project into the newly formulated Autonomous Systems and Avionics (ASA) project.

The ASA project was 1 of 10 foundational technology development efforts that constituted the new ETDD program. Beginning in fiscal year 2011, the new ETDD program planned to develop and demonstrate new technologies and prototype systems that could enable new classes of human spaceflight capabilities and flagship-class mission demonstrations. The ETDD program had only started to make progress in fiscal year 2011 when it was decided that the technology efforts within the program would be further integrated into the newly formed Office of Chief Technologist's Space Technology Program. As of October 1, 2011, the ETDD program had been dissolved and its technology contents absorbed by the Space Technology Program.

Regardless of the project title or the programmatic structure supporting it, the development of avionics and electronics capable of operating within harsh and extreme radiation and thermal environments will continue to be a critical need for NASA. Plans for the exploration of destinations beyond low Earth orbit are only now beginning to emerge in the wake of the Constellation program cancellation. As these new plans for exploration mature, they will certainly have requirements for the advanced avionic technologies initiated and developed within the RHESE project.

References

1. NASA, *Vision for Space Exploration*, Washington, DC, 2004.
2. NASA, *Exploration Systems Architecture Study*, Washington, DC, 2005.
3. E. Crowley et al., A constrained space exploration technology program: A review of NASA's Exploration Technology Development Program, National Academies Press, Washington, DC, Contract No. NNH05CC16C, Final Report, 2008.
4. A. S. Keys et al., Developments in radiation-hardened electronics applicable to the vision for space exploration, AIAA-2007-6269, *AIAA SPACE 2007 Conference and Exposition*, Long Beach, CA, 2007, pp. 1–10.
5. A. S. Keys et al., A review of NASA's radiation-hardened electronics for Space Environments Project, AIAA-2008-7673, *AIAA SPACE 2008 Conference and Exposition*, San Diego, CA, 2008, pp. 1–7.
6. A. S. Keys et al., Advanced Avionics and Processor Systems for space and lunar exploration, AIAA-2009-6783, *AIAA SPACE 2009 Conference and Exposition*, Pasadena, CA, 2009, pp. 1–7.
7. A. S. Keys et al., Advanced Avionics and Processor Systems for a flexible space exploration architecture, AIAA-2010-8783, *AIAA SPACE 2010 Conference and Exposition*, Anaheim, CA, 2010, pp. 1–17.

8. A. C. Tribble, *The Space Environment*, Princeton University Press, Princeton, NJ, 1995, pp. 137–167.
9. K. Greisen, End to the cosmic ray spectrum? *Phys. Rev. Lett*., 16, 1966, 748–750.
10. G. T. Zatsepin and V. A. Kuzmin, Upper limit of the spectrum of cosmic rays, *J. Exp. Theor. Phys. Lett.,* 4(3), 1996, 114–117.
11. L. W. Townsend et al., Large solar flare radiation shielding requirements for manned interplanetary missions, *J. Spacecraft Rockets*, 26(2), 1989, 126–128.
12. L. Sterpone and M. Violante, Analysis of the robustness of the TMR architecture in SRAM-based FPGAs, *IEEE Trans. Nucl. Sci*., 52(5), 2005, 1545–1549.
13. J. F. Wakerly, Microcomputer reliability improvement using triple-modular redundancy, *Proc. IEEE*, 64(4), 1976, 889–895.
14. M. M. Dickinson et al., Saturn V launch vehicle digital computer and data adapter, *AFIPS'64 Fall Joint Computer Conference*, San Francisco, CA, October 1964, pp. 501–516.
15. R. B. Roncoli and J. M. Ludwinski, Mission design overview for the Mars exploration rover mission, AIAA Paper AIAA-2002-4823, *AIAA/AAS Astrodynamics Specialist Conference and Exhibit*, Monterey, CA, 2002, pp. 1–10.
16. D. Y. Lam et al., SEE-hardened-by-design area-efficient SRAMs, *2005 IEEE Aerospace Conference*, Big Sky, MT, 2005, pp. 1–7.
17. K. A. LaBel et al., Emerging radiation hardness assurance (RHA) issues: A NASA approach for space flight programs, *IEEE Trans. Nucl. Sci*., 45(6), 2727–2736, 1998.
18. J. C. Mankins, Technology readiness levels [Online]. Available: http://www.hq.nasa.gov/office/codeq/trl/trl.pdf
19. A. J. Tylka et al., CREME96: A revision of the cosmic ray effects on micro-electronics code, *IEEE Trans. Nucl. Sci*., 44(6), 2150–2160, 1997.
20. R. A. Weller et al., Monte Carlo simulation of single event effects, *IEEE Trans. Nucl. Sci*., 57(4), 1726–1746, 2010.
21. S. Agostinelli et al., GEANT4—A simulation toolkit, *Nucl. Instrum. Methods Phys. Res. Sect. A: Accel. Spectrom. Detect. Assoc. Equip*., 506(3), 250–303, 2003.
22. J. Allison et al., Geant4 developments and applications, *IEEE Trans. Nucl. Sci*., 53(1), 270–278, 2006.
23. Cosmic ray effects on micro electronics—Monte Carlo homepage, Vanderbilt University, Institute for Space and Defense Electronics [Online]. Available: https://creme-mc.isde.vanderbilt.edu
24. M. C. Patrick, Reconfigurable computing concepts for space missions: Universal modular spares, *2008 IEEE Aerospace Conference*, Big Sky, MT, 2008, pp. 1–8.
25. R. L. Akamine et al., Error mitigation of point-to-point communication for fault-tolerant computing, *2011 IEEE Aerospace Conference*, Big Sky, MT, March 5–12, 2011.
26. C. Gauer et al., Spatial avoidance of hardware faults using FPGA partial reconfiguration of tile-based soft processors, *2010 IEEE Aerospace Conference*, Big Sky, MT, March 6–13, 2010.
27. B. J. Lameres et al., Design of a radiation tolerant computing system based on a many-core FPGA architecture, *Military and Aerospace Programmable Logic Devices Conference*, Greenbelt, MD, September 1–4, 2009.
28. B. J. Lameres et al., Position sensitive radiation detector integrated with an FPGA for radiation tolerant computing, *IEEE Sensors 2010 Conference*, Waikoloa, HI, November 1–4, 2010.
29. J. D. Cressler, On the potential of SiGe HBTs for extreme environment electronics, *Proc. IEEE*, 93(9), 1559–1582, 2005.
30. J. D. Cressler, Using SiGe HBTs for extreme environment electronics, *Proceedings of the 2005 IEEE Bipolar/BiCMOS Circuits and Technology Meeting*, Santa Barbara, CA, 2005, pp. 248–251.
31. J. D. Cressler, SiGe HBT reliability issues associated with operation in extreme environments, *2006 IEEE Topical Meeting on Silicon Monolithic Integrated Circuits in RF Systems*, San Diego, CA, 2006, pp. 3–7.
32. J. D. Cressler et al., SiGe integrated electronics for extreme environments, *Proceedings of the 2007 GOMAC-Tech—Government Microcircuit Applications and Critical Technology Conference*, 2007, Lake Buena Vista, FL, pp. 327–331.
33. J. D. Cressler, SiGe BiCMOS technology: An IC design platform for extreme environment electronics applications, *Proceedings of the 2007 IEEE International Reliability Physics Symposium*, Phoenix, AZ, 2007, pp. 141–149.
34. N. R. Augustine et al., *Seeking a Human Spaceflight Program Worthy of a Great Nation*, National Aeronautics and Space Administration, Washington, DC, 2009.
35. National Aeronautics and Space Administration Authorization Act of 2010, Public Law 111-267, United States Government Printing Office, Washington, DC, 2010.

5

Role of Extreme Environment Electronics in NASA's Aeronautics Research

Gary W. Hunter
National Aeronautics and Space Administration

Dennis Culley
National Aeronautics and Space Administration

5.1 Introduction

NASA aeronautical research is focused on a myriad of technologies including those that involve embedding high-performance sensing and control in gas turbine engine systems. Future aeronautic propulsion systems are challenged to meet increasing requirements for reduced maintenance and emissions, improved capability, and increased safety. The inclusion of in situ computational and control capabilities into the propulsion system operation can significantly enable advances in propulsion technology. However, the use of conventional electronics is problematic given the high-temperature and harsh environments typical within an engine. This chapter discusses the use and potential of extreme environment electronics and their impact on associated sensor systems to enable more intelligent engine systems with a distributed control architecture resulting in improved engine capabilities.

The following sections describe two areas where high-temperature electronics can impact future systems: distributed engine controls and smart sensor systems. It is suggested that the capability to embed operational electronics in extreme environments is critical to revolutionary change and the key to bringing forth the next generation of complex, high-performance engines. These changes are enabled through a combination of high-temperature electronics with a range of other technologies, including sensors, power supplies, packaging, communication, and actuators.

5.2 Distributed Engine Controls

5.2.1 Brief History of Gas Turbine Engine Control

There have been at least two revolutionary changes to the architecture of turbine engine control systems since the invention of the jet engine. The first was the application of electronics to initially supplement, and then eventually replace, intricate hydromechanical controls. While hydromechanical controls were certainly capable of providing acceptable control functionality, their size, weight, and expense constrained the ability to expand the number of control variables, which is a measure of control system complexity. The compactness and flexibility of early electronics technology enabled an increase in system complexity even though the initial capability and reliability of these electronics were primitive by today's commercial standards.

Early in this period, circa 1970, electronics were limited to supervisory or trim functions. Over time, many of the initial deficiencies were rectified and electronics provided innovations that far surpassed the capability of hydromechanical control. Eventually, electronic systems would advance to the point that they were capable of performing as "full authority," meaning they could control the entire operation of an engine from startup to shutdown according to the pilot's throttle command.

The second revolutionary change to gas turbine engine control architecture occurred when full authority control was implemented with digital electronics and software, known as a Full Authority Digital Engine Control (FADEC). This change was not significant because of the transition from analog to digital electronics, but rather because it represented a change in control law implementation from the physical domain of hardware to the virtual domain of software. The unlimited flexibility of software provided an unsurpassed capability for quickly implementing system improvements via software without the need to make hardware modifications. Whereas analog electronic control was a representation of individual, localized hydromechanical control functions, software-driven control architecture consolidated all of the engine control laws into one physically central location from which it could be easily modified. Consequently, the control laws themselves have become much more aware of the system state, limited mainly by the available computational power. This centralized control hardware architecture, introduced circa 1985, remains the state of the art for present-day turbine propulsion systems.

Early hydromechanical controls were, in effect, distributed control systems in that they operated locally on a very limited set of input data. Ironically, the next revolutionary change in control architecture will replicate this physical distribution of control functionality; however, it will also preserve the unifying centrality of FADEC architecture. This will be achieved through a networked system of embedded electronic controls. Not surprisingly, these changes are being driven by familiar constraints such as weight, volume, and cost, as well as new concerns about the expanding complexity of engine and integrated vehicle control.

Distributed engine control architecture will not be achieved in a single step change; rather it will occur in a progression of changes as new technologies enable the partitioning of control functionality across the entire environment of the engine system. Distributed control technology development is largely, but not completely, focused on extending the capability, packaging, and availability of electronic systems and components in harsh engine environments. This investment will enable them to reliably function in extreme conditions while requiring minimal need for isolation from the ambient thermal environment.

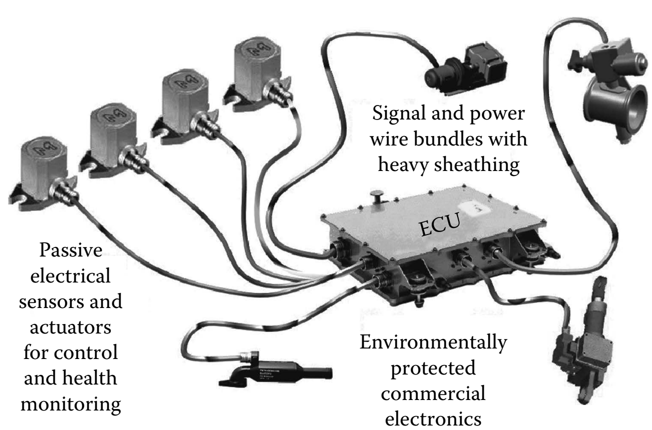

FIGURE 5.1 Traditional engine control architecture.

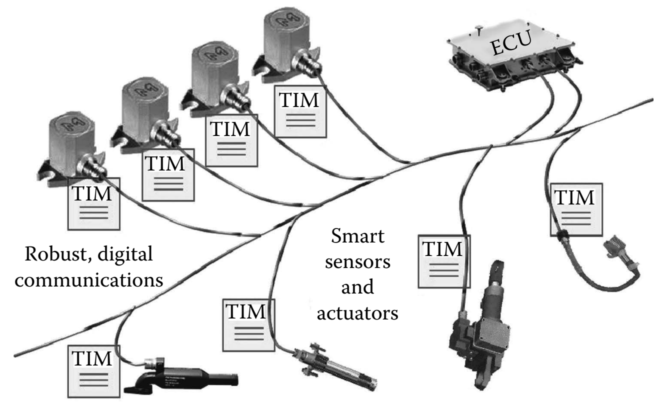

FIGURE 5.2 Distributed engine control architecture.

Examples of traditional and distributed control architectures are depicted in Figures 5.1 and 5.2, respectively. Distributed control, in its fully realized form, would embed highly integrated electronics into each control system device so that they could communicate over a common communication network.

5.2.2 Constraints on Current Engine Control System

The constant integration of new technologies has been responsible for the continuous evolution of gas turbine engine system capability. The manifestation of these improvements, whatever the source, is inevitably reflected in two primary metrics: decreasing core size for a constant engine thrust and increasing temperature in the hot gas path. Both of these parameters increase the difficulty of implementing engine control system technologies.

Modern engines are highly integrated systems and are independent in that they include all elements for their control. The exception to this general rule is turboshaft engines used in rotary craft that often integrate vehicle control with engine control because of their unique interdependencies. Since the engine controls are such an integral component of the engine system, designers have very limited opportunity to manage the location or environment of control hardware. From the initial introduction of solid-state electronics in engine control, designers have had to protect these sensitive components from all hazards of the operating environment. These considerations include such conditions as high vibration and shock loads; low pressure from high altitude flight; contamination from water, salt, and hydrocarbons; and the constant threat of lightning or electrical discharges. Arguably the most severe constraint is the extreme-temperature environment due to the close proximity of control system components to the hot engine core and the potentially rapid and extreme fluctuations in temperature especially in high altitude conditions.

In practice, engine electronics are mounted in a single, high integrity package that protects the electronics from these environmental hazards. This package is typically known as an engine control unit (ECU) or, as noted previously, the FADEC. Each control sensor and effector is cabled to the centralized location of the ECU. In commercial engines, the ECU is typically mounted on the fan casing because of the high capacity for cooling the electronics in this region. In military systems, this package is mounted on a cold plate and heat is transferred to the fuel. The need to environmentally protect electronics hardware and the implications on total engine weight are the main forces that have prevented the adoption of distributed control technologies in turbine engine systems.

As engine systems continue to advance, there are diminishing opportunities to locate fragile engine control electronics in environmental conditions in a framework that insures their reliability, but without severely impacting engine system weight or performance. Overall, the goal for more control and its associated electronics is at odds with these engine constraints. Conversely, advances in engine control capability are seen as one of the most likely technologies to improve future engine system performance. A migration to a distributed control system would be a revolutionary change in technology that could maintain the positive trajectory for overall engine system performance.

5.2.3 Goals and Objectives for a Paradigm Shift

There are many reasons that a shift to distributed control architecture is highly desirable. However, all can be put into one or both of the following categories: cost and performance. This narrow point of view exists because customers for these systems only care about capability, not technology. Distributed control is recognized as the means to deliver this capability in the future. High-temperature electronics is the critical technology that is necessary to make distributed control feasible; therefore, high-temperature electronics must be developed that provide a capability that is equivalent or better than existing technology, and do it within a cost structure that is affordable.

Fortunately, distributed control provides great flexibility in parsing engine control functions. The computationally intensive control law processing components can be located remotely from the end effectors, in more benign environs, as long as sufficient communication bandwidth is available to maintain engine stability. The "embedded" control components are then required to perform transducer functions with, perhaps, simple local loop closure while communicating to the supervisory control.

As distributed control technology evolves, the electronics capability is also expected to improve by embedding additional capability that increases local control functionality. Eventually, it could be expected that embedded high-temperature processing capability would be essentially equivalent to today's commercial microprocessors, leading to highly complex subsystems and hierarchical control structures. However, it must be realized that mainstream commercial electronics will always have an extended lead time in capability, perhaps as long as decades.

5.3 Smart Sensor Systems

5.3.1 Smart Sensor System Overview

In order for future aerospace propulsion systems to meet the increasing requirements for decreased maintenance, increased safety, and improved performance and capability, the inclusion of intelligence into the propulsion system design and operation becomes necessary [1,2]. This increased embedded intelligence can contribute to the distributed engine control concept of Section 5.2, as well as other possible impacts including improved system health management capabilities and situational awareness; increased adaptability and performance optimization in changing conditions; and improved autonomy and automated processing in-flight to respond to unforeseen events.

An enabling technology for such improved measurement capabilities is a smart sensor system. A *smart sensor system* is, at a minimum, the combination of a sensing element with local processing capabilities provided by a microprocessor [3]. A more expansive view of a smart sensor system is shown in Figure 5.3, a complete self-contained sensor system that includes the capabilities for data storage and processing, self-contained power, and an ability to transmit or display informative data. This smart sensor system approach can be combined with efforts to miniaturize sensor technology to provide multiparameter detection of a range of parameters within a single microsensor platform. Integration of this multiparameter information can provide increased whole-field information of the environment. The electronics can be programmed to provide specific information required on a regular basis, but can also provide further diagnostic information when needed. Overall, one of the advantages of a smart sensor system is the ability to program new functions into processors and swap out modules within the system, allowing a wide range of adaptability.

An example of sensor system development that demonstrates the aforementioned technology trends is an integrated smart leak detection system, referred to as "lick and stick" technology,

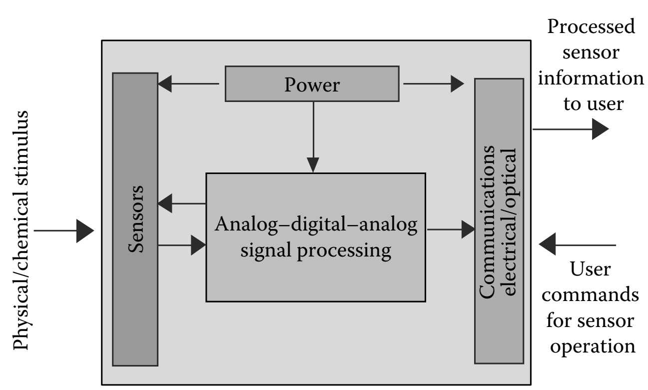

FIGURE 5.3 A smart sensor system as presented herein. The core of a standalone smart sensor system includes sensors, power, communication, and signal processing. (From Hunter, G.W. et al., *Interface Magazine*, 20(1), 66, Winter 2011. Electrochemical Society Inc.)

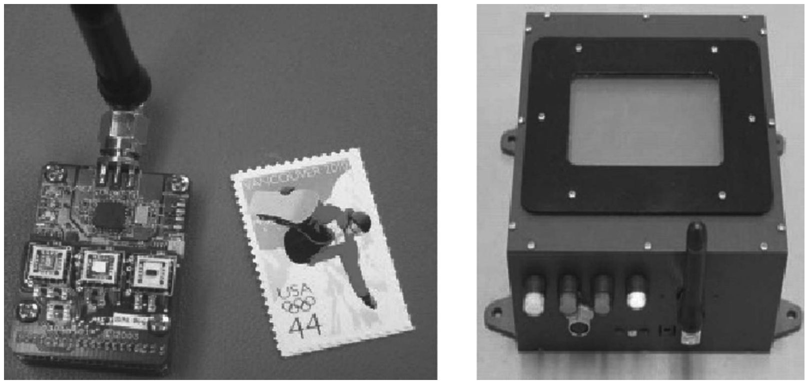

(a) (b)

FIGURE 5.4 (a) A "Lick and Stick" leak detection system with two hydrogen sensors and a hydrocarbon sensor combined with supporting electronics and wireless communication. (b) A wireless hub that is an interface for multiple "Lick and Stick" wireless systems. (From Hunter, G.W. et al., Smart chemical sensor systems for fire detection and environmental monitoring in spacecraft, in *International Conference on Environmental Systems*, Barcelona, Spain, AIAA766637.)

targeted for a range of applications in launch vehicle propulsion systems [4,5]. The smart sensor system shown in Figure 5.4a includes a microsensor array fabricated by microfabrication (often referred to as microelectromechanical system [MEMS])–based technology, featuring two hydrogen sensors and a hydrocarbon sensor used to detect fuel leaks. The sensor array has been incorporated into a smart sensor system that provides a complete unit with signal conditioning electronics, power, data storage, and telemetry. This system has a surface area near the size of a postage stamp and is intended to be applied, like a postage stamp, where and when needed within a vehicle without rewiring of the vehicle system. Other smart sensor systems have been developed for fire detection, environmental monitoring, and emissions monitoring purposes [6,7]. One approach is to place a number of these sensor systems in a region, and the resulting measurements are then fed (wired or wirelessly) into a central processing hub to allow an understanding of the region or environment (Figure 5.4b). The wireless approach has been demonstrated previously for environmental monitoring applications [6].

Overall, smart sensor systems potentially represent a new generation of sensing capability and self-awareness that are essential components of future intelligent systems. Driving intelligence down to the component level through the design of smart sensor systems can have a profound impact on a range of applications [3,8]. Smart sensor systems can possess embedded intelligence to provide critical data in a more rapid, reliable, economical, and efficient manner with a robust interface to the system or user. However, significant challenges exist for application of smart sensor systems in harsh environment of engine applications.

5.3.2 Sensors and Electronics in Harsh Environments

The core of a smart sensor system is the electronic microprocessor. For near-ambient temperature applications, this microprocessor is based on silicon (Si) technology. Electronics based on silicon, as well as silicon-on-insulator (SOI) or gallium arsenide (GaAs), can be considered for temperatures below 300°C, and thus could be of use in some of the cooler regions of the engine.

However, the use of complex electronics to enhance the capabilities and efficiency of engine systems often implies operation at temperatures above 300°C. While silicon-based semiconductors have enabled complex, room-temperature circuits to be miniaturized onto small chips, the direct extension of this technology to temperatures above 300°C is problematic [9,10]. Presently, since today's conventional silicon-based electronics technology cannot function at such high temperatures, these electronics must reside in environmentally controlled areas. This necessitates the use of long wire runs between sheltered electronics and hot-area sensors. Such a low-temperature-electronics approach suffers from serious drawbacks in terms of increased weight, decreased fuel efficiency, and reduced reliability for engine system applications.

The development of engine-compatible electronics is not straightforward. To be useful, such electronics need to be as small, lightweight, and nonintrusive as possible; in addition, these electronics should preferably operate without thermal management overhead in hot regions, at or near very hot combustion chambers and exhaust gas streams. Further challenges for engine system electronics and sensor systems include reliable operation for extended periods in high vibration, as well as in high acoustic and thermal shock environments. A family of high-temperature electronics and sensors that could function in areas as hot as 600°C would enable improved safety, with better vehicle system awareness, as well as substantial performance gains through weight reductions and improved control algorithms.

A leading example of high-temperature electronics with potential for use in these hot sections is silicon carbide (SiC). Wide-bandgap SiC presently appears to be the strongest candidate semiconductor for implementing 400°C–600°C integrated electronics, as other high-temperature electronics materials are less-developed (gallium nitride [GaN], diamond, etc.). Extreme-temperature semiconductor integrated circuits (ICs) are being developed for use in the hot sections of aircraft engines and other harsh-environment applications well above 300°C. Single-crystal wafers of either the 6H or 4H crystal structures of SiC are commercially available with sufficient quality and size to enable foundry mass fabrication of discrete devices and ICs. Such SiC-based electronics can provide a basis for high-temperature smart sensor systems.

5.3.3 Development of High-Temperature Smart Sensor Systems

Development is ongoing toward high-temperature smart sensor systems based on SiC electronics to meet a range of engine application needs [11]. Further description of these circuits will be given in Chapter 62; this chapter will summarize the efforts related to high-temperature smart sensor systems. The following is a sampling of the status and activities associated with producing a high-temperature smart sensor system for use at 500°C. This is not a complete survey, but is a brief overview of some of the challenges and relevant activities toward producing such a system for propulsion system implementation.

This development is based on epitaxial 6H-SiC junction field effect transistors (JFETs) (Figure 5.5). Simple packaged analog amplifier and digital logic gate ICs have been demonstrated for thousands of hours of continuous 500°C operation in oxidizing air atmosphere with minimal changes in relevant electrical parameters. These timeframes are now viable for implementation in engine conditions for extended periods, although other capabilities such as operation over many thermal cycles still need to be demonstrated [12–14]. Nonetheless, this work has been pioneering in demonstrating durability and functionality of SiC electronics for harsh environment applications and allows high-temperature signal processing at temperatures far beyond that capable in silicon electronics. However, the circuits are relatively simple building blocks. They are significantly less complex than corresponding Si or SOI electronics and are the early foundations for more complex systems. Nonetheless, they do allow the capability for simple electronics processing and the basic capabilities are in rough equivalence to that seen historically in the time period of the Mercury manned spaceflight program.

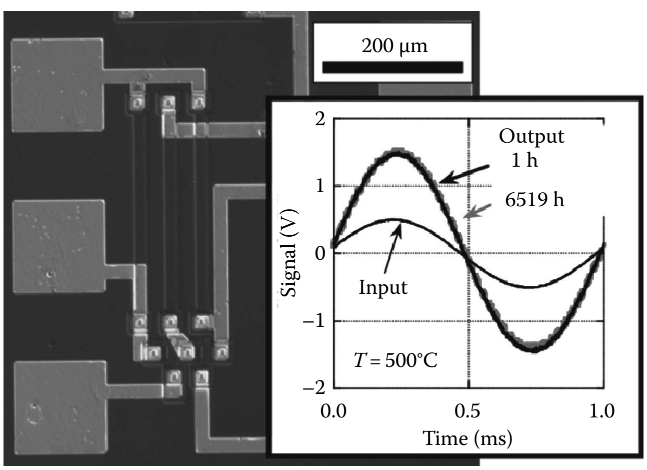

FIGURE 5.5 Optical micrograph of a 500°C durable 6H-SiC JFET differential amplifier IC chip prior to packaging. Digitized waveforms measured during the 1st (solid black) and 6519th (dashed gray) hour of 500°C operational testing show no change in output characteristics. (From Neudeck, P.G. et al., *Phys. Status Solidi A*, 206(10), 2329, 2009.)

In parallel, a range of other components and further technology development are necessary to produce a high-temperature, stand-alone smart sensor system that includes wireless communication, sensors, and power. In brief summary,

- *High-temperature wireless communications*: A range of different approaches can be considered for high-temperature wireless systems [11,15,16]. In relation to an integrated smart sensor system, efforts to design and test a complete wireless circuit have been focused on high-temperature passive components, such as resistors, capacitors, and inductors, as well as the core operating circuit [11,17,18]. Recent work has shown 300°C wireless transmission with commercial SiC circuits integrated with thin-film antenna technology [17], and limited 500°C wired and wireless data transmission using the simple SiC circuits described earlier [19].
- *Power scavenging*: A viable means for providing in situ power in high-temperature environments, such as an engine, is through power scavenging using thermoelectric [11]. High-temperature batteries exist for high-temperature operation [16], but these are larger devices and their integration into an engine environment is problematic.
- *Sensors*: A range of sensors are under development toward possible integration into a high-temperature smart sensor system [11]. Early development of sensors for high-temperature wireless circuits are concentrating on capacitive sensors since they most easily integrated into simple oscillator circuits.

These activities are just a sampling of the activities needed to produce high-temperature smart sensor systems. While capabilities exist to produce smart sensor systems in near-ambient environments, the core capabilities to produce a complete sensor system for high-temperature engine systems do not presently exist. There is a fundamental technology gap between the necessary components for a smart sensor system, and those presently available for operation at high temperatures, and this starts with the high-temperature electronics that are core to such a system. Thus, the revolution envisioned by smart sensor systems for near-ambient temperature operation is more mature than that for the corresponding high-temperature operation applications.

5.4 Conclusions and Future Potential

In a number of commercial markets, advancements in electronics have revolutionized everyday life. Simple examples include advancements in computer technology, smart phones, and digital recording, as well as increased automation and efficiency of a vast range of industrial and commercial processes and systems. But such major changes have not occurred in a number of applications, such as those involving harsh environments, due in part to a lack of basic processing capabilities.

The role of high-temperature electronics in aeronautic engine applications is fundamental toward the expansion of engine capabilities and performance. As described in this chapter, the maturation of high-temperature electronics is core to more intelligent, distributed engine control systems with improved system awareness. Future work in high-temperature circuit development will need to increase the complexity of these circuits to produce increased functionality, eventually leading toward high-temperature wireless circuits. Advancement of wired and wireless sensor nodes will need to be focused on the eventual integration of a sensor, circuitry, and power system that will be operable at temperatures up to 500°C and above. The revolutions seen in smart technology in near–room temperature applications can only be realized at high temperatures with such advancements in high-temperature electronics.

References

1. G. W. Hunter, 2003. Morphing, self-repairing engines: A vision for the intelligent engine of the future. In *AIAA/ICAS International Air & Space Symposium, 100th Anniversary of Flight*, July 14–17, 2003, Dayton, OH, AIAA 2003-3045.
2. G. W. Hunter, L. G. Oberle, G. Baakalini, J. Perotti, and T. Hong. 2011. Intelligent sensor systems for integrated system health management in exploration applications. In S. B. Johnson, T. Gormley, S. Kessler, C. Mott, A. Patterson-Hine, K. Reichard, and P. Scandura, Jr. (Eds.), *System Health Management: With Aerospace Applications*, John Wiley & Sons, Chichester, West Sussex, U.K.
3. G. W. Hunter, J. R. Stetter, P. J. Hesketh, and C. C. Liu. 2011. Smart sensor systems. *Interface Magazine*, 20(1), 66–69. Electrochemical Society Inc.
4. G. W. Hunter, P. G. Neudeck, J. Xu, D. Lukco, A. Trunek, M. Artale, P. Lampard, D. Androjna, D. Makel, B. Ward, and C. C. Liu. 2004. Development of SiC-based gas sensors for aerospace applications. In M. Dudley, P. Gouma, T. Kimoto, P. G. Neudeck, and S. E. Saddow (Eds.), *Silicon Carbide 2004—Materials Processing and Devices*, Materials Research Society Symposium Proceedings 815, Warrendale, PA, pp. 287–298.
5. G. W. Hunter, J. Xu, P. G. Neudeck, D. B. Makel, B. Ward, and C. C. Liu. 2006. Intelligent chemical sensor systems for in-space safety applications. In *42nd AIAA/ASME/SAE/ASEE Joint Propulsion Conference & Exhibit*, July 10–12, 2006, Sacramento, CA, Technical Report AIAA-06-58419.
6. G. W. Hunter, J. C. Xu, L. K. Dungan, B. J. Ward, P. Dutta, A. D. Adeyemo, C. C. Liu, and D. P. Gianettino. 2010. Smart chemical sensor systems for fire detection and environmental monitoring in spacecraft. In *International Conference on Environmental Systems*, Barcelona, Spain, AIAA766637.
7. B. J. Ward, K. Wilcher, and G. W. Hunter. 2010. Gas microsensor array development targeting enhanced engine emissions testing. In *AIAA Infotech@Aerospace 2010*, April 20–22, 2010, Atlanta, GA, AIAA 2010-3327.
8. Nanotechnology-enabled sensing, Report on the National Nanotechnology Initiative Workshop, Arlington, VA, May 5–7, 2009, http://www.nano.gov/
9. P. G. Neudeck. 2000. SiC technology. In W.-K. Chen (Ed.), *The VLSI Handbook, The Electrical Engineering Handbook Series*, CRC Press and IEEE Press, Boca Raton, FL, pp. 6.1–6.24.
10. P. G. Neudeck, R. S. Okojie, and L. Y. Chen. 2002. High-temperature electronics—A role for wide bandgap semiconductors. *Proceedings of the IEEE*, 90, 1065–1076. IEEE Press, Boca Raton, FL.
11. J. Lekki, T. Bencic, A. Gyekenyesi, G. Adamovsky, G. Hunter, R. Tokars, and M. Woike. 2010. Aircraft engine sensors for integrated vehicle health management. In *Proceedings of the 57th Joint Army-Navy-NASA-Air Force (JANNAF) Propulsion Meeting*, Colorado Springs, CO, May 3–7, 2010.
12. D. J. Spry, P. G. Neudeck, L.-Y. Chen, G. M. Beheim, R. S. Okojie, C. W. Chang, R. D. Meredith, T. L. Ferrier, and L. J. Evans. 2008. Fabrication and testing of 6H-SiC JFETs for prolonged 500°C operation in air ambient. In T. Kimoto (Ed.), *Silicon Carbide and Related Materials 2007*, Materials Science Forum, Trans Tech Publications, Switzerland.
13. P. G. Neudeck, D. J. Spry, L. Y. Chen, G. M. Beheim, R. S. Okojie, C. W. Chang, R. D. Meredith, T. L. Ferrier, L. J. Evans, M. J. Krasowski, and N. F. Prokop. 2008. Stable electrical operation of 6H-SiC JFETs and ICs for thousands of hours at 500°C. *IEEE Electron Device Letters*, 29(5), 456–459.
14. P. G. Neudeck, S. L. Garverick, D. J. Spry, L. Y. Chen, G. M. Beheim, M. J. Krasowski, and M. Mehregany. 2009. Extreme temperature 6H-SiC JFET integrated circuit technology. *Physica Status Solidi A*, 206(10), 2329–2345.

15. R. G. DeAnna. 2000. *Wireless Telemetry for Gas-Turbine Applications*, NASA/TM-2000-209815.
16. J. L. Hall, M. Bullock, D. A. Senske, J. A. Cutts, and R. Grammier, *NASA's Flagship Mission to Venus: Final Report of the Venus Science and Technology Definition Team*, April 2009, http://vfm.jpl.nasa.gov
17. G. W. Hunter, G. M. Beheim, G. E. Ponchak, M. C. Scardelletti, R. D. Meredith, F. W. Dynys, P. G. Neudeck, J. L. Jordan, and L. Y. Chen. 2010. Development of high temperature wireless sensor technology based on silicon carbide electronics. *ECS Transactions*, 33, 269–281.
18. Z. D. Schwartz and G. E. Ponchak. 2005. High temperature performance of a SiC MESFET based oscillator. In *IEEE MTT-S International Microwave Symposium Digest*, Long Beach, CA, June 11–17, 2005, pp. 1179–1182.
19. G. E. Ponchak, M. C. Scardelletti, B. Taylor, S. Beard, R. D. Meredith, G. M. Beheim, G. W. Hunter, and W. S. Kiefer. 2012. High temperature, wireless seismometer sensor for Venus. Submitted to *IEEE Topical Conference on Wireless Sensors and Sensor Networks Digital*, Santa Clara, CA, January 15–19, 2012.

6

Technology Options for Extreme Environment Electronics

Jonathan A. Pellish
National Aeronautics and Space Administration

Lewis M. Cohn
Naval Research Laboratory

6.1 Introduction

This chapter will briefly examine a variety of semiconductor microelectronics technologies and comment on their suitability to support various extreme environment applications. The environments to be considered include

1. Extreme temperature, for example, >125°C and <−55°C
2. Extreme radiation environments, for example, $>1 \times 10^{12}$ neutrons/cm^2 (1 MeV equivalent) and $>1 \times 10^6$ rad(SiO_2)
   a. For applications such as nuclear power plant, waste radiation monitoring, and planetary/solar probes—for example, Jupiter, Uranus, etc.
3. Extreme voltage and/or current applications, for example, power generation, conditioning and distribution, etc.
4. All combinations of the above

Although the topic of packaging will not be addressed in this chapter, it is implicit that a robust packaging technology will be required to support many of these applications with special emphasis on the high-temperature applications.

We note that standard complementary metal oxide semiconductor (CMOS) technology has been the workhorse of the industry and has demonstrated capabilities to support applications that range from −120°C to 225°C as well as a variety of high-voltage and radiation effects applications.

Based on this introduction, the following sections will focus on each of the aforementioned extreme environments, relating the application(s) to specific enabling technologies.

6.2 Environments versus Technologies

6.2.1 High-Temperature Applications

This discussion will be separated into two temperature regions: (1) 125°C–225°C with amenable solutions that include silicon-based bipolar transistors, CMOS bulk or silicon-on-insulator (SOI) technologies, and silicon–germanium heterojunction bipolar transistor (SiGeHBT) technologies and (2) the region above 225°C, that is, >300°C addressed by silicon carbide (SiC), gallium nitride (GaN), gallium arsenide (GaAs), diamond technology, thermionic emitters, and other such robust technologies.

Table 6.1 provides a summary of a various semiconductor technologies for a number of selected applications [1–5].

Tables 6.2 and 6.3 provide a summary of the capabilities and present status of these high-temperature technologies [6].

Concerning the temperature operating range of 125°C–225°C, reports exist that identify the successful adaptation of bipolar and CMOS technologies to support this temperature range. Specific instances include

- Honeywell has developed a family of high-temperature electronic component products that use 150 nm SOI technology to support a variety of applications to include digital and analog/mixed-signal very large-scale integration (VLSI) integrated circuits. This technology is designed to continuously operate for at least 5 years at 225°C, and is targeted at sensor signal conditioning, data acquisition, and control applications in hostile environments. It offers significant reliability and performance advantages over

TABLE 6.1 Semiconductor Technologies for Some Selected High-Temperature Electronics Applications

High-Temperature Electronics Application	Peak Ambient (°C)	Chip Power (kW)	Current Technology	Future Technology
Automotive				
Engine control electronics	150	<1	BS and SOI	BS and SOI
On-cylinder and exhaust pipe	600	<1	NA	WBG
Electric suspension and brakes	250	>10	BS	WBG
Electric/hybrid vehicle	150	>10	BS	WBG
Turbine engine				
Sensors, telemetry, control	300	<1	BS and SOI	SOI and WBG
	600	<1	NA	WBG
Electronic actuation	150	>10	BS and SOI	WBG
	600	>10	NA	WBG
Spacecraft				
Power management	150	>1	BS and SOI	WBG
	300	>10	NA	WBG
Venus and mercury exploration	550	~1	NA	WBG
Industrial				
High-temperature processing	300	<1	SOI	SOI
	600	<1	NA	WBG
Deep-well drilling telemetry				
Oil and gas	300	<1	SOI	SOI and WBG
Geothermal	600	<1	NA	WBG

Source: Neudeck, P.G. et al., *Proc. IEEE*, 90(6), 1065. © 2002 IEEE.
BS, Bulk silicon; SOI, silicon-on-insulator; NA, not presently available; WBG, wide bandgap.

TABLE 6.2 Capability of High-Temperature Technologies

Technology	Theoretical Temperature Limit (°C)	Practical Temperature Limit (°C)
Bulk Si	400	225
SOI Si	400	300
GaN	900	600
SiC	900	600
GaAS	500	400
Thermionic vacuum devices	1000	600
Diamond	>1000	800

Source: Mantooth, H.A. et al., *Power Electron. Soc. Newslett.*, 9. © 2006 IEEE.

traditional silicon integrated circuits when the operating temperatures are greater than 150°C [7].

- Analog Devices AD8229 bipolar SOI instrumentation amplifier that has guaranteed operation from −40°C to 210°C as shown in Figure 6.1 [8].
- Texas Instruments ADS1282 is a 4 kS/s delta-sigma SiGeBiCMOS analog-to-digital converter with 31 bits of resolution and a guaranteed operating range of −55°C to 210°C [9]. It was specifically developed for seismic and energy exploration, including down-hole drilling applications such as measurement while drilling and logging while drilling. Other Texas Instruments devices that have been identified in this regime include the Delfino C2000 floating point microcontrollers.

TABLE 6.3 Summary of the Status of High-Temperature Transistor Technologies

Technology	Transistor Type	Operating Voltage	Frequency Limit	Demonstrated Temperature	Power Consumption	Integration Scale
SiC	Normally On	>200 V to kV	200 MHz	500°C	High	Discrete
GaN	Normally On	250 V	100 GHz	300°C	Medium	SSI
Vacuum transistors	Normally Off	>200 V	2 GHz	500°C	High	Discrete
Diamond JFET	TBD	>200 V	>100 GHz	>500°C	Low	Discrete
GaAs	Normally Off	5 V	50 MHz	400°C	Medium	MSI
SOI CMOS	Normally Off	5 V	20 MHz	300°C	Low	VLSI

Source: Mantooth, H.A. et al., *Power Electron. Soc. Newslett.*, 9. © 2006 IEEE.
TBD, to be determined; SSI, small-scale integration; MSI, medium-scale integration.

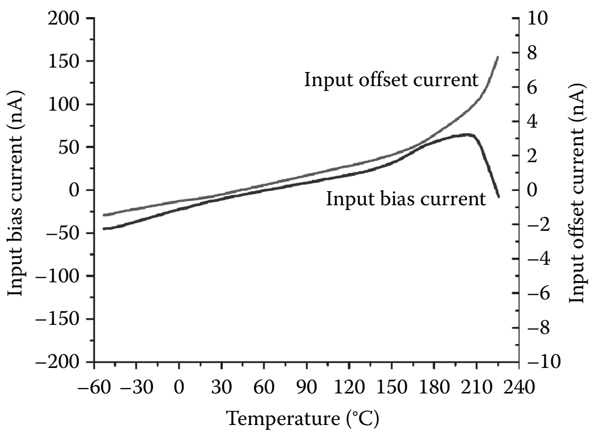

FIGURE 6.1 Analog devices AD8229 1 nV/√Hz low-noise 210°C instrumentation amplifier input bias current and input offset current as a function of temperature. (From 1nV/√Hz low noise 210°C instrumentation amplifier [Datasheet]. Available at http://www.analog.com/static/imported-files/data_sheets/AD8229.pdf)

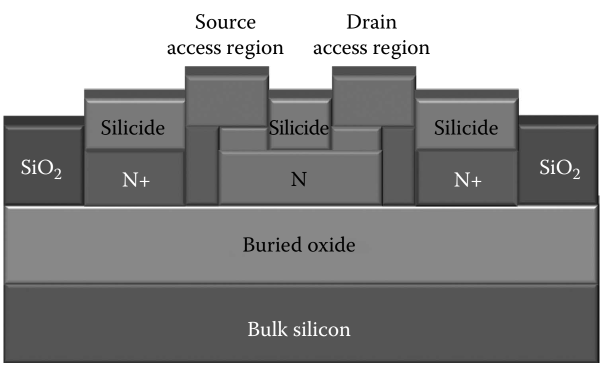

FIGURE 6.2 Cross-sectional SOI MESFET. (From Thornton, T.J. et al., CMOS compatible SOI MESFETs for wide temperature range electronics, *IEEE Aerospace Conference*, pp. 1–9, 2007; Vandersand, J. et al., CMOS compatible SOI MESFETs for extreme environment applications, *IEEE Aerospace Conference*, pp. 1–7, 2005.)

- Metal semiconductor field effect transistor (MESFET) on SOI technology reported by Thornton and Vandersand [10,11] was shown to operate successfully between −180°C and 250°C. In addition, these devices have also demonstrated operation through 5 Mrad(SiO_2) of steady-state total ionizing dose. Figures 6.2 through 6.5 depict the geometry and operation of these transistors and operational transconductance amplifiers (OTA) fabricated using this technology.
- Another technology that has shown promise for both high temperature and radiation performance is the multi-gate SOI FET (SOI MUGFET). As reported by Xiong et al., SOI MUGFET devices have been demonstrated that can operate at temperatures ~300°C and at absorbed dose levels as high as 10 Mrad(SiO_2) [12]. MUGFETs may become particularly important in the future as commercial semiconductor companies develop and productize such devices. As an example, Intel Corporation recently announced that they would begin shipping processors with multi-gate transistors in 2011 [13].

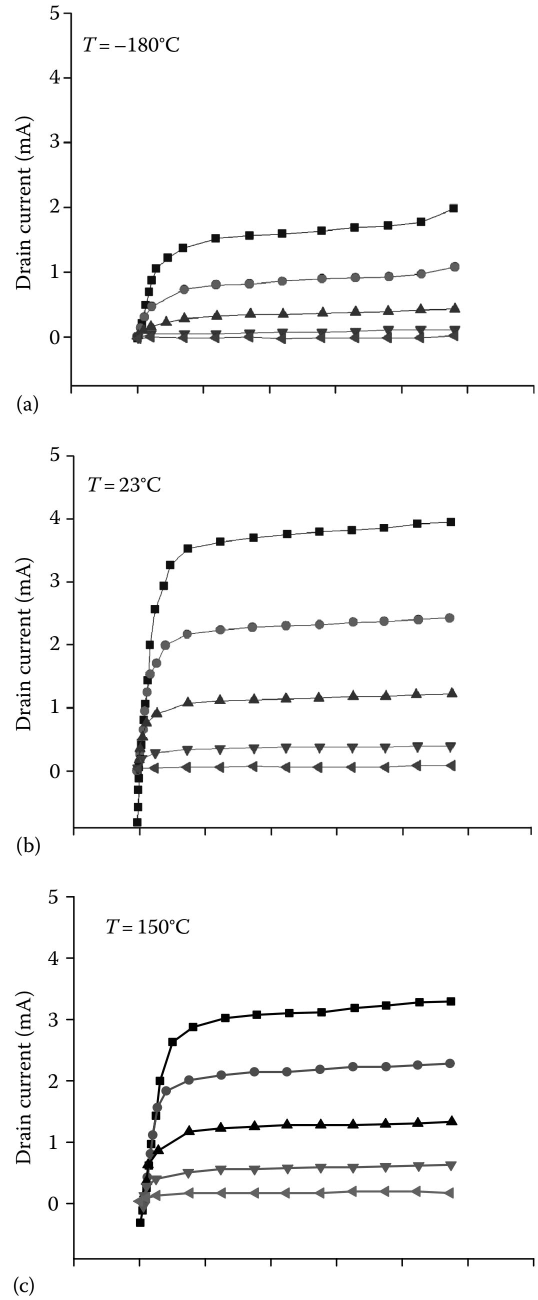

FIGURE 6.3 The I_D–V_{DS} family of curves for (a) −180°C, (b) room temperature, and (c) 150°C. The gate voltages used were 0.5, 0.25, 0, −0.25, and −0.5 V from top to bottom. The dots represent measured data. (From Thornton, T.J. et al., CMOS compatible SOI MESFETs for wide temperature range electronics, *IEEE Aerospace Conference*, pp. 1–9, 2007; Vandersand, J. et al., CMOS compatible SOI MESFETs for extreme environment applications, *IEEE Aerospace Conference*, pp. 1–7, 2005.)

6.2.2 High-Temperature Operation (>300°C)

Concerning operation at temperatures >300°C, the introduction of wide bandgap semiconductor technology (3.0–3.3 eV) becomes imperative and material systems such as SiC, GaN, GaAs, diamond, and thermionic vacuum microelectronics are in use. In addition,

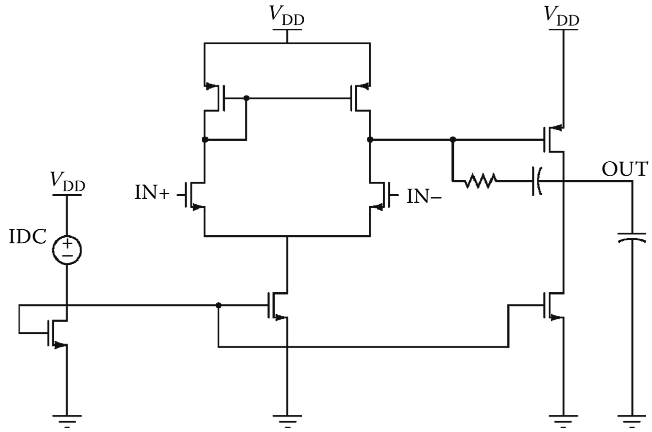

FIGURE 6.4 SOI MESFET operational transconductance amplifier. (From Thornton, T.J. et al., CMOS compatible SOI MESFETs for wide temperature range electronics, *IEEE Aerospace Conference*, pp. 1–9, 2007; Vandersand, J. et al., CMOS compatible SOI MESFETs for extreme environment applications, *IEEE Aerospace Conference*, pp. 1–7, 2005.)

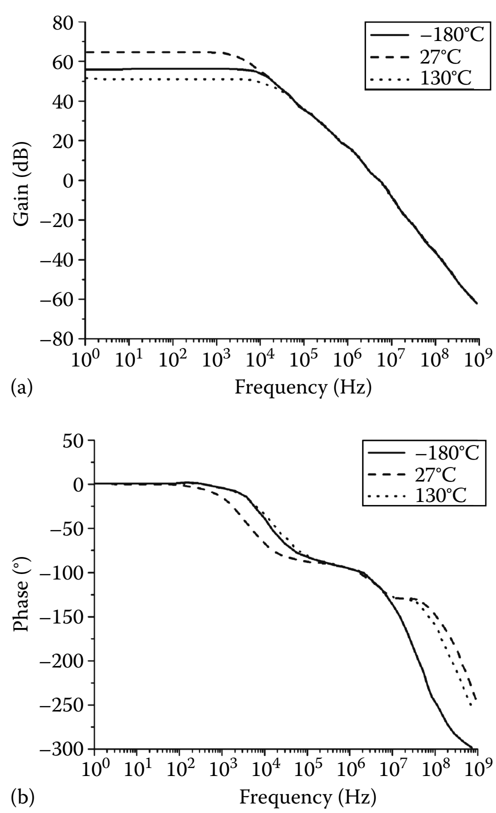

FIGURE 6.5 SOI MESFET operational transconductance amplifier: (a) gain and (b) phase margin performance as a function of frequency for three different temperatures. (From Thornton, T.J. et al., CMOS compatible SOI MESFETs for wide temperature range electronics, *IEEE Aerospace Conference*, pp. 1–9, 2007; Vandersand, J. et al., CMOS compatible SOI MESFETs for extreme environment applications, *IEEE Aerospace Conference*, pp. 1–7, 2005.)

TABLE 6.4 Figures of Merit for Various Semiconductor Technologies

Material	JM[a] $(E_C V_{sat}/\pi)^2$	KM[b] $\lambda(V_{sat}/\varepsilon_\tau)^{1/2}$	QF1[c] $\lambda\sigma_A$[g]	QF2[d] $\lambda\sigma_A E_C$	BM[e] $\sigma_A = \varepsilon_\tau \mu E_C^3$	BHFM[f] μE_C^2
Si	1	1	1	1	1	1
GaAs	7	0.5	36	48	16	11
4H-SiC	278	5.1	594	4357	178	29
GaN	756	1.6	644	7098	744	90

Source: Zhang, N., High voltage GaN HEMTs with low on-resistance for switching applications, PhD dissertation, Electrical and Computer Engineering, University of California, Santa Barbara, CA, 2002.

[a] Johnson's figure of merit for high-frequency devices.
[b] Keyes's figure of merit considering thermal limitation.
[c] Quality factor 1.
[d] Quality factor 2.
[e] Baliga's figure of merit.
[f] Baliga's high-frequency figure of merit.

these technologies have also demonstrated significant capability to withstand high levels of radiation and operating voltage.

The salient properties of the wideband technologies to support high temperature, voltage, and radiation effects, when compared to silicon and GaAs technologies (through the use of four established figures of merit [FM]), are shown in Tables 6.4 through 6.6. These FOM clearly demonstrate the superiority of both SiC and GaN wide bandgap technologies to support both high-temperature and high-voltage applications.

All values are normalized with respect to Si: (1) Johnson's FM for the basic limit on device performance (high power and frequency), (2) Keyes's FM for the switching speed of transistor, (3) Quality factor 1 (thermal FM) for heat sink material and the active device area in power devices, (4) Quality factor 2 is based on the perfect heat sink, (5) Quality factor 3 is based on no assumptions about the sink materials or geometry, and (6) Baliga FM for evaluation of high-frequency applications.

SiC is an ideal semiconductor for power electronics due to its thermal conductivity and wide bandgap. SiC devices have the potential to operate at temperatures near 600°C, eliminating the need for supplementary cooling systems and cutting overall cost. These devices are smaller, lighter, and faster; however, since SiC is a complicated material to grow, the processes associated with it should be developed to reach improved wafer quality with appropriate size and obviously lower cost. Once mature, this material could guide automotive and aircraft technology to higher levels of efficiency.

In Ref. [17], the authors explain the operation of SiC electronics and sensors in extreme environments and discuss such nontraditional applications as the in situ monitoring of volcanic activity, to include immersion in certain types of lavas/magmas, requiring a capability to operate up to 900°C. In Ref. [18], recent trends in SiC power switches are provided with emphasis on bipolar junction transistors (BJTs), insulated gate bipolar transistors (IGBTs), and gate turnoff thyristor (GTOs). BJTs with blocking voltages in 1.2–10 kV range, with current gains >50–100 and operation at 300°C, have been demonstrated [19]. Moreover, p-IGBT devices with breakdown voltages >12 kV and

TABLE 6.5 Physical Properties of SiC and GaN Semiconductors Referenced to Si and GaAs

Property	Si	GaAs	GaN	3C-SiC	6H-SiC	4H-SiC
Bandgap, E_g (eV at 300 K)	1.12	1.43	3.4	2.4	3.0	3.2
Critical field, E_c (V/cm)	2.5×10^5	3×10^5	3×10^6	2×10^6	2.5×10^6	2.2×10^6
Thermal conductivity, λ (W/cm K at 300 K)	1.5	0.5	1.3	3–4	3–4	3–4
Saturated electron drift velocity, V_{sat} (cm/s)	1×10^7	1×10^7	2.5×10^7	2.5×10^7	2×10^7	2×10^7
Electron mobility, μ_n (cm²/V s)	1350	8500	1000	1000	500	950
Hole mobility, μ_p (cm²/V s)	480	400	30	40	80	120
Dielectric constant, ε_r	11.9	13.0	9.5	9.7	10	10

Source: Östling, M., *SCI. CHINA Inform. Sci.*, 54(5), 1087, 2011; Östling, M., Silicon carbide based power devices, *2010 IEEE International Electron Devices Meeting (IEDM)*, 2010, pp. 13.3.1–13.3.4.

TABLE 6.6 Key Electronic Properties for Semiconductor Materials

Semiconductor	Si	SiC-4H	SiC-6H	GaN
Breakdown field (kV/cm)	300	2200	2500	2000
Bandgap (eV)	1.1	3.26	3.05	3.45
Electron mobility (cm²/V s)	1500	1000	500	1250
Thermal conductivity (W/cm·K)	1.5	4.9	4.9	1.3

Source: Zhang, N., High voltage GaN HEMTs with low on-resistance for switching applications, PhD dissertation, Electrical and Computer Engineering, University of California, Santa Barbara, CA, 2002.

super-GTO devices with blocking voltages in the 10–20 kV range have been demonstrated, all with operation at 300°C.

Other examples of the capabilities demonstrated by SiC technologies to support radio frequency (RF) applications include

- SiC BJT with 1800 V breakdown voltage, $R_{on} = 10.8$ mΩ/cm², and $\beta = 20$ capable of sustained operation at 300°C [20]
- Vertical junction field effect transistor (JFET) with 3.5 kV breakdown voltage, 26 mΩ/cm² on-resistance, and sustained operation at 300°C

GaN, on the other hand, has been used in optoelectronics for many years, attaining more developed manufacturing technology. In addition to its wide bandgap, high breakdown field, and better carrier saturation velocity, GaN devices have electron mobility even higher than SiC, though its high-temperature performance is not as good as SiC [21]. GaN technology displays wide bandgap characteristics with high breakdown field performance, saturation velocity, and very high electron mobility, making this technology especially suitable for high-frequency and power applications. GaN–high electron mobility transistor (HEMT) structures (AlGaN/GaN) capable of high power density operation with very low power loss in RF and power systems have been demonstrated [22].

Companies, like Efficient Power Conversion [23], have begun bulk manufacturing of enhancement mode devices with V_{DS} ratings up to 200 V with on-resistances below 30 mΩ. However, with proper processing, the breakdown voltage can be raised significantly—as discussed by Ozbek and Baliga [24], who have demonstrated 1650 V breakdown voltages in Schottky diodes after incorporating special processing techniques. At 3 MV/cm, GaN has a critical field much larger than silicon, so this is an important area of research. The other critical aspect of GaN device development is the manufacture of large-size, high-quality GaN crystals. Many current GaN devices are fabricated on silicon substrates and would benefit from using pure GaN substrates as some lasers do. A small Polish company, Ammono, is pioneering a process to produce 3 and 4 in substrates in the next few years, which would revolutionize GaN device fabrication through economy of scale and device integration capabilities [25]. With GaN wafers of that size, traditional silicon manufacturing techniques would also be feasible.

GaAs and other III–V compound technologies have demonstrated the capability to provide sustained operation at temperatures in the 300°C–500°C range and support various small- to medium-scale density applications that include (but not be limited to) logic, operational amplifiers, and RF amplification. Compounds such as GaAs, AlGaAs/GaAs, AlGaN/GaN, InAs/GaAs materials, and others, configured as MESFETs, MODFETs, JFETs, HEMTs, etc., have been developed as both discrete and integrated circuits to serve high-temperature applications [26]. In addition, GaAs JFET devices have demonstrated high immunity to radiation effects and high temperature, demonstrating operation at 1×10^9 rad(Si) and 10^{16} neutrons/cm² [27].

Thermionic vacuum microelectronics or solid-state vacuum devices (SSVD) have been in development for well over 20 years, and prototypes have been demonstrated using various technologies to include silicon, sapphire, SOI, and SiC. Based on the results of these investigations, they would appear to be a promising technology for power conversion and RF amplification applications requiring high power density and temperatures >700°C. Additionally, they can be integrated into traditional semiconductor process and device technologies [26].

Another recent technology that shows great promise to support both high temperature and radiation effects is carbon nanotube (CNT) nanoelectronics [28–30]. Companies such as Nanterro and Lockheed Martin, who purchased a portion of the original Nanterro, have developed a robust nonvolatile memory technology which has demonstrated a capability to survive and operate at extremes levels of steady-state ionizing radiation and temperature. Figures 6.6 and 6.7 demonstrate this capability showing continued operation at ~10 Mrad(SiO_2) of total ionizing dose and unperturbed retention after prolonged operation at 250°C. Although CNT memory technology is

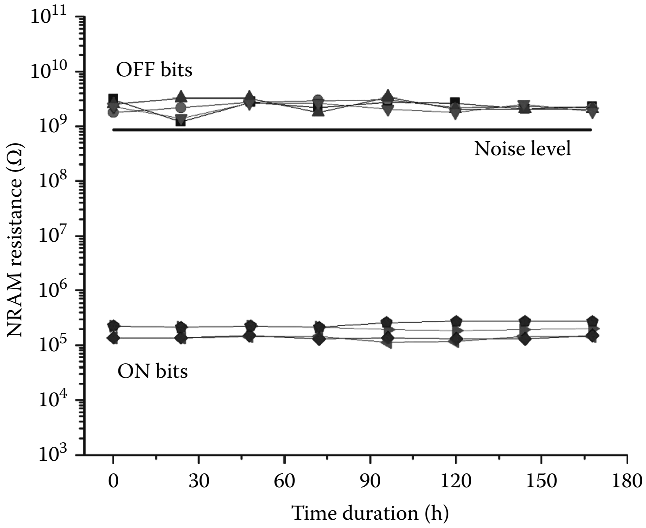

FIGURE 6.6 NRAM data retention at 250°C for 1 week.

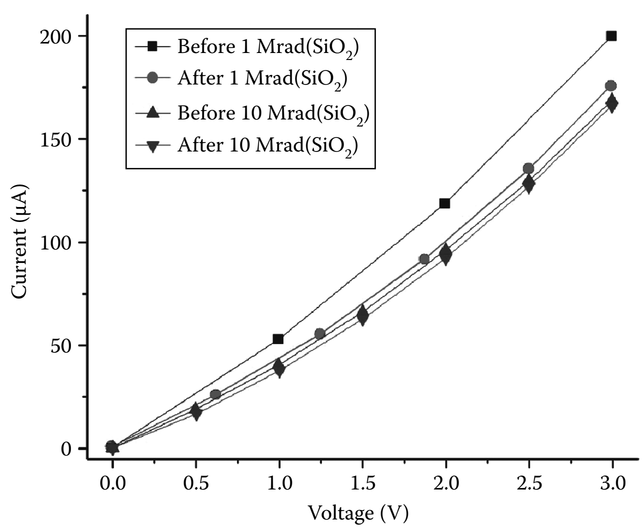

FIGURE 6.7 CNT fabric resistance as a function of steady-state total ionizing dose.

considered to be at an early level of development, for example, National Aeronautics and Space Administration Technology Readiness Level 4 (NASA TRL-4), denoting component and/or breadboard validation in laboratory environment, these data provide some indication of the basic robust nature of the technology and thus its inclusion in this chapter.

The use of diamond-based microelectronics and sensor devices has been explored over the years; however, this technology still remains in the research stage. However, the unique properties of this material would make such devices suitable for very high voltage, power density, and temperature applications, theoretically to above >1000°C.

In 2009, researchers at the University of Glasgow reported on the development of a microsized—50 nm gate length—diamond transistor [31]; this work was formally reported in 2011 [32]. Due to its novel properties—such as large bandgap, high intrinsic mobility, and very high thermal conductivity—diamond is an ideal material for future nanoscale electronic devices and could help the development of nascent technologies such as terahertz imaging and automotive collision detection.

The automotive industry is developing collision detection (or automotive radar) as a safety feature in which a vehicle has an effective radar zone around it that allows it to detect potential collisions from any side well in advance and then take corrective action. Such applications require a very fast and, ideally, high-power transistor technology that needs to be able to operate in adverse weather/temperature conditions, suggested by Moran et al., adding diamond transistor technology would excel in such applications [32]. The diamond material that was used in the device is made synthetically, using chemical vapor deposition by Element Six Ltd. (Ascot, England) through its Diamond Microwave Devices subsidiary. The target is to achieve stable devices with higher frequency and higher power performance than GaN transistors, and to push up the operating frequency of small devices to somewhere around 100 GHz, then enhance power-handling by increasing the device's total gate length.

6.2.3 Low-Temperature Applications

Here again Si-based technologies have demonstrated the capability to support applications at cryogenic temperatures, ≤4.5 K (c.f. [33–37]). However, for operation over an extended temperature range SiGe HBT technology excel. Testing of the IBM 0.5 μm and 130 nm SiGe HBT technologies under the NASA Exploration Technology Development Program (ETDP) has demonstrated operation of this type of technology over a very large temperature range (see Figure 6.8). Data have demonstrated a range of −230°C to >250°C at very significant levels of radiation,

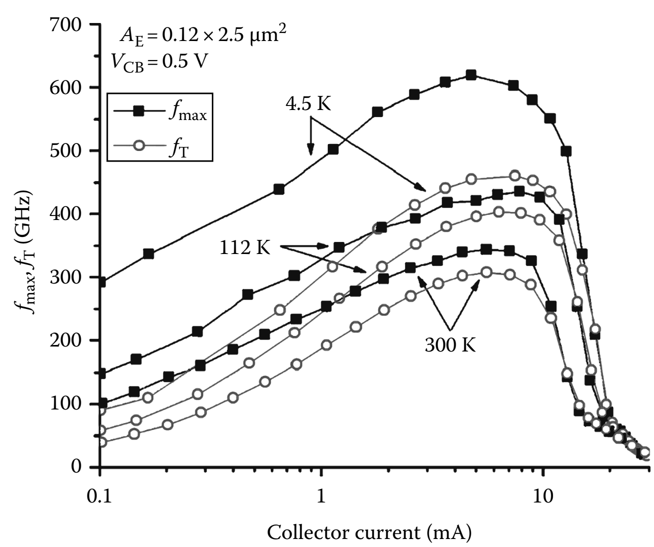

FIGURE 6.8 Measured oscillation and cutoff frequencies as a function of bias at 300, 112, and 4.5 K. (From Jiahui, Y. et al., *IEEE Trans. Electron Devices*, 56(5), 1007, 2009.)

TABLE 6.7 Summary of Fourth-Generation SiGe HBT Parameters at 300, 112, and 4.5 K

Parameter	300 K	112 K	4.5 K
Peak β	827	6504	7693
Peak g_m (mS)	72	110	113
Peak f_{max} (GHz)	343	434	618
Peak f_T (GHz)	309	403	463
Transit time τ_F (fs)	420	330	300
V_{BE} at peak f_{max} (V)	0.90	1.04	1.06
I_C at peak f_{max} (mA)	5.6	7.9	4.8
BV_{CEO} (V)	1.60	1.63	1.62
BV_{CBO} (V)	5.6	5.6	5.6

Source: Jiahui, Y. et al., *IEEE Trans. Electron Dev.*, 56(5), 1007, 2009.

for example, 1 × 10^{14} protons/cm^2. As SiGe technologies scale, their low-temperature performance continues to improve. Table 6.7 shows some SiGe HBT technology parameters of a fourth-generation device at various temperatures.

Another contender for low-temperature operation is laterally diffused CMOS (LDCMOS) technology. This technology has been studied by NASA and the results indicate that it will provide satisfactory performance across a temperature range of −180°C to 100°C [38,39]. The device geometries under study in this investigation are shown later and can operate at voltages from 12 to 1200 V. Some cross sections and data are shown in Figures 6.9 and 6.10 [40].

In addition to LDCMOS and SiGeBiCMOS process technologies, recent testing has shown that the Peregrine Inc. 0.5 μm fully depleted silicon-on-sapphire technology is capable of sustained and undegraded operation at temperatures as low as 10 K at ^{60}Co steady-state total ionizing dose radiation levels of 2 Mrad(Si) [41].

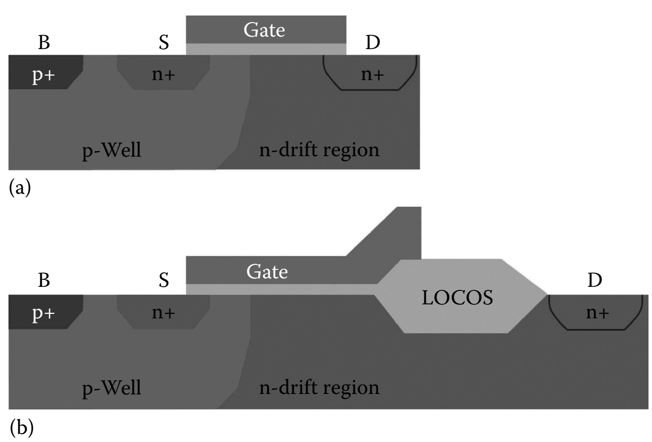

FIGURE 6.9 (a) Low-voltage and (b) high-voltage linear double-diffused metal oxide semiconductor transistors used in the NASA/JPL investigation to characterize low-temperature operation. The unique geometries of these devices and low doping levels support low-temperature operation as shown in Figure 6.10 for a LVDMOS device. (From Kashyap, A.S. et al., Characterization of LDMOS devices in the deep cryogenic regime, presented at the *NASA ETDP Program Review*, Atlanta, GA, 2008.)

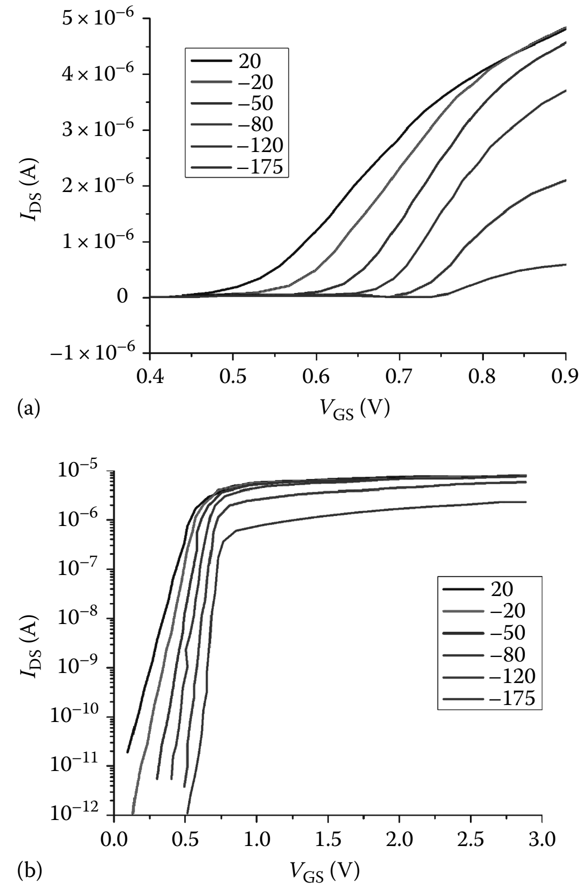

FIGURE 6.10 LDCMOS performance as a function of bias and temperature. (From Kashyap, A.S. et al., Characterization of LDMOS devices in the deep cryogenic regime, presented *at the NASA ETDP Program Review*, Atlanta, GA, 2008.) (a) shows V_{th} variation as a function of temperature and (b) shows I_{DS}–V_{GS} variation as a function of temperature. For both figures, V_{DS} is 0.1 V and V_{SB} is 0 V. The plot legends are in °C.

6.3 Summary

In this chapter, the capabilities of a number of different semiconductor technologies have been assessed for their suitability to support extreme environment applications. A graphic summary of these findings is provided in Table 6.8. It is of interest to note that unless you are at the extreme limits of the environments or require specialized performance, a basic silicon CMOS approach, augmented by an insulating substrate technology, will serve in the majority of the applications.

Since single-event effect performance is, to a large degree, influenced by design only, a qualitative estimate of upset performance is provided, except for SiC power devices that have shown some susceptibility to gate rupture due to heavy ions. Zhang showed that the single-event burnout response of SiC power devices to be ~6× that of silicon-based devices. However, the single-event gate rupture sensitivity was shown to be approximately equal to silicon-based devices [42].

TABLE 6.8 Summary of Semiconductor Exemplar Technologies Operating Capabilities over Environment

	Environment								
	Temperature (°C)					Radiation			Operating Voltage
Technology	<150	<−55 to −150	−55 to ~200	>200 to 500	>500	$>10^6$ Rad(SiO_2) Steady-State Total Ionizing Dose	Single-Event Effects	$>10^{12}$ Neutrons/cm^2 (1 MeV Equivalent)	≥10 kV
CMOS with SOI substrate									Small signal devices
Bipolar with SOI substrate									Small signal devices
SiGe HBT									Small signal devices
GaN RF HEMT/HBT									Small signal devices
SiC power transistor or diode							SEGR		High voltage, $>10^4$ V demonstrated
Vacuum microelectronics									
Diamond JFET									

	Demonstrated reliable operation
	Area of diminished or reduced reliability operation
	Areas where reliable operation is not deemed feasible

Thus, to summarize

1. Temperatures >500°C and high voltage (>1000 V):
   a. SiC BJT type devices (i.e., IGBT, GTO) dominate this application space and discrete devices are available.
   b. GaN JFET technology has also demonstrated a capability to support application up to and exceeding 500°C; however, their application has been focused at RF and fast switching DC/DC converter applications that also require low R_{on}.
   c. Diamond JFET technology may someday serve as an alternative, but still remains a laboratory phenomenon.
   d. Thermionic vacuum technology has shown itself to be a viable candidate for >500°C operation, but at lower voltage; however, this too is not available commercially.
2. Temperature range >300°C to ~400°C:
   a. GaAs and other III–V compound semiconductor technologies for low-voltage applications fall into this category.
3. Room temperature up to 225°C:
   a. Silicon-based CMOS and BJT transistors using SOI substrate technology provide VLSI-type integrated circuits in this range with various commercial off-the-shelf solutions available.
   b. SiGe HBT devices provide a technology to serve this area.
5. Room temperature down to mK:
   a. Both SiGe HBT and CMOS silicon technologies have demonstrated the capability to support this temperature range.

References

1. P. G. Neudeck, R. S. Okojie, and L. Y. Chen, High-temperature electronics—A role for wide bandgap semiconductors? *Proceedings of the IEEE*, 90(6), 1065–1076, 2002.
2. P. G. Neudeck, D. J. Spry, C. Liang-Yu, G. M. Beheim, R. S. Okojie, C. W. Chang, R. D. Meredith et al., Stable electrical operation of 6H-SiC JFETs and ICs for thousands of hours at 500 deg C, *IEEE Electron Device Letters*, 29(5), 456–459, 2008.
3. P. G. Neudeck, S. L. Garverick, D. J. Spry, L. Y. Chen, G. M. Beheim, M. J. Krasowski, and M. Mehregany, Extreme temperature 6H-SiC JFET integrated circuit technology, *Physica Status Solidi A—Applications and Materials Science*, 206(10), 2329–2345, 2009.
4. P. G. Neudeck, D. J. Spry, L. Y. Chen, C. W. Chang, G. M. Beheim, R. S. Okojie, L. J. Evans, et al., Prolonged 500 degrees C operation of 6H-SiC JFET integrated circuitry, in *Silicon Carbide and Related Materials 2008*, Materials Science Forum Vols. 615–617, A. PerezTomas et al., Eds., 2009, pp. 929–932, 2009, Trans Tech Publications, Zurich, Switzerland.
5. P. G. Neudeck, M. J. Krasowski, L. Y. Chen, and N. F. Prokop, Characterization of 6H-SiC JFET integrated circuits over a broad temperature range from −150 degrees C to +500 degrees C, in *Silicon Carbide and Related Materials 2009, Pts 1 and 2*, Vol. 645–648, A. J. Bauer et al., Eds., 2010, pp. 1135–1138.
6. H. A. Mantooth, M. M. Mojarradi, and R. W. Johnson, Emerging capabilities in electronics technologies for extreme environments. Part I—High temperature electronics, *Power Electronics Society Newsletter*, 9–14, 2006.

7. Honeywell. SSEC—High temperature electronics—Honeywell Aerospace. Available at http://honeywell.com/Pages/Home.aspx, 2011.
8. 1 nV/√Hz low noise 210°C instrumentation amplifier [Datasheet]. Available at http://www.analog.com/static/imported-files/data_sheets/AD8229.pdf
9. ADS1282 ultra high resolution delta sigma ADC with PGA for seismic and energy exploration [Datasheet]. Available at http://focus.ti.com/docs/prod/folders/print/ads1282.html
10. T. J. Thornton, J. Ervin, A. Balijepalli, A. Shanmugam, W. Lepkowski, K. Holbert, and B. Bakkaloglu, CMOS compatible SOI MESFETs for wide temperature range electronics, *IEEE Aerospace Conference*, Big Sky, MT, March 3–10, 2007, pp. 1–9.
11. J. Vandersand, V. Kushner, J. Yane, B. Blalock, and T. Thornton, CMOS compatible SOI MESFETs for extreme environment applications, *IEEE Aerospace Conference*, 2005, pp. 1–7.
12. W. Xiong, C. R. Cleavelin, C. H. Hsu, M. Ma, T. Schulz, K. Schruefer, P. Patruno, and J. P. Colinge, Multi-gate SOI MOSFET operations in harsh environments, *2007 IEEE International SOI Conference*, Indian Wells, CA, October 1–4, 2007, pp. 29–30.
13. Transistors go 3-D, *Spectrum, IEEE*, 48(6), 12, 2011. DOI: http://dx.doi.org/10.1109/MSPEC.2011.5779772.
14. N. Zhang, High voltage GaN HEMTs with low on-resistance for switching applications, PhD dissertation, Electrical and Computer Engineering, University of California, Santa Barbara, CA, 2002.
15. M. Östling, High power devices in wide bandgap semiconductors, *SCIENCE CHINA Information Sciences*, 54(5), 1087–1093, 2011.
16. M. Östling, Silicon carbide based power devices, *2010 IEEE International Electron Devices Meeting (IEDM)*, San Francisco, CA, December 6–8, 2010, pp. 13.3.1–13.3.4.
17. A. Horsfall and N. Wright, Sensing the extreme, *Physics World*, 19(5), 34–39, May 2006.
18. A. Agarwal, Z. Qingchun, A. Burk, R. Callanan, and S. Mazumder, Prospects of bipolar power devices in silicon carbide, *34th Annual Conference of IEEE Industrial Electronics, 2008. IECON 2008*, 2008, pp. 2879–2884.
19. C. Jonas, C. Capell, A. Burk, Q. Zhang, R. Callanan, A. Agarwal, B. Geil, and C. Scozzie, 1200 V 4H-SiC bipolar junction transistors with a record β of 70, *Journal of Electronic Materials*, 37(5), 662–665, 2008.
20. M. Östling, S. M. Koo, S. K. Lee, E. Danielsson, M. Domeij, and C. M. Zetterling, SiC device technology for high voltage and RF power applications, *23rd International Conference on Microelectronics, MIEL 2002*, Niš, Yugoslavia, May 12–15, Vol. 1, 2002, pp. 31–39.
21. T. P. Chow, V. Khemka, J. Fedison, N. Ramungul, K. Matocha, Y. Tang, and R. J. Gutmann, SiC and GaN bipolar power devices, *Solid State Electronics*, 44(2), 277–301, 2000.
22. W. Saito, Reliability of GaN-HEMTs for high-voltage switching applications, *2011 IEEE International Reliability Physics Symposium (IRPS)*, Monterey, CA, April 10–14, 2011, pp. 4E.1.1–4E.1.5.
23. Efficient power conversion. Available at http://epc-co.com/epc/
24. A. M. Ozbek and B. J. Baliga, Planar nearly ideal edge-termination technique for GaN devices, *IEEE Electron Device Letters*, 32(3), 300–302, 2011.
25. R. Stevenson, The world's best gallium nitride, *IEEE Spectrum*, 47(7), 40–45, 2010.
26. L. P. Sadwick, R. J. Hwu, J. H. Chern, C. H. Lin, L. Del Castillo, T. Johnson, and IEEE, 500 C electronics for harsh environments, *2005 IEEE Aerospace Conference*, Vols. 1–4, IEEE, Piscataway, NJ, 2005, pp. 2681–2691.
27. D. Palmer, B. Draper, and G. Carlson, Extreme radiation tolerance of high temperature solid-state microelectronics, *IEEE Transactions on Components, Hybrids, and Manufacturing Technology*, 4(4), 466–471, 1981.
28. V. Ayres, B. Jacobs, S. Song, R. Ronningen, A. Zeller, M. Crimp, J. Halpern, M. He, M. Petkov, D. Liu, and H. Shaw, Nanotube, nanowire, and nanocircuit behavior in simulated space environments, *Proceedings of SPIE*, 5897(1), 589702, 2005.
29. C. D. Cress, J. J. McMorrow, J. T. Robinson, A. L. Friedman, and B. J. Landi, Radiation effects in single-walled carbon nanotube thin-film-transistors, *IEEE Transactions on Nuclear Science*, 57(6), 3040–3045, 2010.
30. N. A. Duncan, Changes to electrical conductivity in irradiated carbon nanocomposites, MSc thesis, Department of Engineering Physics, Air Force Institute of Technology, Wright-Patterson Air Force Base, OH, 2011.
31. S. Bush, Glasgow Uni develops diamond transistor with 50 nm gate. Available at http://www.electronicsweekly.com/Articles/13/08/2010/45900/glasgow-uni-develops-diamond-transistor-with-50nm-gate.htm, 2009.
32. D. A. J. Moran, O. J. L. Fox, H. McLelland, S. Russell, and P. W. May, Scaling of hydrogen-terminated diamond FETs to sub-100-nm gate dimensions, *IEEE Electron Device Letters*, 32(5), 599–601, 2011.
33. C. Tianbing, K. Wei-Min Lance, Z. Enhai, L. Qingqing, J. Zhenrong, J. D. Cressler, and A. J. Joseph, On the high-temperature (to 300°C) characteristics of SiGe HBTs, *IEEE Transactions on Electron Devices*, 51(11), 1825–1832, 2004.
34. J. D. Cressler, On the potential of SiGe HBTs for extreme environment electronics, *Proceedings of IEEE*, 93(9), 1559–1582, 2005.
35. R. Krithivasan, Y. Lu, J. D. Cressler, J.-S. Rieh, M. H. Khater, D. Ahlgren, and G. Freeman, Half-terahertz operation of SiGe HBTs, *IEEE Electron Device Letters*, 27, 567–569, 2006.
36. L. Najafizadeh, J. S. Adams, S. D. Phillips, K. A. Moen, J. D. Cressler, S. Aslam, T. R. Stevenson, and R. M. Meloy, Sub-1-K operation of SiGe transistors and circuits, *IEEE Electron Device Letters*, 30(5), 508–510, 2009.

37. Y. Jiahui, J. D. Cressler, R. Krithivasan, T. Thrivikraman, M. H. Khater, D. C. Ahlgren, A. J. Joseph, and R. Jae-Sung, On the performance limits of cryogenically operated SiGe HBTs and its relation to scaling for terahertz speeds, *IEEE Transactions on Electron Devices*, 56(5), 1007–1019, 2009.
38. A. S. Kashyap, H. A. Mantooth, T. A. Vo, and M. Mojarradi, Compact modeling of LDMOS transistors for extreme environment analog circuit design, *IEEE Transactions on Electron Devices*, 57(6), 1431–1439, 2010.
39. A. S. Kashyap, M. Mudholkar, H. A. Mantooth, T. Vo, and M. Mojarradi, Cryogenic characterization of lateral DMOS transistors for lunar applications, *Aerospace Conference, 2009 IEEE*, 2009, pp. 1–8.
40. A. S. Kashyap, M. Mudholkar, H. A. Mantooth, M. Mojarradi, and T. Vo, Characterization of LDMOS devices in the deep cryogenic regime, presented at the *NASA ETDP Program Review*, Atlanta, GA, 2008.
41. J. McGaritty, in *Peregrine SOS Low-Temperature and Radiation Performance*, L. M. Cohn, Ed., College Park, MD, 2011.
42. X. Zhang, Failure mechanisms in wideband semiconductor power devices, PhD dissertation, Mechanical Engineering, University of Maryland, College Park, MD, 2006.

II

Background

John D. Cressler
Georgia Institute of Technology

Introduction

A meaningful discussion of extreme environment electronics must necessarily assume a requisite background understanding in several subjects, including the physics of temperature, temperature's impact in semiconductor behavior and device operation over wide operating temperature ranges, the nature of radiation and radiation transport physics, and the interaction of various radiation types with semiconductor materials and devices. Part II provides the reader with this fundamental background, and is thus an excellent "jumping off point" for the rest of the book.

Chapter 7 by John Cressler and Kurt Moen of Georgia Tech provides fundamental background related to the physical meaning of temperature and its influence on carrier transport properties in semiconductors and the various devices built from them. In Chapter 8 by Robert Reed of Vanderbilt University and Janet Barth of NASA-GSFC, the reader is introduced to important concepts from radiation transport physics that pertain to radiation effects in electronics. Chapter 9 by Ken Galloway and Ron Schrimpf of Vanderbilt University provide background on the influence of radiation on semiconductors and semiconductor device operation. Each chapter of this part contains numerous references for further reading.

7 Physics of Temperature and Temperature's Role in Carrier Transport

John D. Cressler
Georgia Institute of Technology

Kurt A. Moen
Georgia Institute of Technology

7.1 Introduction

"'Thermal physics' is the fruit of the union of statistical and mechanical principles."* Thermal physics is commonly referred to by the much more intimidating name "statistical mechanics," a complex subject which is often the bane of many physics students, and which unifies the bedrock of macroscopic thermodynamics with the microscopic world of quantum mechanics. Said another way, statistical mechanics derives the results of thermodynamics using (statistical) quantum mechanics, from first principles. As such, it is one of the more beautiful and elegant constructs of the human mind.

Mechanics deals with the nature of "work," whereas thermal physics deals with the nature of "heat." Because of this fundamental difference, new concepts must be necessarily introduced in thermal physics, namely, entropy and temperature, which are closely related. Clearly, within the context of extreme environments (this book), temperature is a key concept to get your hands around, and while it clearly has an intuitive basis (our body's sensations of "hot" and "cold"), placing temperature on a firm theoretical grounding is important. We will start there. Next we will examine the theoretical basis of thermal activation (Arrhenius behavior), which touches much of transistor physics, circuit response, device and packaging reliability, etc. (the list is long), and which is a direct consequence of our definition of temperature and how it couples to a two energy level system. Given these results, the logical question then becomes how does temperature enter transistor physics, and with that, all of electronics? Inevitably, the answer to this admittedly deep question is traceable to the carrier (electron and hole) distribution functions, arguably the most important result of thermal physics as it relates to electronic devices, circuits, and systems. These derivations are worth seeing and are shown next. Finally, we examine the important role temperature plays on carrier transport, since this coupling has a direct bearing on the operation of electronic devices across a wide temperature range.

7.2 Physics of Temperature

First things first. What, formally, is "temperature"? Well, let us start with "entropy." At its deepest level, entropy measures the number of quantum states accessible to a system. The statistical bedrock is this: the quantum states of the system in question, whatever that might be, are assumed to be either accessible or inaccessible to the system, and the system is equally likely to be in one accessible state as any other accessible state. Given g accessible states, the entropy is defined to be

$$\sigma = \ln g \tag{7.1}$$

From this perspective, the entropy will necessarily be a function of the total system energy (U), the number of particles (N) within the system, and the volume (V) of the system. Other parameters may also enter the scene, depending on the exact nature of the system in question.

When two systems, each with specific energy, are brought into intimate "thermal contact," they may transfer energy from

* For the first three sections of this chapter, I am leaning heavily on the refreshingly intuitive approach to thermal physics pioneered by Charles Kittel [1,2].

one to the other, and while the total energy is fixed, the constraints on each systems' respective energy are removed (this is formally what we mean by thermal contact). A transfer of energy in one direction or the other may increase the product of their respective accessible states (g_1g_2), which measures the number of accessible states of the combined systems. The fundamental assumption of statistical mechanics biases the final outcome in favor of that allocation of the total energy between the two systems that maximizes the number of accessible states. The net: more accessible states is the result preferred by nature, and thus more likely to happen (statistically speaking). This statement is simply a statistical mechanical statement of the law of the increase of entropy; that is, the second law of thermodynamics.

Back to the problem at hand. Having brought two systems into thermal contact, what is the most probable outcome? Well, one system will gain energy at the expense of the other (the total energy is fixed), and the total entropy of the two systems will increase. Eventually, the entropy will reach a maximum for a given total energy (a.k.a., a fundamental definition of what we mean by "equilibrium"). It can be shown [1] from first principles that the maximum entropy will be attained when $(\partial\sigma/\partial U)_{N,V}$ for one system is equal to the value of the same quantity for the second system. This equality property of two systems in thermal contact is exactly the property we intuitively expect for the temperature. Thus, we formally define the "fundamental temperature" according to [1]

$$\frac{1}{\tau} \equiv \left.\frac{\partial\sigma}{\partial U}\right|_{N,V} \tag{7.2}$$

Clearly, τ has dimensions of energy. The use of $1/\tau$ in this definition ensures that the energy flows from high τ to low τ, again, consistent with our intuitive expectation of temperature. It then follows that the Kelvin temperature, the so-called "absolute temperature," is directly proportional to τ via Boltzmann's constant ($k = 8.617 \times 10^{-5}$ eV/K) (refer to Appendix B for more information). Thus we have

$$\tau = kT \tag{7.3}$$

In this formalism, the conventional entropy (S) is then simply given by $S = k\sigma$. As you can see, temperature, while clearly intuitive to our body's sensory organs as a measure of "hotness" and "coldness," is also deeply embedded in the fundamental statistical mechanical nature of reality.

7.3 Origins of Thermal Activation

Let us now briefly examine the fundamental origins of "thermal activation," sometimes referred to as "Arrhenius behavior." The Arrhenius equation is a well-known formula for the temperature dependence of the reaction rate constant, and therefore, the rate of a chemical reaction. The equation was first proposed by the Dutch chemist J.H. van Hoff in 1884, and 5 years later in 1889, the Swedish chemist S. Arrhenius provided a physical justification and interpretation for it. The Arrhenius equation is given by

$$R = Ae^{-E_a/kT} \tag{7.4}$$

and shows (in a chemistry context) that the reaction rate constant (R) in proportional to the exponential of an "activation energy" (E_a), divided by the fundamental temperature (kT). This result is often viewed as simply an empirical equation for describing various data. Nothing could be further from the truth. A clue is given in the fact that Arrhenius behavior is observed in virtually all fields of study: chemistry, certainly, but also biology, cosmology, metallurgy, and, yes, transistor physics, especially as it relates to the temperature dependence of electronics. The list is semi-infinite. This diversity of appearance is clearly indicative of a more fundamental origin, and that is easily obtained from basic thermal physics, as illustrated here.

Consider a simply "toy model" consisting of only two energy states: one at energy level 0 (a.k.a. the "ground state") and one at energy level E (Figure 7.1). Let this simple two-state system be held in intimate thermal contact with a "large" system that we call a "thermal reservoir" (note that it only need be large relative to the energy of the two-state system). Let the total energy of the combined system be U_0, and thus when the two-state system has energy 0, the reservoir has energy U_0 and $g(U_0)$ quantum states accessible to it. On the other hand, when the small system is in state E, the reservoir will have energy $U_0 - E$ and $g(U_0 - E)$ quantum states accessible to it. By the fundamental assumption of statistical mechanics, the ratio of the probability of finding the small system with energy E to the probability of finding it with energy 0 is simply

$$\frac{P(E)}{P(0)} = \frac{g(U_0 - E)}{g(U_0)} = \frac{e^{\sigma(U_0 - E)}}{e^{\sigma(U_0)}} \tag{7.5}$$

Now, the reservoir entropy σ can be expanded in a Taylor Series (because the small system is negligible in size compared to it) such that

$$\sigma(U_0 - E) = \sigma(U_0) - E\frac{\partial\sigma}{\partial U_0} + \cdots = \sigma(U_0) - \frac{E}{\tau} \tag{7.6}$$

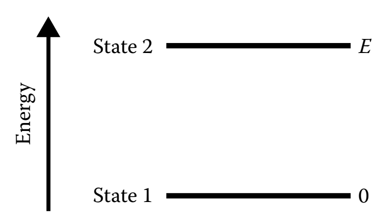

FIGURE 7.1 Conceptual view of a general two-state system at energy 0 and energy E.

by the definition of the fundamental temperature. Dropping higher-order terms, and simplifying, we obtain

$$\frac{P(E)}{P(0)} = e^{-E/\tau} = e^{-E/kT} \tag{7.7}$$

This is the so-called Boltzmann factor, and is the fundamental origin of thermal activation: Arrhenius behavior. Any system which can be simplified into two energy levels, and which obeys statistical occupancy probabilities, by whatever means, will necessarily be governed in a manner proportional to the Boltzmann factor. Note that this concept can be extended into an exceptionally diverse set of realms. In general, any scenario when one configuration of a given system (at energy 1) dynamically changes to another configuration (at energy 2) will yield thermal activated behavior. As an example, consider solid-state diffusion (energy 1 represents the diffusing atom in lattice position one, and energy 2 represents the diffusing atom in position two). Other examples include trap kinetics and defect formation in solids. This list is long. Closer to home, we can apply this two-state system idea to carrier transport in semiconductors. The energy bandgap (E_G) is a fine two energy level system (e.g., E_C and E_V—Figure 7.2). Thus, any action involving the bandgap will necessarily involve thermally activated behavior. For instance, the intrinsic carrier density can be written as

$$pn = n_i^2 = e^{-E_G/kT} \tag{7.8}$$

Given the exponential dependence on temperature that is driven by the Boltzmann factor, temperature thus couples very strongly to semiconductor properties, and in particular transistor physics, especially when it is tied to excitation of carriers across the bandgap (e.g., minority carrier transport devices—*pn* junctions, bipolar transistors, MOSFETs in subthreshold regime, etc.).

As a concrete transistor example, consider the ratio of the current gain (β) in a SiGe HBT to that in a Si BJT (refer to Chapter 18):

$$\left.\frac{\beta_{\mathrm{SiGe}}}{\beta_{\mathrm{Si}}}\right|_{V_{BE}} \simeq \left\{\frac{\tilde{\gamma}\tilde{\eta}\Delta E_{g,\mathrm{Ge}}(\mathrm{grade})/kT e^{\Delta E_{g,\mathrm{Ge}}(0)/kT}}{1 - e^{-\Delta E_{g,\mathrm{Ge}}(\mathrm{grade})/kT}}\right\} \tag{7.9}$$

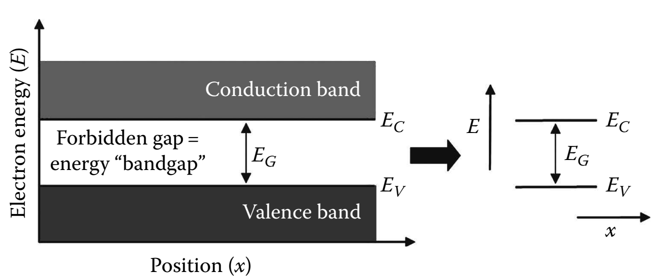

FIGURE 7.2 Conceptual view of the energy band diagram.

In this case, the band-edge changes induced by the addition of the smaller bandgap SiGe alloy produce thermally activated behavior in the current gain ratio, and in this instance each *kT* factor is favorably aligned to improve transistor current gain with cooling, opening the door to operation of SiGe HBTs at cryogenic temperatures.

Finally, note that even complex processes involving many different energy configurations, not just two, can be approximated as a piecewise linear collection of two-state events, again pulling in thermal activation into the driving mechanism.

7.4 Fermi–Dirac and Boltzmann Distribution Functions

At the deepest level, temperature most strongly enters the physical equations governing transistor operation via the carrier distribution functions. That is, given an accessible quantum state in the conduction or valence band, what is the probability that this state is filled (or emptied) by an electron? This is the carrier distribution function. Since electrons (and holes) are fermions, the governing distribution function for semiconductor devices is ultimately the Fermi–Dirac distribution function ($f_{FD}(E, T)$) [1]. In the limit of low carrier densities, the Fermi–Dirac distribution function reduces to the Boltzmann distribution function ($f_B(E, T)$). The well-known "density-of-states" function ($g_C(E, T)$) which determines the number of allowed quantum states in the conduction and valence bands per unit energy per unit volume, is given by,

$$g_C(E,T) = \frac{1}{2\pi^2}(2m_n^*/\hbar^2)^{3/2}\sqrt{E - E_C} \tag{7.10}$$

The multiplication of f_{FD} with g_C and integration from E_C to infinity, physically "counts" the electrons present in the conduction band (Figure 7.3), which might, for instance, be available for transport in response to an applied field (i.e., generating current flow). Both f_{FD} and g_C can be derived from very general arguments. Given its significance in the coupling of temperature to carrier transport in semiconductor devices, we here show how simple arguments can be used to arrive at f_{FD} [1]. More sophisticated (and rigorous) approaches are easily found in books on *Statistical Mechanics* (e.g., see [3]).

Let us reconsider two systems, but now allow for not only energy exchange between them, but also particle exchange. For two systems in both thermal and diffusive contact, the entropy will be a maximum with respect to the transfer of both particles and energy. Thus, not only must $(\partial\sigma/\partial U)_{N,V}$ be equal for both systems, but $(\partial\sigma/\partial N)_{U,V}$ must also be equal for both systems, where N is the number of particles (e.g., electrons). For this scenario we introduce a new concept, the "chemical potential" (μ), such that

$$-\frac{\mu}{\tau} \equiv \left.\frac{\partial\sigma}{\partial N}\right|_{U,V} \tag{7.11}$$

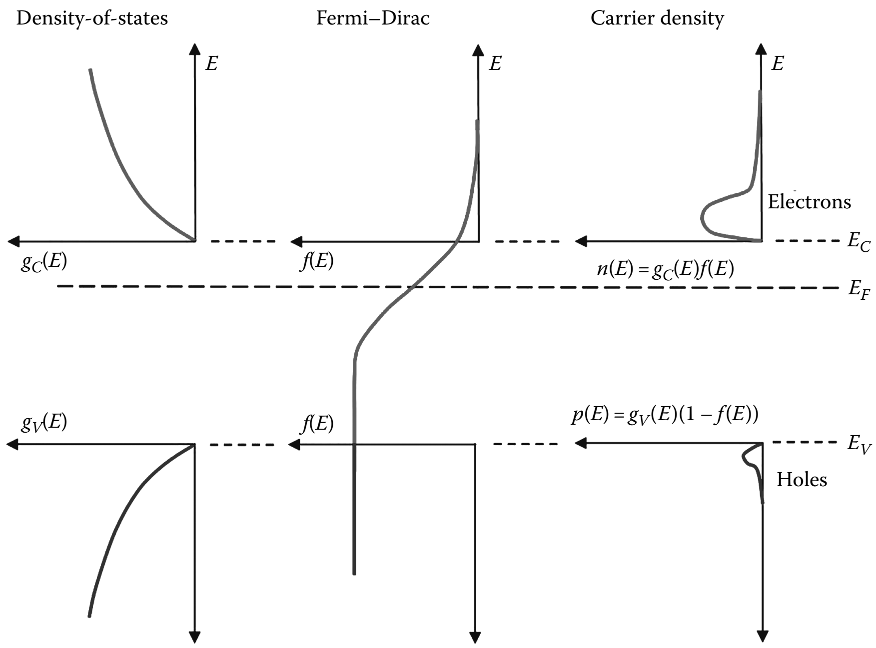

FIGURE 7.3 Illustration of the use of the Fermi–Dirac distribution function to calculate the electron density in the conduction band.

The negative sign is chosen to ensure that the direction of particle flow as equilibrium is approached is from high chemical potential to low chemical potential. Given sufficient time to reach equilibrium, we have that for two systems in thermal and diffusive contacts, $\tau_1 = \tau_2$ and $\mu_1 = \mu_2$.

Now let us return to the two-state system discussed earlier, but now we also include particles (Figure 7.4). Assume that one state has 0 particle and 0 energy, and the second state has 1 particle and energy E. As earlier, this system is in contact with a reservoir at fundamental temperature τ and chemical potential μ. Following the same path, we find

$$\begin{aligned}\sigma(U_0 - E; N_0 - 1) &= \sigma(U_0; N_0) - E\frac{\partial\sigma}{\partial U_0} - 1\frac{\partial\sigma}{\partial N_0} + \cdots \\ &= \sigma(U_0; N_0) - \frac{E}{\tau} + \frac{\mu}{\tau}\end{aligned} \tag{7.12}$$

By analogy with our original example, we have

$$\frac{P(1,E)}{P(0,0)} = e^{(\mu - E)/\tau} = e^{(\mu - E)/kT} \tag{7.13}$$

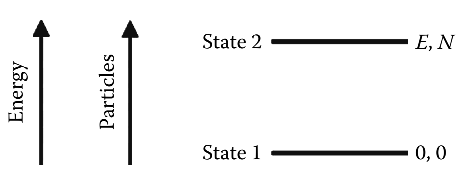

FIGURE 7.4 Conceptual view of a general two-state system with 0 particle at energy 0 and N particles at energy E.

for the ratio of the probability that the system is occupied by 1 particle at energy E to the probability that the system is unoccupied with energy 0. After normalization, we finally obtain

$$P(1,E) = f_{FD}(E,T) = \frac{1}{e^{(E-\mu)/\tau} + 1} = \frac{1}{e^{(E-E_F)/kT} + 1} \tag{7.14}$$

where by convention when working with semiconductors, we have changed chemical potential (μ) to the "Fermi energy" (E_F). This is the Fermi–Dirac distribution function. It easily follows then that in the limit of small values of $P(1, E)$ (with respect to 1), this reduces to the familiar Boltzmann distribution:

$$P(1,E) = f_B(E,T) \cong e^{-(E-\mu)/\tau} = e^{-(E-E_F)/kT} \tag{7.15}$$

From these distribution functions, one is then set to tackle the counting of electron (and hole) densities in the conduction (and valence) bands of a semiconductor. The reader is referred to any good book on semiconductor devices for those standard derivations (e.g., [4,5]).

7.5 Role of Temperature in Carrier Transport

Given this background on the fundamentals of temperature, we now briefly turn to the more practical topic of how temperature couples to the carrier transport parameters in real semiconductor devices. At the end of the day, carrier transport (in essence, how electrons and holes move from point A to point B as time elapses) determines the functional utility of any given semiconductor device, whether that device is designed for high speed or high voltage or both, for an electronic application or a photonic application or both. When one speaks of transport parameters, the items that come to mind would be the carrier lifetimes ($\tau_{n,p}$), the carrier drift mobilities ($\mu_{n,p}$), and the impact of high electric fields on carrier velocity (saturation velocity, carrier overshoot, the impact of drift fields induced by compositional grading of the bandgap [e.g., with SiGe alloys], or strain-induced drift fields, etc.). Secondarily, because it directly influences carrier transport, one also cares about the percentage of dopants that are ionized and contribute to conduction at a given temperature (i.e., carrier freeze-out), the bandgap narrowing involved in the inevitable use of high doping densities in practical devices, and the impact both have on carrier densities, velocities, and lifetimes. We must also be concerned with the temperature dependence of the resistivity ($\rho = 1/(q(\mu_n n + \mu_p p))$) of the various semiconductor layers needed to build a given device, since at the end of the day, a device with high parasitic resistances is rarely useful for most application needs.

From a practical standpoint, one desires not only robust data for such transport parameters over temperature (data which are surprisingly sparse in the literature, an indication of the difficulty in measuring it), but also physical models which adequately describe their various dependencies mathematically and which can be used in TCAD for device design. As one might logically guess, no such comprehensive dataset presently exists, even for silicon, the most studied material on the planet (by far). That said, we will now present some results for things that have been recently measured [6], and which should prove useful to device engineers contending with operation of their devices in extreme environments. In this instance, the various semiconductor layers in a first-generation SiGe BiCMOS technology platform were used for the investigation, but many of those layers are common to most, if not all, silicon-based integrated circuit technologies (e.g., a lightly doping p-type substrate).

7.5.1 Carrier Lifetime

We begin first with the carrier lifetime.* A convenient expression of the SRH recombination lifetime for a defect of energy level E_T is given by

$$\tau_{\text{SRH}} = \tau_{n0}\left[\frac{p_0 + p_1 + \Delta n}{p_0 + n_0 + \Delta n} + k\frac{n_0 + n_1 + \Delta n}{p_0 + n_0 + \Delta n}\right] \tag{7.16}$$

where

n_0 and p_0 are the equilibrium densities of electrons and holes
n_1 and p_1 are the SRH densities
Δn is the excess carrier density

τ_{n0} and τ_{p0} are the respective capture time constants of electrons and holes, defined as

$$\tau_{n0} \equiv (N_T\sigma_n v_{th})^{-1} \quad \text{and} \quad \tau_{p0} \equiv (N_T\sigma_p v_{th})^{-1} \tag{7.17}$$

with inverse dependencies on the thermal velocity, v_{th}, the defect concentration, N_T, and the capture cross sections σ_n and σ_p. In Equation 7.16, a symmetry factor k has been defined that depends only on the defect structure rather than on the absolute quantities of N_T and $\sigma_{n,p}$:

$$k \equiv \frac{\sigma_n}{\sigma_p} = \frac{\tau_{p0}}{\tau_{n0}} \tag{7.18}$$

Having introduced the symmetry factor k, the absolute defect parameters N_T and σ_n only appear in the electron capture time constant τ_{n0}, which is a common factor of both terms of Equation 7.16. Consequently, τ_{n0} acts solely as a scaling factor for τ_{SRH}, whereas the relative defect parameters E_T and k form the basis for the interrelated injection and temperature dependencies of the SRH lifetime.

Considering p-type material, the temperature-dependent terms are n_1, p_1, and τ_{n0}. The majority carrier concentration p_0 is also temperature-dependent due to carrier freeze-out. This is clearly critical at cryogenic temperatures, but must also be considered across all temperatures for doping levels near the Mott transition. Assuming a trap center above mid-bandgap, the low-level injection SRH lifetime reduces to

$$\tau_{\text{SRH}}^{\text{LLI},p} = \tau_{n0}(T)\left[1 + k\frac{n_1(T)}{p_0}\right] \tag{7.19}$$

Observe that there are two contributions to the overall temperature dependence of the SRH lifetime: τ_{n0}, which merely reflects the temperature dependencies of the capture cross section σ_n and the thermal velocity v_{th}, and the SRH density, n_1, which increases exponentially with increasing temperature. The thermal velocity has a power law dependence on temperature, whereas the SRH density derives its temperature dependence from the conduction band density-of-states N_C. The temperature dependence of σ_n typically follows a power law, but depends entirely on the nature of the trap in question.

At moderate temperatures, the contribution of n_1 to the overall temperature dependence can be neglected. Therefore, the temperature dependence of the SRH lifetime is given directly by $\tau_{n0}(T)$, and is proportional to the inverse product $(\sigma_n(T)v_{th}(T))^{-1}$. From this dependence, the superimposed dependence of the thermal velocity can be removed, revealing the capture cross-sectional temperature dependence. As the temperature increases, n_1/p_0 cannot be neglected and eventually begins to dominate (Equation 7.19), resulting in a steep increase in the SRH lifetime. The critical temperature for the onset of this steep

* We follow the analysis of Ref. [6], and the reader is referred to references within that work.

increase is largely driven by the trap energy level. A shallow trap will manifest this increase at a much lower temperature than a deep level trap, due to its higher SRH density. Consequently, the trap energy level can be determined from either the onset temperature itself or the slope of the lifetime for temperatures above the onset temperature.

The measured temperature dependence of the substrate minority electron lifetime is given in Figure 7.5, in which the bias current is fixed in order to decouple the lifetime injection dependence. Also shown in Figure 7.5 is the *n*-well minority hole lifetime, which exhibits a similar temperature dependence to that of the electron lifetime. Lifetime extraction was limited to a temperature range of 90–425 K due to excessive parasitics at the temperature extremes that caused the measured voltage decay curves to depart from the expected behavior. The fact that both the electron and hole lifetimes increase with increasing temperature indicates that their respective capture cross sections have an inverse dependence on temperature. The lack of a rapid increase in lifetime up to a temperature of 425 K indicates that the dominant trap energy level is fairly deep or near the middle of the bandgap. Proton irradiation experiments were conducted in order to assess the effects of displacement and ionization damage of the minority carrier lifetimes. The diode test structures were subjected at room temperature to 63.3 MeV proton irradiation up to a total accumulated dose of 1 Mrad(Si). Temperature-dependent measurements of the irradiated samples were carried out, with the results also given for both electron and hole lifetimes in Figure 7.5. As expected intuitively and from the diode *I*–*V* characteristics, both hole and electron lifetimes decrease substantially due to the increased recombination associated with displacement and ionization damage. Furthermore, the slope of the temperature dependence flattens, indicating the presence of additional defect types.

The temperature- and injection-dependent data for minority electron SRH lifetimes can be used to develop calibrated theoretical models that can then be inserted into commercial TCAD software. In addition, considering these data in light of SRH recombination theory and the analytical techniques of lifetime spectroscopy, it is possible to characterize the dominant trap levels within this particular SiGe BiCMOS technology. The extracted trap parameters for the present data are given in Table 7.1, where the trap is labeled as T_p. In Figure 7.6, the resulting temperature-dependent model is plotted against the measured lifetimes. A trap energy level of 0.32 eV above E_C was used for this calculation. The irradiated electron lifetime data can be modeled by introducing additional trap energy levels. The primary energy levels produced by electron irradiation in *p*-type silicon are the E1 (vacancy-oxygen complex) and E4 (divacancy) defects. These defects can be introduced as a starting point for our postirradiation lifetime calculations. By maintaining the same T_n trap density and increasing the trap densities of the E1 and E4 levels, it was possible to closely fit the measured temperature dependence of the 30 krad sample.

TABLE 7.1 Trap Parameters for Calibrated Carrier Lifetime Models

Trap	Energy (eV)	$\sigma_p(T)$ (cm^2)	k	N_T (cm^{-3})
T_n	$E_C - 0.5$	$1 \times 10^{-15} \times (T/300)^{-3.49}$	3.5	4.5×10^{12}
T_p	$E_V + 0.32$	$3.1 \times 10^{-15} \times (T/300)^{-3.05}$	1	4.3×10^{12}

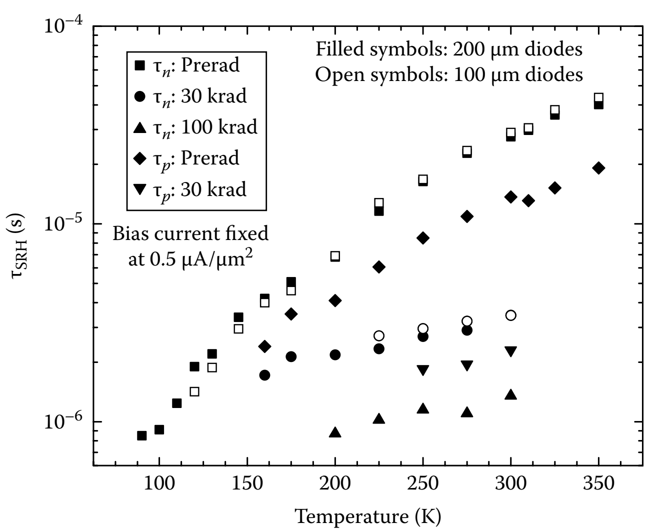

FIGURE 7.5 Radiation response of minority electron and hole lifetimes across temperature. Filled symbols correspond to 200 μm diodes at various levels of irradiation and open symbols correspond to 100 μm diodes. (From Moen, K.A. and Cressler, J.D., Measurement and modeling of carrier transport parameters applicable to SiGe BiCMOS technology operating in extreme environments, *IEEE Trans. Electron Dev.*, 57, 551–561, 2010. © 2010 IEEE.)

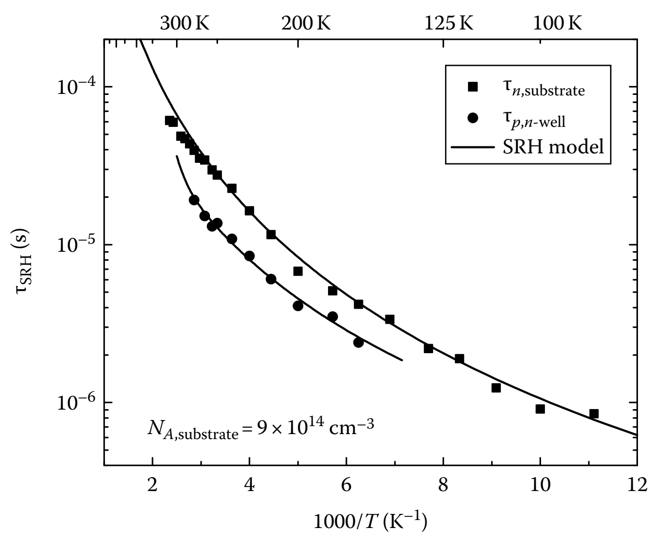

FIGURE 7.6 SRH model fit of minority electron and hole lifetimes versus temperature. (From Moen, K.A. and Cressler, J.D., Measurement and modeling of carrier transport parameters applicable to SiGe BiCMOS technology operating in extreme environments, *IEEE Trans. Electron Dev.*, 57, 551–561, 2010. © 2010 IEEE.)

7.5.2 Carrier Mobility and Resistance

The Philips unified mobility model [7,8] is a physics-based analytical model that unifies the descriptions of the majority and minority carrier mobilities. Besides lattice, donor, and acceptor scattering, this model also incorporates the effects of impurity screening by charge carriers, electron–hole scattering, clustering of impurities, and a full temperature dependence for both majority and minority carrier mobility. Moreover, since the model gives the carrier mobility as an analytical function of the donor, acceptor, electron, and hole concentrations, it is a natural fit for implementation within a TCAD device simulator.

The strong temperature-dependent nature of the lattice scattering mobility is explicitly shown in its definition:

$$\mu_{i,L} = \mu_{\max}\left(\frac{T}{300}\right)^{\theta_i} \tag{7.20}$$

Similarly, the majority impurity scattering mobilities, $\mu_{e,D}$ and $\mu_{h,A}$, directly depend on temperature and are expressed as

$$\mu_{i,I}(N_I, c) = \mu_{i,N}\left(\frac{N_{ref,1}}{N_I}\right)^{\alpha_1} + \mu_{i,c}\left(\frac{c}{N_I}\right) \tag{7.21}$$

where (i, I) stands for (e, D) or (h, A). For the majority impurity scattering mobility at low temperatures, $\mu_{i,N}$ will dominate, since it has a direct power law dependence on temperature and $\mu_{i,c}$ has a inverse power law dependence. The minority impurity and electron–hole scattering mobilities derive their temperature dependence both from their direct dependence on the majority impurity expression and from the parameter P_i within their respective mobility ratio functions $G(P_i)$ and $F(P_i)$ [7]. Assessing which of these scattering components drives the overall temperature dependence of the mobility at extremely low temperatures is an important step in evaluating and calibrating an accurate mobility model for use down to cryogenic temperatures. From Figure 7.7, it is clear that the lattice scattering mobility dominates the temperature dependence of the carrier mobility at lower doping concentrations and higher temperatures, whereas the combined majority/minority impurity and carrier scattering mobility increasingly dominates the temperature dependence for higher doping concentrations and lower temperatures. This provides a reasonable starting point for evaluating the mobility model against experimental resistivity measurements across temperature and doping concentration.

An accurate model for the incomplete ionization of dopants is necessary not only to meaningfully link experimental resistivity data to theoretical mobility values, but also in its own right a critical component of accurate low-temperature device models. A new model [9,10] was recently derived based on a parameterization of the density-of-states near the band edge of doped silicon and subsequently applied to calculate dopant ionization level. In that model derivation, the dopant band was shown to only touch the conduction band at the Mott transition and to merge with the conduction band at considerably higher doping levels, agreeing with the experimental data that at these high doping levels the dopants are completely ionized. Marked occupation of dopant states occurs when the Fermi level is located near the dopant level, leading to incomplete ionization of dopant atoms and a diminished free carrier density. Up to 25% of dopant atoms may be nonionized for certain doping concentrations. Consequently, incomplete ionization at moderate temperatures is an important concern for doping levels from roughly 1×10^{17} to 1×10^{19} cm^{-3}, as clearly shown in Figure 7.8. This incomplete ionization model has been used for all relevant calculations presented, including the carrier lifetime modeling of the preceding section. It provides an accurate depiction of dopant ionization across doping concentration from the deep cryogenic through high-temperature regimes. Together with the Philips mobility model, this model establishes a solid foundation for evaluating and calibrating an accurate resistance model based on experimental data.

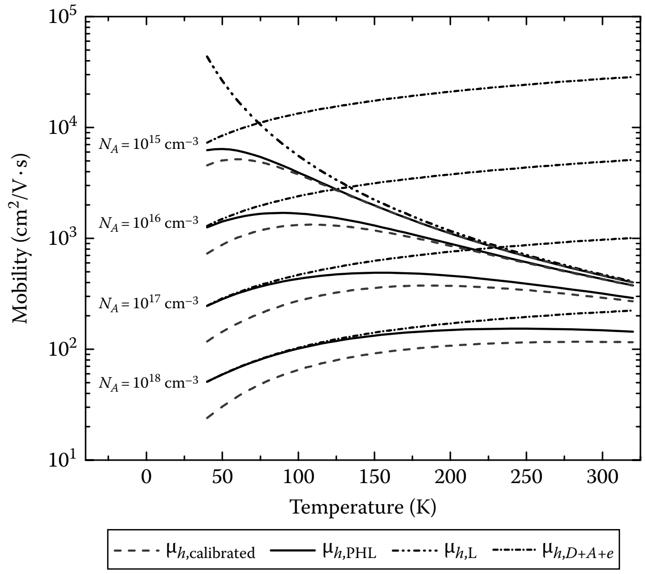

FIGURE 7.7 Comparison of the temperature dependence of scattering mechanisms used in Philips unified mobility model for various doping concentrations. The effective hole mobility from the calibrated model is shown by the dashed lines. (From Moen, K.A. and Cressler, J.D., Measurement and modeling of carrier transport parameters applicable to SiGe BiCMOS technology operating in extreme environments, *IEEE Trans. Electron Dev.*, 57, 551–561, 2010. © 2010 IEEE.)

In Figure 7.9, the p-type temperature-dependent resistance data are shown, including the substrate resistivity, intrinsic base sheet resistance, and p^+ diffusion sheet resistance. For the lightly doped substrate, a significant increase in resistivity is seen as the temperature decreases below 100 K. This can be attributed to the significant degree of incomplete ionization that is expected for a boron density of 9×10^{14} cm^{-3}. The decrease in substrate resistivity from room temperature down to 100 K can be attributed solely to the expected increase in mobility, since the dopants are completely ionized in this temperature range. In contrast, the intrinsic

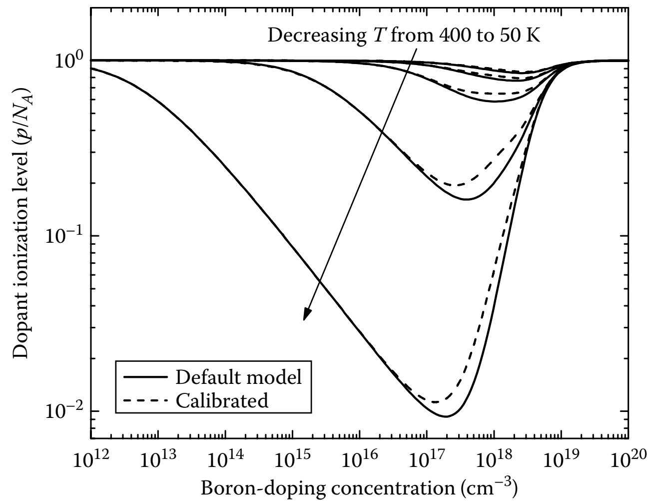

FIGURE 7.8 Ionization level as a function of boron doping concentration across a wide temperature range. The dashed lines reflect the ionization level from the calibrated ionization model. (From Moen, K.A. and Cressler, J.D., Measurement and modeling of carrier transport parameters applicable to SiGe BiCMOS technology operating in extreme environments, *IEEE Trans. Electron Dev.*, 57, 551–561, 2010. © 2010 IEEE.)

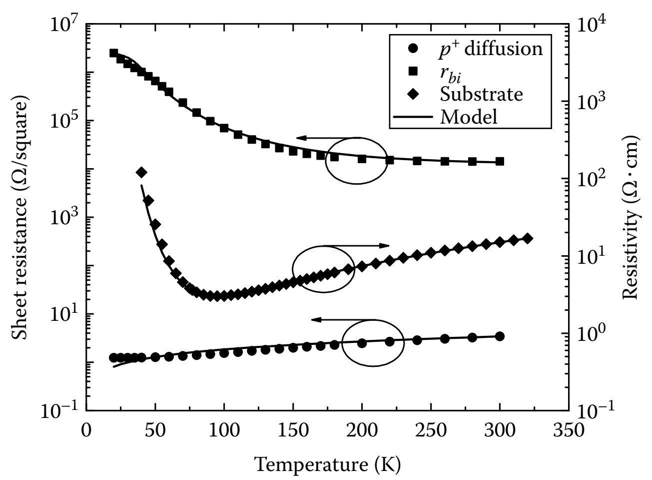

FIGURE 7.9 Resistivity and sheet resistance measurements for p-type silicon of various doping levels in a first-generation SiGe BiCMOS technology. (From Moen, K.A. and Cressler, J.D., Measurement and modeling of carrier transport parameters applicable to SiGe BiCMOS technology operating in extreme environments, *IEEE Trans. Electron Dev.*, 57, 551–561, 2010. © 2010 IEEE.)

base sheet resistance exhibits clear signs of incomplete ionization even at temperatures above 200 K, due to its higher doping concentration. Reexamining Figure 7.8 for doping levels near 1×10^{18} cm^{-3}, incomplete ionization is already in effect at room temperature and the level of ionization steadily decreases with decreasing temperature, albeit at a slower rate than for lower doping concentrations. This overrides the mobility-related decrease in resistance and leads to an increase in r_{bi} with decreasing temperature, accelerating as the temperature decreases below 200 K. Finally, the p^+ diffusion sheet resistance exhibits very little temperature

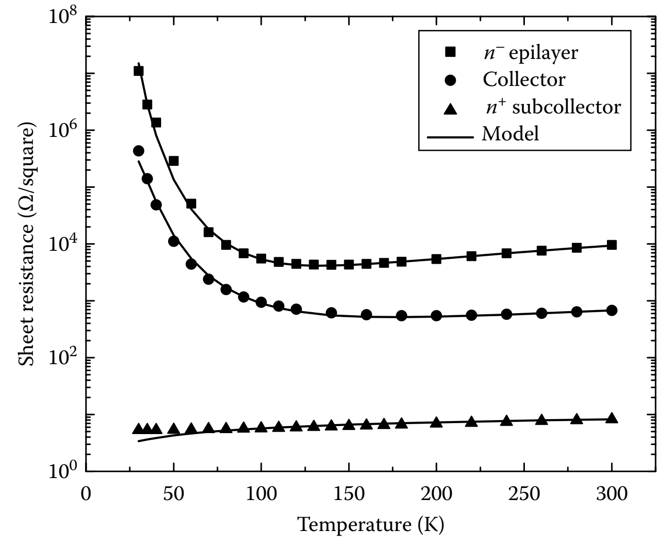

FIGURE 7.10 Resistivity and sheet resistance measurements for n-type silicon of various doping levels in a first-generation SiGe BiCMOS technology. (From Moen, K.A. and Cressler, J.D., Measurement and modeling of carrier transport parameters applicable to SiGe BiCMOS technology operating in extreme environments, *IEEE Trans. Electron Dev.*, 57, 551–561, 2010. © 2010 IEEE.)

dependence due to its extremely high doping concentration. Complete ionization of dopants holds across the entire temperature range, and thus the slight decrease (less than 3×) in sheet resistance from 300 to 20 K can be attributed to a corresponding increase in mobility with cooling.

Figure 7.10 shows the n-type temperature-dependent resistance data, including the sheet resistances of the n^- epilayer, HBT collector, and n^+ HBT subcollector. The n^- epilayer, which has a relatively higher doping concentration than that of the substrate, displays a similar temperature dependence. The weaker dependence at higher temperatures reflects the fact that the mobility dependence is also weaker due to the higher doping concentration. The collector layer is merely the n^- epilayer after ion implantation. Thus, the collector sheet resistance demonstrates a similar overall temperature dependence compared to the n^- epilayer, with several key differences: the overall magnitude is lowered due to a higher carrier density; the moderate temperature region is suppressed, reflecting a reduction in mobility due to increased impurity scattering; and the onset of incomplete ionization occurs at a higher temperature due to the higher doping concentration. Finally, the n^+ subcollector sheet resistance data mirror that of the p^+ diffusion layer, indicating complete ionization across all temperatures.

Proton irradiation experiments were conducted in order to assess the effects of displacement and ionization damage on the substrate resistivity. Resistivity test structures were subjected at room temperature to 63.3 MeV proton irradiation up to a total accumulated dose of 1 Mrad(Si). Figure 7.11 shows the changes induced in the temperature-dependent resistivity at accumulated doses of 100 krad, 300 krad, and 1 Mrad. By normalizing the irradiated resistivities to the preirradiation data, the specific nature of

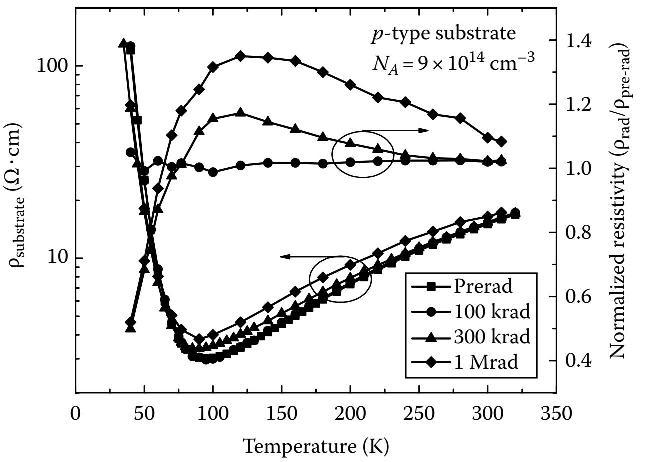

FIGURE 7.11 Proton radiation response of the substrate resistivity across temperature. (From Moen, K.A. and Cressler, J.D., Measurement and modeling of carrier transport parameters applicable to SiGe BiCMOS technology operating in extreme environments, *IEEE Trans. Electron Dev.*, 57, 551–561, 2010. © 2010 IEEE.)

the radiation-induced changes to resistivity is more easily seen. At moderate temperatures, the increase in resistivity indicates that radiation-induced displacement damage results in higher lattice scattering. Below 100 K, however, where impurity scattering dominates at this particular doping concentration, the resistivity decreases. This decrease could be caused by boron dopant deactivation from radiation damage. Dopant deactivation would cause a temperature-independent increase in resistivity due to a lower carrier concentration, along with decreased ionized impurity scattering that would be manifested as decreased resistance at low temperatures. Moreover, the lower carrier concentration would lead to a relatively lower degree of incomplete ionization, resulting in lower resistivity in the deep cryogenic temperature regime.

Although it is fairly easy to obtain an accurate model fit for a particular set of data by freely tuning the model parameters, maintaining a high level of accuracy across a wide range of conditions with one set of model parameters is much more challenging. In order to develop mobility and ionization models that together produce accurate models of resistivity for the doping-dependent p-type and n-type resistance data presented here, the most reliable approach is to retain models that are physics-based and focused on material systems rather than particular technologies. This approach minimizes the reliance on assumptions that could potentially break down under conditions for which the models have not been experimentally tested. Models that are purely empirical or have been developed specifically for a particular technology often do not extend well to other technologies or physical conditions. Consequently, the approach described here has been to carefully calibrate the parameters of the Philips mobility model and the Altermatt ionization model, since both of these models were developed out of fundamental theory and aimed for silicon-based systems in general. All of the experimental data were fit using a single set of model parameters. The modified parameters used for the calibrated Philips model and the calibrated Altermatt model are given in Tables 7.2 and 7.3.

TABLE 7.2 Calibrated Parameters Used in Mobility Model for Arsenic-, Phosphorus-, and Boron-Doped Silicon

Parameter	As	P	B
$N_{ref,1}$ (cm^{-3})	1.45×10^{17}	1.1×10^{17}	1.5×10^{17}
$N_{ref,I}$ (cm^{-3})	1.0×10^{22}	1.0×10^{22}	1.0×10^{22}
α_1	0.85	0.65	0.8
θ_i	1.72	1.72	1.82

TABLE 7.3 Calibrated Parameters Used in Incomplete Ionization Model for Arsenic-, Phosphorus-, and Boron-Doped Silicon

Parameter	As	P	B
N_{ref} (cm^{-3})	3.0×10^{18}	7.0×10^{17}	8.5×10^{17}
C	1.5	0.8	1.4
N_b (cm^{-3})	9.0×10^{18}	6.0×10^{18}	4.5×10^{18}
D	1.8	1.3	2.4

Figure 7.9 shows the calibrated model fits for the p-type resistance data. The substrate resistivity was used to calibrate θ_i, since at moderate temperatures lattice scattering dominates and incomplete ionization is negligible. Properly accounting for the low-temperature increase in resistivity due to carrier freeze-out, combined with the increasing influence of impurity scattering, required simultaneous tuning of the impurity scattering temperature coefficient α_1 and the ionization model parameters. The resulting model produces close fits to the three datasets across the entire temperature range.

Calculation of the intrinsic base sheet resistance also required the highly variable doping concentration across the base to be properly taken into account. Substituting an effective base doping is insufficient, since mobility and ionization level are strong functions of doping concentration. For that reason, the variable base profile was discretized into very thin layers of constant doping using data from SIMS measurements. The resistivity and corresponding sheet resistance for each layer was calculated, then all of these individual sheet resistances were added together as parallel resistances in order to determine the total effective base sheet resistance.

Following the same procedure as for the p-type models, the n-type resistance data were used to calibrate the n-type mobility and incomplete ionization parameters. The resulting model fits are given in Figure 7.10. For the calculations of n^- epilayer and collector sheet resistance, a constant effective doping level was used. For the n^+ subcollector, however, the known doping profile was discretized in the same manner as the base profile in order to account for the varying doping concentration through the subcollector. Since both the modeled p^+ diffusion and n^+ subcollector sheet resistances begin to diverge from the data below 70 K, the error can be attributed to inadequate modeling of ultrahigh doping effects in the mobility model. Finally, a good model to data fit for the changes in substrate resistivity due to radiation exposure is shown in Figure 7.11.

References

1. C. Kittel, *Introduction to Solid State Physics*, 6th Edn. New York: John Wiley & Sons, 1986.
2. C. Kittel and H. Kroemer, *Thermal Physics*, 2nd Edn. San Francisco, CA: W.H. Freeman & Sons, 1980.
3. D.A. McQuarrie, *Statistical Mechanics*. New York: Harper & Row, 1976.
4. J.D. Cressler, *Silicon Earth: Introduction to the Microelectronics and Nanotechnology Revolution*. New York: Cambridge University Press, 2009.
5. B.L. Anderson and R.L. Anderson, *Fundamentals of Semiconductor Devices*. New York: McGraw-Hill, 2005.
6. K.A. Moen and J.D. Cressler, Measurement and modeling of carrier transport parameters applicable to SiGe BiCMOS technology operating in extreme environments, *IEEE Transactions on Electron Devices*, 57, 551–561, 2010.
7. D.B.M. Klaassen, A unified mobility model for device simulation I. Model equations and concentration dependence, *Solid-State Electronics*, 35(7), 953–959, 1992.
8. D.B.M. Klaassen, A unified mobility model for device simulation II. Temperature dependence of carrier mobility and lifetime, *Solid-State Electronics*, 35(7), 961–967, 1992.
9. P.P. Altermatt, A. Schenk, and G. Heiser, A simulation model for the density of states and for incomplete ionization in crystalline silicon. I. Establishing the model in Si:P, *Journal of Applied Physics*, 100(11), 113714, 2006.
10. P.P. Altermatt, A. Schenk, and G. Heiser, A simulation model for the density of states and for incomplete ionization in crystalline silicon. II. Investigation of Si:As and Si:B and usage in device simulation, *Journal of Applied Physics*, 100(11), 113715, 2006.

8

Overview of Radiation Transport Physics and Space Environments

Robert Reed
Vanderbilt University

Janet Barth
National Aeronautics and Space Administration

In this chapter of the reference manual, we will describe radiation environments that produce effects in electronics. We will begin the discussion by defining those effects, and then we will define important concepts from radiation transport physics that pertain to the effects. Then we will provide an overview of the important radiation environments.

8.1 Introduction to Radiation Effects in Electronics

Microelectronic and photonic components are manufactured in very controlled environments. During certain phases of the manufacturing process, even the slightest change in conditions like temperature or impurity concentration can induce changes in the overall molecular structure that cause the component to fail functional or parametric performance metrics. Devices that rely on carefully grown, well-defined microscopic structures can have very low tolerance for slight changes in their characteristics. When a component is exposed to radiation, the radiation transfers some of its energy to the component materials, changing the localized material properties (either temporarily or permanently). This can have significant effects on component functionality and/or parametrics, with the end result depending on the type of radiation, where the energy deposition occurred, and the type of component. Three important effects that occur when a component is exposed to radiation are single-event effects (SEEs) and effects due to total ionizing dose (TID) and displacement damage (DD).

An SEE is simply any effect on an integrated circuit (IC) that is the result of energy deposition by a single incoming ionizing particle. Ionization of a target material occurs when the incident particle loses energy via interactions with the target electrons. This generates charge carriers, called electrons and holes, which are free to move within the semiconductor (see Section 8.2). Two common SEEs are (1) single-event transient (SET), which is a radiation-induced current (or voltage) pulse occurring at a circuit node of an IC and (2) single-event upset (SEU), which is a radiation-induced change in a circuit's static logic state. An SEU is the manifestation of an SET on a specific sensitive circuit node.

Damage from TID is caused by the electron–hole pairs generated by ionizing radiation passing through an oxide near the active regions of an IC. In most cases, the basic cause of TID degradation is the trapping of charge in the oxide. Once trapped in the oxide, these charges can gradually change the performance of an electronic component, with the level of change depending on the total ionizing energy absorbed. Generally, TID changes the characteristics of the materials that make up a component, resulting in gradual parametric degradation and changes in functionality.

Proper IC function depends critically on the semiconductor having a near pristine crystalline lattice. However, this lattice can be damaged when an energetic particle, such as a neutron, electron, proton, or heavy ion, displaces one or more nuclei within the crystalline lattice, creating electrically active defects. As this damage to the crystalline lattice—called the DD—increases, the device can degrade parametrically, and eventually stop functioning all together.

8.2 Radiation Transport Physics

8.2.1 Ion Stopping

A detailed understanding of the interaction of charged particles with matter is required to quantify the energy deposited by the particle. Some of the earliest studies of charged-particle penetration were conducted by pioneers of physics; people like E. Rutherford, J. J. Thomson, N. Bohr, H. Bethe, C. Møller, F. Bloch, and others. This work continues today. In 2005, the International Commission on Radiation Units and Measurements (ICRU) released a new document detailing the stopping of ions heavier than helium [1]. This document provides the most comprehensive study to date of stopping force for these ions. In 1993, the ICRU released a document that describes ion stopping for helium and protons [2].

Electronic stopping is considered to be the most important for SEEs. Electronic stopping occurs when the ion electromagnetically scatters through elastic Coulomb collisions between the incident ions and the field of the atomic electrons in the material. The result is the excitation (known as ionization) of the target atom's electrons. The target nuclei remains at a fixed location because the energy transfer is smaller than the energy required to release it from the bond between the atom and its nearest neighboring atoms. The incident ion is deflected only very slightly from its original direction with essentially no momentum transfer to atomic nuclei. Of course, there will be an ensemble of interactions between many target atoms as the ion passes through the semiconductor and liberates a large number of electrons. This process is known as direct ionization.

All SEEs and TID effects are a result of ionizations that occur within the sensitive region of a component. For SEE, this can be direct ionization produced by a single primary ion or ionization from secondary ions produced by reactions between the primary ion and the target nuclei (see below). TID effects are produced via an accumulation of charge produced by an ensemble of ion-induced direct ionization events. (Note: ionization from secondary particles is known as indirect ionization.)

Nuclear stopping of ions in matter happens as a consequence of the interaction of the ion with the target atoms. The incident ion collides elastically with the atom through Coulomb collisions between the ion and the atom nucleus field and screened by the atom electrons. This interaction causes changes in the ion and target motion. The primary difference between electronic stopping and nuclear stopping is the motion of the ion and target nuclei after the collision. In a nuclear stopping collision, the incoming ion approaches the target nucleus at a fairly small distance, and undergoes a sufficient deflection to transfer momentum to the target nucleus, possibly resulting in its ejection from its lattice site. Direct and indirect ionization occurs during a nuclear stopping event. (Note: nuclear stopping should not be confused with nuclear reactions; see Section 8.2.2.)

As an ion passes through matter, it will lose energy during each Coulomb interaction with the target electrons and nuclei. While this energy is typically very small for each interaction, especially with the electrons, the net effect of all interactions is to slow the ion down and, if the target is thick enough, eventually stop the particle within the target.

One key parameter used to characterize the penetration of charged particles is the average energy loss per unit path length ($-dE/dx$), that is, stopping power or stopping force. The SEE community commonly uses mass stopping force, called linear energy transfer (LET), as the metric for average energy deposited per unit path length:

$$\mathrm{LET} = -\frac{1}{\rho}\frac{dE}{dx} \tag{8.1}$$

where
ρ is the density of the target material
LET unit is typically $\mathrm{MeV \cdot cm^2/mg}$

Currently, for SEE, the primary energy loss mechanism is electronic stopping, so for the remainder of this chapter we use the term $\mathrm{LET_{elec}}$ to mean the electronic stopping, $\mathrm{LET_{nuc}}$ to denote nuclear stopping, and $\mathrm{LET} = \mathrm{LET_{elec}} + \mathrm{LET_{nuc}}$.

Ion transport through matter can be simulated using advanced computer codes that employ Monte Carlo techniques and detailed physical models. However, electronic and nuclear stopping can also be estimated using lookup tables computed from theory. While the latter approach is simpler and more typically accessible than the Monte Carlo approach, these calculations are for average LET values, and some do not consider fluctuations in energy loss.

The computed LET (electronic and nuclear) versus ion energy for iron incident on silicon is shown in Figure 8.1 using the Stopping and Range of Ions in Matter (SRIM) code [3]. First let us focus on the electronic stopping curve (black line tagged with a square). One can think of these data as a prediction of the average $\mathrm{LET_{elec}}$ of an ensemble of ions as they move through the target material. So, for an ensemble of iron ions all with an initial energy 100 GeV, a decrease in energy (until near 100 MeV) results in an increase in the average $\mathrm{LET_{elec}}$. The average $\mathrm{LET_{elec}}$ is a maximum value near 100 MeV, after that the average $\mathrm{LET_{elec}}$ decreases with decreasing energy. The peak in the electronic stopping LET curve is known as the Bragg peak.

This trend over energy occurs for all ions in all materials. The magnitude and location of the Bragg peak will be different depending on the ion and target material. The trend of LET with

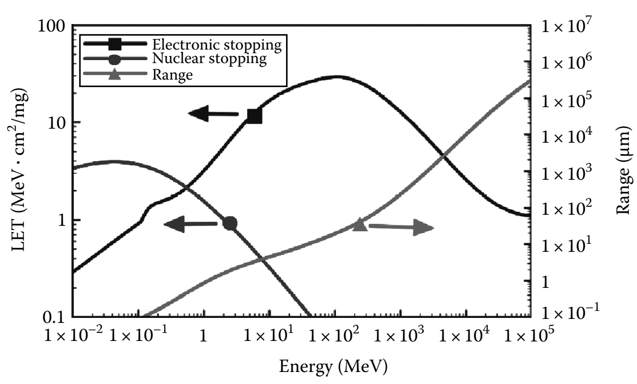

FIGURE 8.1 SRIM results for iron in silicon. The curves tagged with a square and circle are the computed LET versus ion energy for iron incident on silicon for electronic and nuclear stopping. The curve tagged with a triangle shows the predicted ion range.

charge of the nucleus (atomic number, Z) is simpler than that with energy; for two ions, $Z_1 > Z_2$, incident on the same material with the same energy, the LET_{elec} for Z_1 will be greater than that for Z_2.

The nuclear stopping average LET (line tagged with a circle) has a similar trend over energy as the electronic stopping, except the peak value occurs at a much lower energy (note the abscissa is plotted on logarithm scale). Nuclear stopping does not ionize the target directly, but the recoil that results from nuclear stopping will produce ionization (known as indirect ionization). A nuclear stopping event results in a transfer of the incident ion energy to the target nuclei; this can result in a dramatic (almost instantaneous) change in the ions electronic stopping power.

The ion's average range (line tagged with a triangle) is also shown in Figure 8.1. As expected, the ion range decreases as the ion energy decreases. In general, ions with energies near the Bragg peak have limited range as compared to dimension-sensitive regions within an IC.

8.2.2 Ion-Induced Nuclear Inelastic Reactions

Particles contained within the nucleus are coupled together via the strong force. When the nucleus absorbs a particle (e.g., a neutron, proton, or some other heavy ion), the ensemble of particles are subject to these forces. A nuclear reaction (also known as "hadronic" reaction) will ensue. This strong force has a much shorter interaction range than the interactions described earlier, which were characterized by Coulomb forces. The strong force becomes effective for charged particles (ions) when the ion energy is higher than the Coulomb barrier generated between the incident ion and the target nucleus. (We note that neutrons are neutral; therefore, they are free to enter the nucleus unimpeded by the Coulomb field emitted by the nucleus.)

During an inelastic nuclear reaction, part of the ion's total kinetic energy is transferred to the excitation and/or the breakup of the target nucleus. When the incident ion penetrates the target nucleus, a variety of particles are emitted including nucleons (protons and neutrons), photons, alpha particles (helium ions), and other heavier fragments (known as recoil nuclei). Excited states may later decay by gamma ray or other forms of radiative emission, or further breakups. These types of interactions are very complicated, and are the least understood of all the interactions. No single theory of inelastic nuclear reactions exists.

The recoiling nuclei and other fragments transport through the semiconductor, losing energy along the way via the stopping force. Similar to the ionization from recoiling nuclei resulting from nuclear stopping, the ionization produced by secondary products from nuclear reactions is also known as indirect ionization. The fragments may also interact with other target nuclei via nuclear processes; however, this is very rare and is often ignored when studying radiation effects in electron devices. Ionization due to nuclear reactions can produce SEEs and DD effects and, to date, TID effects are considered to be negligible.

8.2.3 Nuclear Fission

The final nuclear reaction that is important for SEEs is nuclear fission. Nuclear fission is a process in which the nucleus of an atom splits into two or more smaller nuclei as fission products, and possibly some by-product particles. This can be induced by particle capture by the nucleus. For example, a thermal (very low energy, say <1 keV) neutron that enters the nucleus may result in a splitting of the target nucleus into two smaller fragments (this may be accompanied by a gamma emission). Fission of heavy elements is an exothermic reaction. The fragments can move away with substantial amounts of kinetic energy.

The fission fragments transport through the semiconductor, losing energy along the way via the stopping force. Similar to the ionization from recoiling nuclei resulting from nuclear stopping and nuclear reactions, the ionization produced by secondary products from nuclear fission is also known as indirect ionization. Thermal neutron capture has been identified as a critical SEE issue for technologies using borophosphosilicate glass (BPSG) [4].

8.3 Space Radiation Environment

Earth-orbiting and interplanetary spacecraft face a variety of radiation-related threats. Determining the survival probability of a spacecraft during its mission requires not just accurate ground-based test data for the device and a validated model for predicting the device performance in space from the ground-based data, it also requires accurate prediction of the space radiation environment. Although a complete description of the environment is beyond the scope of this reference manual, its importance demands that we give at least a cursory treatment here. An excellent description of the space radiation environment, as well as the use, validity, and limitations of the relevant models thereof, can be found in the Nuclear and Space Radiation Effects Conference 1997 [5] and 2006 [6] Short Courses.

The radiation environment encountered by a spacecraft depends on several factors. The path of the spacecraft relative to the planets, the level of solar activity, and the mission duration determine the radiation levels incident on the spacecraft. For some radiation effects, the spacecraft's ability to shield sensitive components from radiation can be crucial in determining whether radiation effects will degrade the performance of those components. Finally, the threat of manmade radiation environments (not addressed in this course) can be an important consideration. Typically, these variables are used as inputs to computer codes that predict the space radiation environment encountered by a spacecraft and how this environment affects the spacecraft's mission.

There are two major components of the natural space radiation environment: the transient environment and that trapped by the magnetic fields of most planets. As might be expected, Earth's trapped radiation environment is better characterized than that of other planets. Our brief discussion of the radiation environment will focus on the naturally occurring radiation

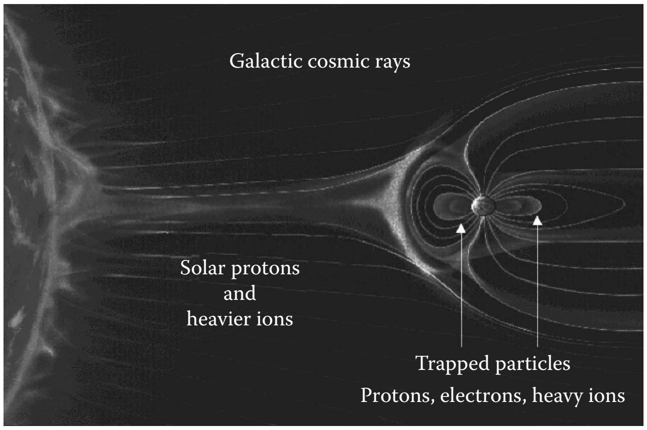

FIGURE 8.2 Cartoon showing the components of the space radiation environment important for microelectronic and photonic performance degradation evaluations. (From Barth, J., Modeling space radiation environments, Notes from 1997 IEEE Nuclear and Space Radiation Effects Conference Short Course; Courtesy of K. Endo, Nikkei Science, Inc., Tokyo, Japan.)

environments in Earth-orbiting spacecraft. Deep-space missions passing near other planets environments have similar particle constituents, but differ in magnitude.

Figure 8.2 is an artist's conception of Earth's radiation environment. The solar and galactic radiation environments will be discussed first, followed by a discussion of the near Earth–trapped particle environment.

8.3.1 Transient Environment

Although many types of radiation make up the transient environment, the two most important components for radiation effects in spacecraft are the galactic cosmic rays (GCRs) and particles emitted during solar events.

The sources of GCRs are sufficiently far from our solar system that the fluxes of these particles are essentially isotropic in free space regions. Interactions in the vicinity of Earth between the solar wind and our planet's magnetic field change individual particle trajectories and energies. However, the net GCR flux is still essentially omnidirectional.

The GCR particle composition is roughly 83% protons, 13% alpha particles, 3% electrons, and 1% heavier ions ($Z > 2$). The ion energies range from 10s of MeV/nuc to 100s of GeV/nuc and beyond, and most ions are fully ionized. Some of these ions have sufficient energy to penetrate most shielding provided by a spacecraft structure.

The CRÈME [7] website can be used to model the GCR space environment. Figure 8.3 shows the iron and full GCR differential flux computed for geostationary orbit (GEO) for solar minimum using a shielding of 100 mils of aluminum. Notice the iron flux peaks near a few 100 MeV/nuc (Figure 8.3a). Also note that in Figure 8.3b the peak flux of most all ions is near this value. The five most abundant ions are highlighted with symbols (called the "top five" ions for the remainder of this chapter). The black lines represent the model results for all other ions. Loosely speaking, the flux at a particular energy value decreases with increasing atomic number. One exception is iron, with a Z of 26; it appears in the top five ions in the space environment and, because of its high stopping power, is very important. For any specific energy, it has a stopping power that is much larger than any of the other top five ions. These top five ions will dominate the response for most circuits that are sensitive to direct ionization (or LET_{elec}), in particular the iron flux is greater than 40% of the total environment that can induce soft errors when the circuit response is dominated by LET_{elec}; this is discussed in more detail later.

A common soft-error rate prediction technique combines the entire space environment into an integrated dataset of ion flux versus LET_{elec} (called a Heinrich spectrum [8]). The technique is to create an integrated LET_{elec} distribution by summing the flux for all ions for each specific LET_{elec} in the target material. Application of this environment definition assumes that one can show that average LET_{elec} is a valid metric for determining soft-error performance of the specific circuit.

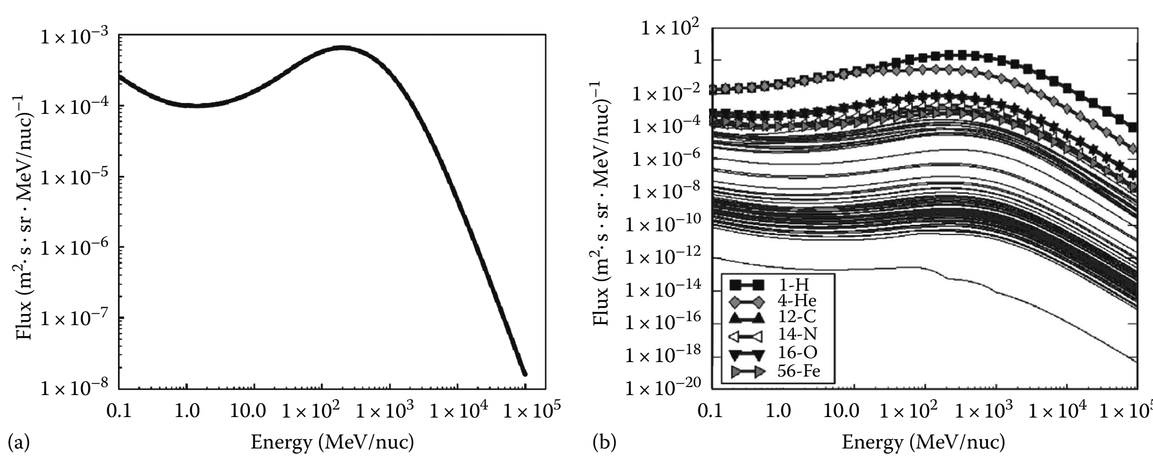

FIGURE 8.3 Modeled GCR environment at geostationary orbit. (a) Iron flux at solar minimum behind 100 mils of aluminum shielding. (b) Ion flux at solar minimum behind 100 mils of aluminum shielding.

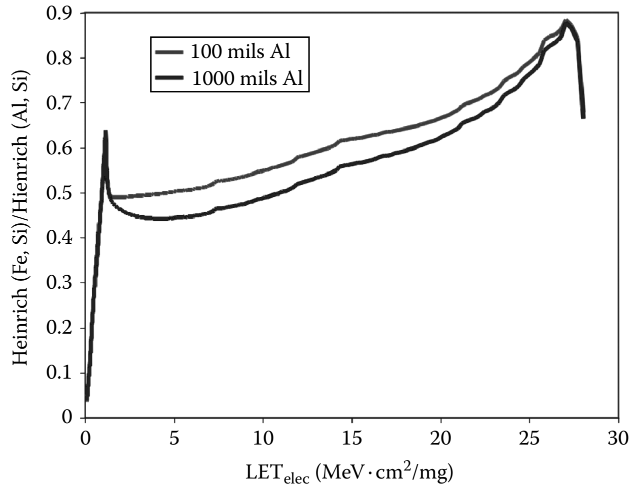

FIGURE 8.4 Fraction of iron in GEO heavy ion environment.

Figure 8.4 shows the ratio of the Heinrich spectrum for iron in silicon, Heinrich(Fe, Si), to that for all ions in silicon, Heinrich(Al, Si), for two different spherical aluminum shielding thicknesses for a GEO environment. First, note that increasing shielding does not mitigate the fraction of iron in the total spectrum; it is also true that shielding cannot reduce the absolute magnitude of the spectrum. Iron is more than 40% of the flux environment for ion LET$_{elec}$ greater than 0.5 MeV·cm^2/mg.

The iron flux is 75% of the space environment for ion LET$_{elec}$ greater than 25 MeV·cm^2/mg. Iron ions with an LET$_{elec}$ greater than 20 MeV·cm^2/mg have a range of <80 μm, and those with an LET$_{elec}$ greater than 25 MeV·cm^2/mg have a range <45 μm. Note that shielding has very little effect on the relative contribution. This means that a significant fraction of the highly ionizing space environment is coming to rest in the microelectronic device. This is especially important for radiation-hardened circuits designed to mitigate effects from ions with LET$_{elec}$ below 15 MeV·cm^2/mg. This is often the target number for circuits designed to be hardened to the proton environment; the Bragg peak of silicon in silicon is near this value.

Not all of radiation impinging on Earth originates from such distant sources. The Sun can be thought of as a boiling pot of plasma that emits charged particles most of the time. When the Sun is "quiescent," most of the particles it emits do not have sufficient energy to penetrate through even a small amount of spacecraft shielding. However, during times of high activity, conditions occur that can accelerate a spectrum of charged particles with a large range of energies for varying durations. The duration of such events is usually between a few hours and several days. The average frequency of these solar events varies roughly sinusoidally with the 11 year sunspot cycle. Figure 8.5 illustrates this variation over the last three solar cycles—showing solar proton integral fluences (the spikes) for large solar proton events over a 30 year period superimposed over the sunspot numbers (smooth curve) [5].

Two important classes of events that occur during this high activity period are Coronal Mass Ejections (CMEs) and solar flares. CMEs have been correlated with events that have a high probability of producing protons that reach the Earth, whereas solar flares seem to be correlated to heavy ion-rich solar particle events [9]. Figure 8.6 plots proton, alpha, oxygen, and iron fluence data taken by three spacecraft (ACE, SAMPEX, GOES-11) during a solar energetic particle (SEP) event that occurred on January 20, 2005 [10]. The intensity and composition of the spectra will vary from event to event. Solar flares and CMEs can occur at the same time giving rise to events with very high intensity and can contain all naturally occurring elements (Z = 1–92). The total integral fluences during these rare events can exceed average GCR fluxes by 3 orders of magnitude or more.

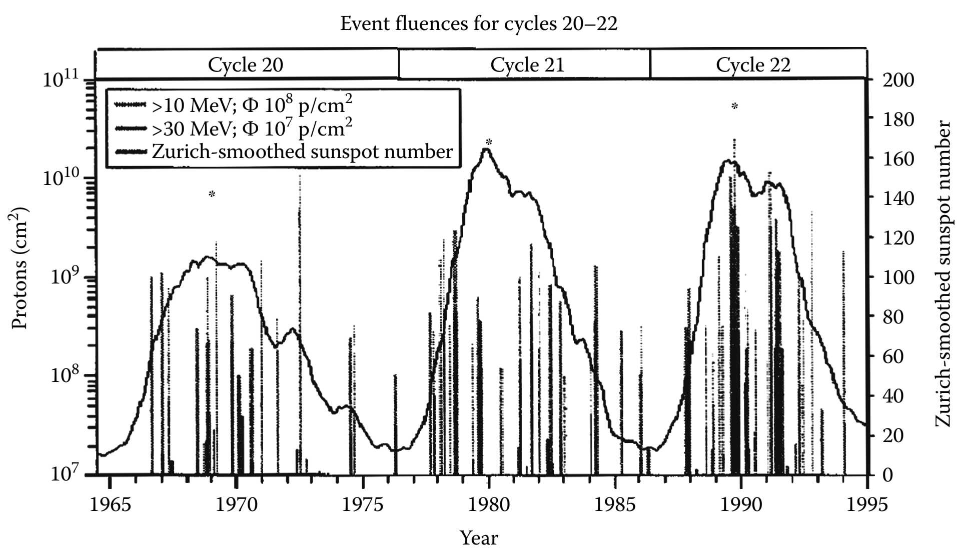

FIGURE 8.5 Correlation of the occurrence of several large solar proton events over a 30 year period (vertical light lines) with the Zurich sun spot number (single solid dash line). (From Barth, J., Modeling space radiation environments, Notes from 1997 IEEE Nuclear and Space Radiation Effects Conference Short Course.)

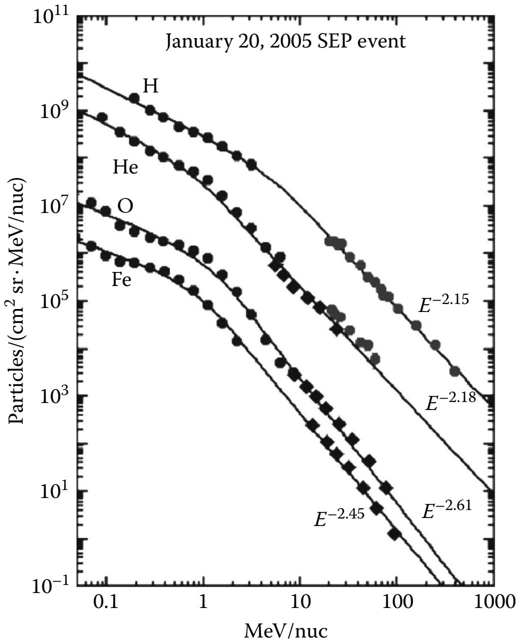

FIGURE 8.6 Particle flux data taken by ACE, SAMPEX, GOES-11 for an SEP. (From Mewaldt, R.A. et al., Solar-particle energy spectra during the large events of October–November 2003 and January 2005, *29th International Cosmic Ray Conference Pune,* pp. 101–104, 2005.)

8.3.2 Trapped Protons and Electrons

Particles with the proper charges, masses, energies, and trajectories can be captured by the Earth's magnetic field (Figure 8.7) [5]. In simplified approximations of these environments, they form a toroid with Earth at the center and Earth's magnetic pole defining the toroid's central axis. (The geographic pole is roughly 11° off center from the magnetic pole.) As shown in the figure, the proton flux is confined to a single toroid, and electrons form two high intensity toroids. The region between the two electron zones is known as the slot region. Earth's atmosphere and magnetic field and their interaction with the solar wind and the solar magnetic field define the details of the flux of each particle toroid. The particles roughly follow Earth's magnetic field lines.

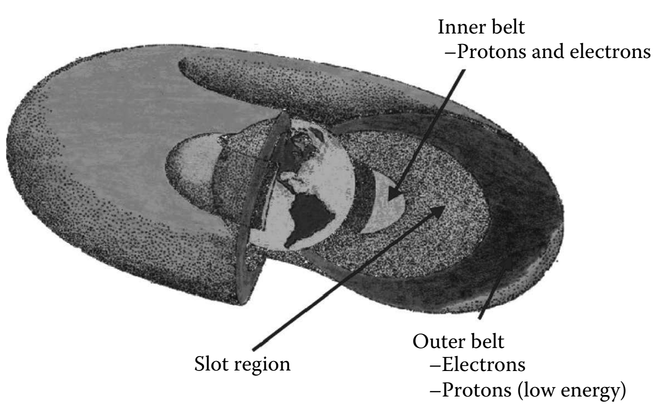

FIGURE 8.7 Trapped particle belts surrounding the Earth. (From Barth, J., Modeling space radiation environments, Notes from 1997 IEEE Nuclear and Space Radiation Effects Conference Short Course.)

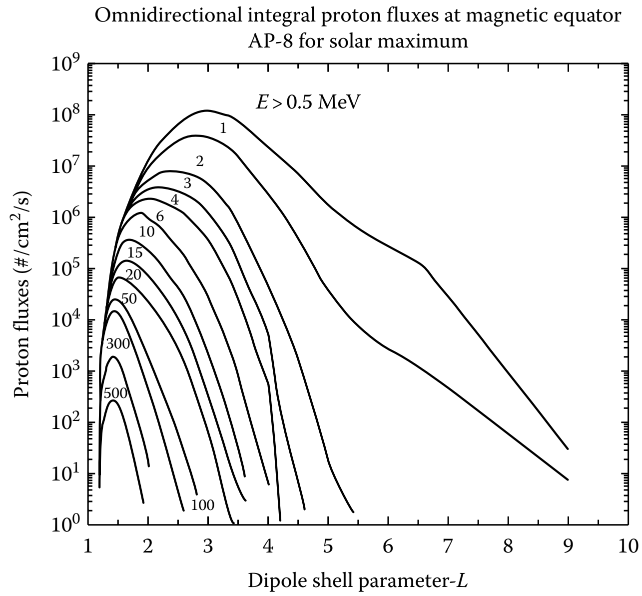

FIGURE 8.8 Proton flux as predicted by AP-8. (From Barth, J., Modeling space radiation environments, Notes from 1997 IEEE Nuclear and Space Radiation Effects Conference Short Course.)

Of the particles confined by Earth's magnetic field, protons have the greatest effect on soft-error performance of spaceflight hardware. Figure 8.8 shows cross sections through a dipole plot of these several proton populations as predicted with the AP-8-trapped particle models [5]. Each curve is labeled with the minimum energy found at this L-shell. L-shell is the dipole shell number of the Earth's magnetic field. At the magnetic equator, L is the distance in Earth radii from the center of the Earth. As the angle of inclination moves away from the magnetic equator, the value of L is corrected for the magnetic field strength. The values of L in Figure 8.8 refer to that at the magnetic equator.

In the inner region, $L < 3.5$, electron and proton toroids overlap, while for $3.5 > L > 8.5$, the trapped particles are mostly electrons. No significant particle trapping occurs for values of $L > 11$. In the trapped regions, the flux is considered to be approximately omnidirectional.

Although Figure 8.8 presents a static view of the shape, regional flux, and orientation of the toroids, in reality, these belts are very dynamic, growing and shrinking over time. Occasionally, new toroidal regions form and disappear, especially in the slot region. The dynamic nature of the trapped radiation belts is not very well understood and is poorly modeled. Research has shown that fluxes can change dramatically with solar activity, but quantitative models of this variability do not yet exist for short-term averages.

One temporal variation that has been quantified is the variation of the flux levels in the toroids with the 11 year solar cycle. (During solar maximum the integral fluences for protons are lower for low Earth orbit than during solar minimum, while for electrons the reverse is true.) It is the short-duration temporal variations that are the most difficult to quantify.

Another modification to the simple toroidal model results from the fact that Earth's magnetic field is multipolar in nature, causing the magnetic field strength contours to sink toward the earth. This multipolar field causes the South Atlantic Anomaly (SAA)—a dip toward the Earth in proton and inner electron flux contours over the South Atlantic. For equal altitudes, the particle flux will be higher for locations in the SAA than for those outside of it.

8.3.3 Trapped Heavier Ions

Ions with $Z > 1$ can also be trapped by Earth's magnetic field, although the intensities for these ions are lower than those for protons and electrons. The trapped heavy ions have energies on the order of 10s of MeV/nuc, so most of them will not penetrate even the thinnest spacecraft shielding. Effects of these particles on microelectronic and photonic systems are second order in most cases.

8.4 Terrestrial Radiation Environment

8.4.1 Alpha Particle Decay

Alpha particles are produced by radioactive decays of nuclei. An alpha particle is simply a helium ion that was ejected from the nucleus. The energy is <10 MeV. The range in silicon is <100 μm. Traces of alpha emitters are found in semiconductor process and packing material. Purification of production materials and shielding can mitigate the alpha environment.

8.4.2 Environment from GCR Interaction with Atmosphere

Neutron (n), proton (p), and muon (μ) showers are produced from interaction of GCR ions with the atmosphere. The particle flux depends strongly on altitude. For example, Denver, CO has higher flux than Hawthorne, NY. Protons and muons interact via direct ionization. Neutrons are not charge particles; therefore, they interact with target nuclei. Two processes dominate: (1) fission energies less than a few MeV and (2) nuclear reaction energies greater than 1 MeV or so. Thermal neutron–induced decay of ^{10}B into a lithium, alpha, and gamma is an issue for microelectronic circuits fabricated with BPSG.

References

1. Stopping of ions heavier than helium, *Journal of the ICRU*, Report 73, 2005.
2. Stopping power and ranges for protons and alpha particles, *Journal of the ICRU*, Report 49, 1993.
3. J. Ziegler. www.srim.org
4. R. Baumann and E. B. Smith, Neutron-induced 10B fission as a major source of soft errors in high density SRAMs, *Elsevier Microelectronics Reliability*, 41(2), 211, 2001.
5. J. Barth, Modeling space radiation environments, Notes from 1997 IEEE Nuclear and Space Radiation Effects Conference Short Course.
6. M. Xapsos, Modeling the space radiation environment, Notes from 2006 IEEE Nuclear and Space Radiation Effects Conference Short Course.
7. Vanderbilt University's Institute for Space and Defense Electronics. https://creme.isde.vanderbilt.edu
8. W. Heinrich, Calculation of LET spectra of heavy cosmic ray nuclei at various absorber depths, *Journal of Radiation Effects*, 34, 143, 1977.
9. D. V. Reames, Solar energetic particles: A paradigm shift, *Reviews of Geophysics (Suppl.)*, 33, 585, 1995.
10. R. A. Mewaldt, M. D. Looper, C. M. S. Cohen, G. M. Mason, D. K. Haggerty, M. I. Desai, A. W. Labrador, R. A. Leske, and J. E. Mazur, Solar-particle energy spectra during the large events of October–November 2003 and January 2005, *29th International Cosmic Ray Conference Pune*, pp. 101–104, 2005.